PRICE-BASED OPTIMAL RESOURCE ALLOCATION IN MULTI-HOP WIRELESS NETWORKS

BY

YUAN XUE

B.S., Harbin Institute of Technology, 1998
M.S., University of Illinois at Urbana-Champaign, 2002

DISSERTATION

Submitted in partial fulfillment of the requirements
for the degree of Doctor of Philosophy in Computer Science
in the Graduate College of the
University of Illinois at Urbana-Champaign, 2005

Urbana, Illinois

Abstract

Recent advances in wireless communications and digital electronics have enabled rapid development of a variety of wireless network technologies. The undeniable popularity of wireless network is due to its ubiquity and convenience, which is appreciated by the users.

In this dissertation, we study the problem of *resource allocation* in multihop wireless networks (so called ad hoc networks). A wireless ad hoc network consists of a collection of wireless nodes without a fixed infrastructure. Two wireless nodes communicate with each other directly, if they are within the transmission range of each other. Otherwise, the communication is achieved through the relays of intermediate nodes. Compared with traditional wireline networks, the unique characteristics of wireless networks pose fundamental challenges to the design of effective resource allocation algorithms that are *optimal* with respect to resource utilization and *fair* across different network flows. Particularly, the following issues of wireless networks need fresh treatment: (1) *Interference of wireless communication*. Flows not only contend at the same node (contention in the time domain), but also compete for shared channel if they are within the interference ranges of each other (contention in the spatial domain). (2) *Multiple resource usage*. Sending data from one wireless node to another needs to consume multiple resources, most notably wireless bandwidth and battery energy. (3) *Autonomous communication entities*. The wireless nodes usually belong to different autonomous entities. They may lack the incentive to contribute to the network functionality in a cooperative way. (4) *Rate diversity*. Wireless nodes can adaptively change the transmission bit rate based on perceived channel conditions. This leads to a wireless network with *rate diversity*, where competing flows within the interference range transmit at different rates.

None of the existing resource allocation algorithms in wireless ad hoc networks have realis-

tically considered end-to-end flows spanning multiple hops. Moreover, strategies proposed for wireline networks are not applicable in the context of wireless ad hoc network, due to its unique characteristics.

In this dissertation, we propose a new price-based resource allocation framework in wireless ad hoc networks to achieve *optimal* resource utilization and *fairness* among competing end-to-end flows. We build our pricing framework on the notion of *maximal cliques* in wireless ad hoc networks, as compared to individual links in traditional wide-area wireline networks. Based on such a price-based theoretical framework, we present a two-tier iterative algorithm. Distributed across wireless nodes, the algorithm converges to a global network optimum with respect to resource allocations. Further, we present a *price pair* mechanism to coordinate multiple resource allocations, and to provide incentives simultaneously such that cooperation is promoted and the desired global optimal network operating point is reached by convergence with a fully decentralized self-optimizing algorithm. Such desired network-wide global optimum is characterized with the concept of Nash bargaining solution, which not only provides the Pareto optimal point for the network, but is also consistent with the fairness axioms of game theory. Finally, we present a *channel aware* price generation scheme to decompose the bit rate adjustment and the flow rate allocation. The allocation result achieves channel time fairness where user fairness and channel utilization is balanced.

The major achievements of this dissertation are outlined as follows.

1. *It models a system-wide optimal operation point of a wireless network, and outlines the solution space of resource allocation in a multihop wireless network*;

2. *It presents a price-based distributed resource allocation algorithm to achieve this global optimal point*;

3. *It presents a low overhead implementation of the price-based resource allocation algorithm*;

4. *It presents an incentive mechanism that enables the resource allocation algorithm when users are selfish.*

TO MY PARENTS AND YI

Acknowledgments

First and foremost, my deepest gratefulness goes to my thesis advisor, Professor Klara Nahrstedt, for her invaluable guidance and support throughout my Ph.D. study. Her insights and suggestions have enlightened me not only on academic thinking, and technical problem solving, but also on career choice. To me, she has been a great advisor and an irreplaceable role model. I will always be grateful for her consistent encouragement and belief in me during my periods of doubt and frustration. I feel extremely lucky to have Klara as my advisor, who is always dedicated to the success of her students.

I would like to thank the members of my thesis committee: Professor Jennifer Hou, Professor P. R. Kumar, and Professor Nitin Vaidya, for their helpful discussions on the ideas of my work. Their insightful comments on my thesis have greatly helped me to improve the quality of this work. I am also deeply indebted for their advice and supports in my career choices.

I would also like to extend my special thanks to Professor Robin Kravets and Professor Roy Campbell for their encouragement and support during my Ph.D. study. I would like to thank Professor Baochun Li from University of Toronto and Professor Dongyan Xu from Purdue University for their invaluable advice on how to conduct valuable research. Working with them has greatly benefited my graduate study and research career.

I am grateful for the help and support from all current and former members of the MONET (Multimedia Operating Systems and Networking) research group. Particularly, I would like to thank Kai Chen, Samarth Shah, Chui Sian Ong and Hoang Nguyen for many insightful discussions and fruitful collaborations. I am also thankful to Li Xiao, Xue Yang, Rong Zheng for the helpful discussions and comments. My gratitude also goes to Bin Yu, Jin Liang, Wenbo He, Jingwen

Jin, Wanghong Yuan, Xiaohui Gu, Duangdao Wichadakul, Jun Wang, King-Shan Lui, Won Jeon, William Conner and Adam Slagell.

Last but not least, my parents deserve special recognitions for their unconditional love and continuous support. Without them, all that I have achieved would not have been possible. I am also grateful to my husband Yi for his love and support during my graduate study. His companionship makes this long journey a joyful experience. This dissertation is dedicated to them.

Table of Contents

List of Tables . . . . . **xi**

List of Figures . . . . . **xii**

Chapter 1 Introduction **1**
1.1 Background 1
1.2 Problem Description and Research Goal 2
1.3 Our Approach 4
1.4 Contribution 6
1.5 Thesis Outline 6

Chapter 2 Generalized Price-based Resource Allocation Framework **7**
2.1 Resource Allocation: An Optimization Problem 7
2.1.1 An abstract network model 7
2.1.2 Objective: maximizing aggregated utility 8
2.1.3 Constraint: resource element and its capacity 8
2.1.4 Putting things together 10
2.2 Decentralized Solution: A Price-based Approach 12
2.3 Notations 14

Chapter 3 Bandwidth Allocation in Multihop Wireless Networks **16**
3.1 Overview 16
3.2 Resource Model of Multihop Wireless Networks 17
3.2.1 Network model 17
3.2.2 Identifying resource element 19
3.2.3 Approximating resource element 22
3.3 Distributed Algorithm 26
3.3.1 Dual problem 26
3.3.2 First tier algorithm: per-clique price calculation 29
3.3.3 Second tier algorithm: decentralized clique construction 33
3.3.4 Two-tier algorithm: integration choices 35
3.3.5 Towards asynchrony 36
3.3.6 Improvement for multi-rate wireless network 45
3.4 Performance Evaluation 47
3.4.1 Deployment issues 48

3.4.2 Convergence . . . 50
3.4.3 Impact of realistic wireless interference . . . 56
3.4.4 Overhead . . . 60
3.4.5 k-hop heuristic . . . 62
3.4.6 Impact of mobility . . . 64
3.5 Related Work . . . 67
3.6 Summary . . . 69
3.7 Notations . . . 69

Chapter 4 Multi-Resource Allocation and Incentives Arbitration in Multihop Wireless Networks . . . 71
4.1 Overview . . . 71
4.2 Network Model and Resource Constraints . . . 73
4.2.1 Characterizing wireless ad hoc networks . . . 73
4.3 Problem Formulation . . . 76
4.3.1 Nash Bargaining Solution: a game theoretical formulation . . . 76
4.3.2 Network operating points: optimal and fair rate allocations . . . 79
4.3.3 Local strategies: self-optimizing decisions . . . 82
4.4 Proof of Theorem 4.3.3 . . . 84
4.5 Algorithm . . . 86
4.5.1 Dual problem . . . 86
4.5.2 Distributed algorithm . . . 87
4.6 Proof of Theorem 4.5.1 . . . 90
4.6.1 Implementation issues . . . 94
4.7 Simulation Results . . . 94
4.7.1 Convergence . . . 95
4.7.2 Impact of resource capacity . . . 97
4.7.3 Network performance with incentives . . . 101
4.8 Related Work . . . 102
4.9 Summary . . . 104
4.10 Notations . . . 104

Chapter 5 Software Architecture and System Implementation . . . 106
5.1 Software Architecture . . . 106
5.2 System Implementation . . . 108
5.2.1 Data structure . . . 108
5.2.2 Router . . . 109
5.2.3 Queue monitor . . . 110
5.2.4 Bandwidth estimator . . . 110
5.2.5 Data bit rate monitor . . . 111
5.3 Experiment Results . . . 112
5.4 Limitations of Price-based Resource Allocation in Wireless Networks . . . 117

Chapter 6 Concluding Remarks and Future Directions 119
6.1 Concluding Remarks 119
6.2 Future Directions 120

References 122

Vita 125

List of Tables

2.1 Notations in Chapter 2 15

3.1 First tier: per-clique resource allocation algorithm 31
3.2 Resource allocation algorithm in multi-rate wireless network. 47
3.3 Number of iterations towards convergence 51
3.4 Rate allocations and equilibrium prices in different networks 59
3.5 Notations in Chapter 3 70

4.1 Distributed algorithm 89
4.2 Flows and their routes 96
4.3 Maximal Cliques 96
4.4 Equilibrium rates and prices 98
4.5 Equilibrium rates and prices when more energy is available at node 11 and 1. . . . 99
4.6 Comparison of Network Performance 102
4.7 Notations in Chapter 4 105

List of Figures

2.1 Resource elements in different networks 9
2.2 Price-based Resource Allocation Framework 14

3.1 Resource model of multihop wireless network 19
3.2 Solution space of wireline network. 22
3.3 Approximate resource model of multihop wireless network 24
3.4 Price-based framework: a comparison. 29
3.5 Example of decentralized clique construction 34
3.6 Measurement-based bandwidth estimation. 49
3.7 4-hop chain topology 50
3.8 Asynchronous experiments of implementation I with different step sizes γ ($\alpha = 0$). 52
3.9 Asynchronous experiments of implementation I with different weights α ($\gamma = 0.05$). 53
3.10 Asynchronous experiments with implementation II. 53
3.11 Convergence with bandwidth estimation. 54
3.12 Convergence under the piggyback-based lightweight communication protocol. . . . 55
3.13 Convergence in random networks. 55
3.14 Convergence in the hidden terminal scenario I. 57
3.15 Convergence in the hidden terminal scenario II. 57
3.16 Convergence in the exposed terminal scenario. 57
3.17 Convergence in the race condition scenario. 58
3.18 Comparison of different interference ranges. 60
3.19 Overhead. 61
3.20 Comparison of price-based resource algorithms and TCP over randomly generated networks. 65
3.21 Throughput comparison over a randomly generated network with 30 node deployed over a $600 \times 600\ m^2$ region. 65
3.22 Impact of node mobility. 66
3.23 Impact of node mobility. 67

4.1 Example of wireless ad hoc network and its subflow contention graph 75
4.2 Example of Nash bargaining solution 79
4.3 An example of the price pair mechanism 82
4.4 Random topology used in the simulation 95
4.5 Convergence of the algorithm on the network shown in Fig. 4.1 97
4.6 Convergence when more energy is available at node 11 and 1. 97

4.7 Energy is dominant factor 100
4.8 Channel is dominant factor 100

5.1 Overview of software architecture. 106
5.2 Details of software architecture. 107
5.3 Measurement-based bandwidth estimation. 111
5.4 Single scenario. 112
5.5 Multihop scenario. 113
5.6 Scenario 2. 113
5.7 Race condition. 114
5.8 Multi-rate scenario 1. 115
5.9 Multi-rate scenario (mobile). 116
5.10 Multi-rate scenario 2. 116
5.11 TCP performance in multi-rate wireless network. 117

Chapter 1

Introduction

1.1 Background

Recent advances in wireless communications and digital electronics have enabled rapid development of a variety of wireless network technologies, such as wireless LAN, home network, multihop ad hoc network, and sensor network. In all these networks, a set of computing devices are interconnected over wireless medium to form a distributed environment. Some networks are interconnected to the Internet via base stations, while others stand alone. The undeniable popularity of wireless network is due to its ubiquity and convenience, which is appreciated by the users. Such a popularity has attracted both academic and industrial efforts to the domain of wireless networking research.

In this dissertation, we mainly consider multihop wireless networks (so called ad hoc networks). A wireless ad hoc network consists of a collection of wireless nodes without a fixed infrastructure. Two wireless nodes communicate with each other directly, if they are within the transmission range of each other; Otherwise, the communication is achieved through the relays of intermediate nodes. Ad hoc networks could be rapidly deployed without the support of fixed infrastructure. Thus they can be used in the situations where temporary network connectivity is needed.

1.2 Problem Description and Research Goal

In this dissertation, we study the problem of *resource allocation* in wireless networks. Compared with traditional wireline networks, the unique characteristics of wireless networks pose new challenges to this problem, and prevent verbatim applications of the existing resource allocation approaches. Particularly, the following issues of wireless networks need fresh treatment.

- *Interference of wireless communication.* Compared with wireline networks where flows only contend at the router that performs flow scheduling (contention in the time domain), the unique characteristics of wireless networks show that, flows also compete for shared channel if they are within the interference ranges of each other (contention in the spatial domain). This presents the problem of designing the topology-aware resource allocation algorithm for contending multi-hop flows.

- *Complex resource usage*. Sending data from one wireless node to another needs to consume multiple resources, most notably wireless bandwidth and battery energy. Wireless bandwidth is shared among neighboring nodes, while battery energy is private to the node itself. Thus end-to-end multihop flows need coordinated resource allocation between bandwidth and energy. In the wireline networks, this kind of complex resource usage does not occur.

- *Autonomous communication entities*. The wireless nodes usually belong to different autonomous entities. They may lack the incentive to contribute to the network functionality in a cooperative way. Here cooperation has two-fold implications. First, each wireless node does not excessively and greedily inject traffic to the shared wireless channel. Second, intermediate nodes are willing to relay traffic for upstream nodes towards the destination at the cost of their own private resources. This presents the problem of designing appropriate incentive mechanisms to not only encourage cooperative behavior of selfish nodes, but also curb unfair and excessive resource usage.

- *Constrained resource condition*. The resource conditions in wireless networks tend to be more stringent than their wireline peers. For example, the energy supply in the portable device is limited, and the wireless channel bandwidth is scarce. Such constrained resource condition poses great challenges in designing the light-weighted resource allocation solution.

- *Rate Diversity*. In wireless networks, the signal strength and noise level of wireless channels vary widely, especially in indoor environments, leading to diverse channel bit error rates (BER). To reduce the BER, the sender can transmit at a lower data rate by using a more resilient modulation scheme. Many vendors of client adaptors and access points implement automatic bit rate control scheme in which the sender adaptively changes the bit rate based on perceived channel conditions. This leads to a wireless network with *rate diversity*, where competing flows within the interference range transmit at different rates.

- *Dynamic environment*. Mobile users of wireless networks create a dynamic networking environment, where network topologies and resource usage patterns are changing with time. Such environments require the resource allocation mechanism to adapt quickly to network and resource dynamics.

In recognition of the above challenges, the goal of our research is to answer the following questions,

1. *how to model a system-wide optimal operation point of a wireless network, given the resource demand of its users*;

2. *how to achieve this global optimal point via distributed algorithms*;

3. *how to implement these distributed algorithms efficiently via low overhead protocols*;

4. *how to enable these resource allocation mechanisms when users are selfish*.

1.3 Our Approach

Towards these goals, we employ a *price*-based approach to the resource allocation problem. In this approach, *price* serves as the key to the design of efficient distributed algorithms. The unique characteristics of the wireless ad hoc network are incorporated into a novel pricing model which is tailed to its resource model.

Specifically, we start with a generalized price-based resource allocation framework, which is established based on an abstract network resource model. In this abstract model, the network resource is characterized by a set of resource elements with independent capacities. Under this model, we formulate the resource allocation problem in a general setting as an optimization problem via a utility-based approach. In this formulation, the concept of *utility* is used to reflect the resource demands of different users. At the system optimum, the aggregated utility of all users is maximized. Under this problem formulation, we illustrate the mathematical foundation of the price-based approach and show how this approach can provide a distributed solution to the optimization problem.

Then we instantiate the generalized resource allocation framework to the case of bandwidth allocation in the setting of multihop wireless networks. The key challenge comes from the *shared-medium multi-hop* nature of such networks, namely location-dependent contention and spatial reuse. Based on solid theoretical analysis, we show that a resource element in a multihop wireless network is a *facet of the polytope defined by the independent set of the contention graph of this network*. The modeling of the system-wide optimal operation point of a wireless network then follows directly from the generalized resource allocation framework.

To achieve this global optimal point, we present a price-based distributed resource allocation algorithm. In this algorithm, price is dynamically adjusted based on the relationship between the resource demand and its supply. And the users make self-optimization decisions on their sending rates to maximize their own net benefits, which is the difference between their utilities and their costs. We show that such a distributed algorithm converges to the unique global optimal network

operation point.

The key challenge to implement the above resource allocation algorithms comes from the computational complexity of identifying resource elements and the communication overhead from the distributed algorithms. To address these challenges, we first present heuristics of these algorithms which approximate the original algorithms at different levels and different degrees by exploring the locality of the wireless network. Then we design low overhead communication protocols which are integrated with the existing ad hoc routing protocols.

Further, we present a price-pair mechanism to coordinate the resource allocation between the wireless bandwidth and the battery energy, and to provide incentives simultaneously, such that cooperation is promoted and the levels of cooperation are adequate to achieve the desired global optimal network operation point. This global optimum is characterized with the concept of Nash Bargaining Solution (NBS), which not only provides the Pareto optimal point for the network, but is also consistent with the fairness axioms of game theory.

We also study the problem of resource allocation in multi-rate wireless networks where transmission bit rates are automatically adjusted by the wireless adaptors based on perceived channel conditions. We show that our price-based resource allocation framework provides a natural solution to decompose the bit rate adjustment and the flow rate adaption. The allocation result achieves channel time fairness where user fairness and channel utilization is balanced.

Finally, we present the software architecture and the system implementation of the price-based resource allocation algorithms. The algorithms are implemented as two entities inside the network. At the end hosts, the price-based rate adaptation is implemented at the application level. At the relaying nodes, the price generation is implemented based on queue monitoring and MAC bandwidth estimation. Our implementation does not require any change to the underlying MAC layer, thus can be easily deployed on open source Linux systems.

1.4 Contribution

The key contributions of the price-based resource allocation solutions for wireless networks presented in this dissertation are summarized as follows.

Theoretically, the generalized price-based framework provides an integrated model for resource allocation in both wireline and wireless networks. It also has the potential to accommodate future networking technologies. Further, the novel pricing model, which reflects the unique resource characteristics of the wireless networks, successfully provides a distributed solution to the resource allocation problem in such networks.

Practically, the design of price-based resource allocation algorithms is evaluated via extensive simulation and test-bed experiment. The results validate that our solution is: (1) able to support efficient and fair resource allocation; (2) light-weighted for the resource constrained wireless networks; and (3) adaptive to the dynamic mobile environments.

1.5 Thesis Outline

The rest of this dissertation is organized as follows: Chapter 2 introduces the generalized resource allocation framework and presents the theoretical fundamentals of the price-based resource allocation approach. Chapter 3 elaborates on our investigations of bandwidth allocation problem in multihop wireless networks. It presents two sets of price-based algorithms and their implementations, and evaluates their performances. Chapter 4 studies the problem of resource coordination between the wireless bandwidth and the battery energy, and presents an incentive mechanism for multihop wireless networks via channel-relay price pair. Chapter 5 presents the software architecture, system implementation, and testbed results of the price-based resource allocation algorithm. Chapter 6 concludes this dissertation and points out our future research directions.

Chapter 2

Generalized Price-based Resource Allocation Framework

In this chapter, we present the generalized price-based theoretical framework for resource allocation in the setting of an abstract network model. We first formulate the resource allocation problem as an optimization problem. We then show that a price-based approach can provide a decentralized algorithm to solve this problem.

2.1 Resource Allocation: An Optimization Problem

2.1.1 An abstract network model

In our abstract network model, a network is represented as a set of *resource elements* E. A resource element $e \in E$ can be a wireline link, a shared wireless channel, etc. Each element has a fixed and finite capacity C_e. Note that the most important nature of a resource element is the independence of its capacity. Specifically, how resource is allocated can not affect the capacity of a resource element. In this sense, a wireline link is a resource element, while a wireless link is not, as its bandwidth may vary depending on the traffic in its neighborhood.

Consider the network is shared by a set of end-to-end flows F. A flow $f \in F$ has a rate of x_f. f must traverse a sequence of resource elements (end-to-end path) to reach its destination. Let R_{ef} be the amount of resource e used by a unit flow of f, and y_e be the amount of traffic generated by all flows at resource element e. Obviously $y_e = \sum_{f \in F} R_{ef} \cdot x_f$.

2.1.2 Objective: maximizing aggregated utility

We associate each end-to-end flow $f \in F$ with a *utility function* $U_f(x_f) : \Re_+ \rightarrow \Re_+$, which represents the degree of satisfaction of its associated end user. Here we make the following assumptions about $U_f(x_f)$:

- **A1**. On the interval $[0, \infty)$, the utility function $U_f(\cdot)$ is increasing, strictly concave and continuously differentiable.
- **A2**. U_f is additive so that the aggregated utility of rate allocation $\boldsymbol{x} = (x_f, f \in F)$ is $\sum_{f \in F} U_f(x_f)$.

We investigate the problem of optimal resource allocation in the sense of *maximizing the aggregated utility function* of all users, which is also referred to as the *social welfare* in the literature. Formally, this objective is given as follows,

$$\textbf{maximize} \sum_{f \in F} U_f(x_f)$$

This optimization objective is of particular interest, because as we will demonstrate, such an objective achieves Pareto optimality with respect to the resource utilization, and also realizes different fairness models — including proportional and max-min fairness — when appropriate utility functions are specified.

2.1.3 Constraint: resource element and its capacity

Recall that each element $e \in E$ in the network has a finite capacity C_e, and y_e is the amount of traffic generated by all flows at resource element e. The constraints from resource capacities are given as follows,

$$\forall e \in E, y_e \leq C_e$$

As R_{ef} is the amount of resource e used by a unit flow of f, and thus $y_e = \sum_{f \in F} R_{ef} \cdot x_f$, we have

$$\forall e \in E, \sum_{f \in F} R_{ef} \cdot x_f \leq C_e$$

or in concise form,

$$\boldsymbol{R} \cdot \boldsymbol{x} \leq \boldsymbol{C}$$

where $\boldsymbol{R} = (R_{ef})_{|E| \times |F|}$ is a matrix with element R_{ef} at row e and column f, and $\boldsymbol{x} = (x_f, f \in F)$, $\boldsymbol{C} = (C_e, e \in E)$ are vectors of flow rates and resource capacities respectively.

The definition of resource element and its capacity can be very diverse for different types of networks. Sometimes it is very hard to define the resource constraint of a network, especially for a multihop wireless network with the presence of spatial reuse. In what follows, we will illustrate the concept of resource element in two simple network settings, and present their resource constraints. Based on these intuitive examples, we will further define the resource model of multihop wireless networks in Chapter 3, which establishes the foundation of theoretical study on resource allocation in this type of networks.

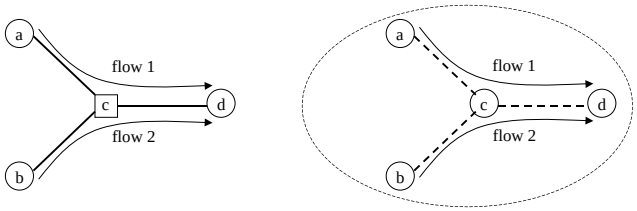

(a) Wireline network (b) Wireless network without spatial reuse

Figure 2.1: Resource elements in different networks

Wireline networks

In wireline networks, flows only contend with each other if they share the same physical link. In this case, the resource element e is a wireline link, its resource capacity C_e is the link capacity. In

this case, $\boldsymbol{R}$ can be understood as the routing matrix defined as follows.

$$R_{ef} = \begin{cases} 1 & \text{if } f \text{passes through } e \\ 0 & \text{otherwise} \end{cases}$$

In the example shown in Fig. 2.1 (a), the constraints on resource allocations of flows 1 and 2 can be expressed as

$$\begin{pmatrix} 1 & 0 \\ 0 & 1 \\ 1 & 1 \end{pmatrix} \begin{pmatrix} x_1 \\ x_2 \end{pmatrix} \leq \begin{pmatrix} C_{ac} \\ C_{bc} \\ C_{cd} \end{pmatrix}$$

Wireless networks without spatial reuse

In wireless networks where nodes are within the transmission range of each other as shown in Fig. 2.1 (b), flows not only contend at the same wireless link, but also in a geographical vicinity: only one node can transmit at any time instance in this vicinity. In this case, the flows in the network share one wireless channel. Hence this is the only resource element, whose capacity is C_{chan} – the wireless channel capacity. Then the constraints on resource allocations of flows 1 and 2 can be expressed as

$$\begin{pmatrix} 2 & 2 \end{pmatrix} \begin{pmatrix} x_1 \\ x_2 \end{pmatrix} \leq C_{chan}$$

2.1.4 Putting things together

Summarizing above discussions, we formulate the resource allocation problem in a generalized form as follows.

$$\mathbf{S}: \quad \textbf{maximize} \quad \sum_{f \in F} U_f(x_f) \tag{2.1}$$

$$\textbf{subject to} \quad \boldsymbol{R} \cdot \boldsymbol{x} \leq \boldsymbol{C} \tag{2.2}$$

$$\boldsymbol{x} \geq \mathbf{0} \tag{2.3}$$

The objective function in Eq. (2.1) of the optimization problem maximizes the aggregated utility of all flows. The constraint of the optimization problem (Inequality (2.2)) is the resource constraint. We now demonstrate that, by optimizing towards such an objective, both *optimal resource utilization* and *fair resource allocations* may be achieved among *end-to-end* flows.

Pareto optimality

With respect to optimal resource utilization, we show that the resource allocation is *Pareto optimal* if the optimization problem $\mathbf{S}$ can be solved. Formally, the Pareto optimality is defined as follows.

Definition 2.1.1. (Pareto optimality) *A rate allocation $\boldsymbol{x} = (x_f, f \in F)$ is* **Pareto optimal***, if it satisfies the following two conditions: (1) $\boldsymbol{x}$ is feasible,* i.e., *$\boldsymbol{x} \geq \mathbf{0}$ and $\boldsymbol{R} \cdot \boldsymbol{x} \leq \boldsymbol{C}$; and (2) $\forall \boldsymbol{x}'$ which satisfies $\boldsymbol{x}' \geq \mathbf{0}$ and $\boldsymbol{R} \cdot \boldsymbol{x}' \leq \boldsymbol{C}$, if $\boldsymbol{x}' \geq \boldsymbol{x}$, then $\boldsymbol{x}' = \boldsymbol{x}$. In the second condition, The $\geq$ relation is defined such that, two vectors $\boldsymbol{x}$ and $\boldsymbol{x}'$ satisfy $\boldsymbol{x}' \geq \boldsymbol{x}$, if and only if for all $f \in F$, $x'_f \geq x_f$.*

Proposition 2.1.1. *A rate allocation $\boldsymbol{x}$ is Pareto optimal, if it solves the problem* $\mathbf{S}$*, with increasing and strictly concave utility functions $U_f(x_f)$, for $f \in F$.*

Proof. Let $\boldsymbol{x}$ be a solution to the problem $\mathbf{S}$. If $\boldsymbol{x}$ is not Pareto optimal, then there exists another vector $\boldsymbol{x}' \neq \boldsymbol{x}$, which satisfies $\boldsymbol{R} \cdot \boldsymbol{x}' \leq \boldsymbol{C}$ and $\boldsymbol{x}' > \boldsymbol{x}$. As $U_f(\cdot)$ is increasing and strictly concave, we have that $\sum_{f \in F} U_f(x'_f) > \sum_{f \in F} U_f(x_f)$. This leads to a contradiction, as $\boldsymbol{x}$ is the solution to $\mathbf{S}$ and hence maximizes $\sum_{f \in F} U_f(x_f)$. □

Fairness

By choosing appropriate utility functions, the optimal resource allocation can implement different fairness models among the flows. We illustrate this fact using two commonly adopted fairness models: *weighted proportional* fairness and *max-min* fairness.

Definition 2.1.2. (weighted proportional fairness) *A vector of rates* $\boldsymbol{x} = (x_f, f \in F)$ *is* **weighted proportionally fair** *with the vector of weights* w_f*, if it satisfies the following two conditions: (1)* $\boldsymbol{x}$ *is feasible,* i.e., $\boldsymbol{x} \geq 0$ *and* $\boldsymbol{R} \cdot \boldsymbol{x} \leq \boldsymbol{C}$*; and (2) for any other feasible vector* $\boldsymbol{x}' = (x'_f, f \in F)$*, the aggregate of proportional changes is zero or negative:*

$$\sum_{f \in F} w_f \frac{x'_f - x_f}{x_f} \leq 0.$$

Proposition 2.1.2. *A rate allocation* $\boldsymbol{x}$ *is weighted proportional fair with the weight vector* w_f*, if and only if it solves the problem* **S***, with* $U_f(x_f) = w_f \log x_f$ *for* $f \in F$*.*

Proof. As shown in [19], by the optimality condition (2.1), this proposition can be derived according to the following relation:

$$\sum_{f \in F} \frac{\partial U_f}{\partial x'_f}(x_f)(x'_f - x_f) = \sum_{f \in F} w_f \frac{x'_f - x_f}{x_f} < 0$$

where the strict inequality follows from the strict concavity of U_f. □

Definition 2.1.3. (max-min fairness) *A vector of rates* $\boldsymbol{x} = (x_f, f \in F)$ *is* **max-min fair***, if it satisfies the following two conditions: (1)* $\boldsymbol{x}$ *is feasible,* i.e., $\boldsymbol{x} \geq 0$ *and* $\boldsymbol{R} \cdot \boldsymbol{x} \leq \boldsymbol{C}$*; and (2) for any* $f \in F$*, increasing* x_f *can not be achieved without decreasing the fair share* $x_{f'}$ *of another flow* $f' \in F$ *that satisfies* $x_f \geq x_{f'}$*.*

Proposition 2.1.3. *A rate allocation* $\boldsymbol{x}$ *is max-min fair if and only if it solves the problem* **S***, with* $U_f(x_f) = -(-\log x_f)^\zeta$*,* $\zeta \to \infty$ *for* $f \in F$*.*

Again, these results straightforwardly follow their counterparts in wireline networks [19].

2.2 Decentralized Solution: A Price-based Approach

We proceed to study how to derive a decentralized solution to the problem **S** so that the optimal resource allocation can be achieved.

By assumption **A1**, the objective function of $\mathbf{S}$ in Eq. (2.1) is differentiable and strictly concave. In addition, the feasible region of the optimization problem in Inequality (2.2) is convex and compact. By non-linear optimization theory, there exists a unique maximizing value of argument $\boldsymbol{x}$ for the above optimization problem. Let us consider the Lagrangian form of the optimization problem $\mathbf{S}$:

$$\begin{aligned} L(\boldsymbol{x};\boldsymbol{\mu}) &= \sum_{f\in F} U_f(x_f) + \boldsymbol{\mu}^T(\boldsymbol{C}-\boldsymbol{R}\boldsymbol{x}) \\ &= \sum_{f\in F}(U_f(x_f) - x_f\sum_{e\in E}\mu_e R_{ef}) + \sum_{e\in E}\mu_e C_e \end{aligned} \tag{2.4}$$

where $\boldsymbol{\mu} = (\mu_e, e \in E)$ is a vector of Lagrange multipliers. Given global knowledge of utility functions, $\mathbf{S}$ is mathematically tractable. However, in practice, such knowledge is unlikely to be available. In addition, it may be infeasible to compute and allocate resources in a centralized fashion. Here we seek a decentralized solution. The key to decentralization is pricing.

In the Lagrangian form specified in Eq. (2.4), the Lagrange multipliers μ_e may be regarded as the implied cost, or the *shadow price*, of a unit flow using resource e. Such a price μ_e reflects the traffic load y_e at this resource element e. Flow $f \in F$ will then be charged with a flow price λ_f which is the sum of the costs at all resource elements it uses, the cost at each resource element being the product of its price and the amount of resource used by a unit flow of f, namely,

$$\lambda_f = \sum_{e\in E} R_{ef}\mu_e$$

Through this price signal, flow f can make a self-optimized decision to adjust its sending rate x_f. The aggregated sending rate $y_e = \sum_{f\in F} R_{ef} \cdot x_f$ of all flows through resource element e in turn affects its price μ_e. To summarize, Fig. 2.2 illustrates the price-based resource allocation framework. Here we deem each component in the diagram as abstract entities capable of computing and communicating. The functioning of the framework involves no central authority, but purely depends on local decision of each component and exchange of control signals among them.

In each cycle, a resource element e calculates its load y_e, the total amount of flows passing through it, then derives its penalty μ_e and sends it to all these flows. Meanwhile, a flow f, on receiving signals from all resource elements it traverses, derives its flow price λ_f, then adjusts flow rate x_f. Such a cycle repeats itself, and finally converges to the equilibrium point.

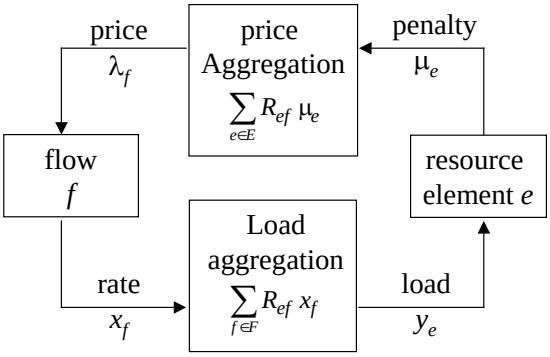

Figure 2.2: Price-based Resource Allocation Framework

The presented framework is a generalized form of the framework proposed by Kelly et al. in [20, 19] for wireline networks. As we will show in Chapter 3 and 4, such a generalization is critical for us to study the resource allocation problem in multihop wireless networks. In Chapter 3, we apply it to the bandwidth allocation of multihop wireless networks. In Chapter 4, it is applied to the resource coordination between battery energy and wireless bandwidth.

2.3 Notations

We list all notations introduced in Chapter 2 as follows.

Notation	Definition
$f \in F$	End-to-end flow in the network
$e \in E$	Resource element of the network
$\boldsymbol{x} = (x_f, f \in F)$	Rate vector of flow $f \in F$
$\boldsymbol{C} = (C_e, e \in E)$	Capacity vector of resource element $e \in E$
$\boldsymbol{R} = (R_{ef})_{\|E\|\times\|F\|}$	Resource constraint matrix
$U_f(x_f)$ $(f \in F)$	Utility function of flow $f \in F$
$\boldsymbol{y} = (y_e, e \in E)$	Aggregated traffic load at resource element $e \in E$
$\boldsymbol{\mu} = (\mu_e, e \in E)$	Price of resource element $e \in E$
λ_f $(f \in F)$	Price of flow $f \in F$

Table 2.1: Notations in Chapter 2

Chapter 3

Bandwidth Allocation in Multihop Wireless Networks

3.1 Overview

In a multihop wireless network, each node in the network forwards packets for its peer nodes, and each *end-to-end flow* traverses multiple wireless links from a source to a destination. Compared with wireline networks where flows only contend at the router that performs flow scheduling (contention in the time domain), the unique characteristics of multihop wireless networks show that, flows also compete for shared channel if they are within the interference ranges of each other (contention in the spatial domain). This presents the problem of designing a topology-aware bandwidth allocation algorithm that is both *optimal* with respect to bandwidth utilization and *fair* across contending multi-hop flows.

In this chapter we seek to answer the following question: how much bandwidth should we allocate to each of the end-to-end flows, so that scarce bandwidth in a wireless network may be optimally and fairly utilized? To answer this question, we apply the price-based resource allocation framework to the setting of bandwidth allocation in multihop wireless networks. We first instantiate the abstract network model of the generalized framework to the case of multihop wireless network in Section 3.2. Based on solid analysis, we show that a resource element in a multihop wireless network is a facet of the polytope defined by the independent set of the contention graph of this network. It can further be approximated by a maximal clique in this contention graph.

Following the generalized resource allocation framework, we formulate the system-wide optimal operation point of a multihop wireless network with a utility-based approach. Based on this formulation, achieving the global network optimum becomes an optimization problem.

We then proceed to employ the price-based approach to solve this problem so that the global optimum can be achieved. In Section 3.3, we present a two-tier distributed algorithm to compute the bandwidth allocation for each of the end-to-end flows. The first tier of the algorithm constitutes an iterative algorithm that determines per-clique shadow prices and end-to-end flow resource allocations. We show that this algorithm converges to the unique equilibrium where the aggregated utility is maximized. The second tier of the algorithm constructs the maximal cliques in a distributed manner. To facilitate its deployment in practical network environments, the algorithm is further improved to accommodate asynchronous communications.

Finally we present the implementation of our algorithms and their performance study in Section 3.4, discuss related work in Section 3.5 and summarize this chapter in Section 3.6.

3.2 Resource Model of Multihop Wireless Networks

3.2.1 Network model

Consider a multihop wireless network that consists of a set of nodes N. Each node $i \in N$ has a transmission range d_{tx} and an interference range d_{int}. Packet transmission in such a network is subject to location-dependent contention. There exist two models for packet transmission in wireless networks in the literature [13], generally referred to as the *protocol model* and the *physical model*. In the case of a single wireless channel, these two models are presented as follows.

1. *The Protocol Model*: In the protocol model, the transmission from node i to j, ($i, j \in N$) is successful if (1) the distance between these two nodes d_{ij} satisfies $d_{ij} < d_{tx}$; (2) any node $k \in N$, which is within the interference range of the receiving node j, $d_{kj} \leq d_{int}$ is not transmitting. This model can be further refined towards the case of IEEE 802.11-style MAC protocols, where the sending node i is also required to be free of interference as it needs to receive the link layer acknowledgement from the receiving node j. Specifically, any node $k \in N$, which is within the interference range of the nodes i or j (*i.e.*, $d_{kj} \leq d_{int}$

or $d_{ki} \leq d_{int}$), is not transmitting.

2. *The Physical Model*: This model is directly related to the physical layer characteristics. The transmission from node i to j is successful if the signal-to-noise ratio at the node j, SNR_{ij}, is not smaller than a minimum threshold: $SNR_{ij} \geq SNR_{thresh}$.

In this dissertation, we focus our attention on solving problems of resource allocation based on the protocol model, with a particular interest in IEEE 802.11-style MAC protocols due to their popular deployment in realistic wireless systems. The problems of resource allocation under the physical model is beyond the scope of this dissertation, and left as a future research direction. Further, unless notified otherwise, we assume that the transmission range d_{tx} is the same as the interference range d_{int}.

Under the protocol model, a wireless ad hoc network can be regarded as a *bidirectional* graph $G = (N, L)$. $L \subseteq 2^N$ denotes the set of *wireless links*, which are formed by nodes that are within the transmission range of each other. A wireless link $l \in L$ is represented by its end nodes i and j, *i.e.*, $l = \{i, j\}$.

In such a network, there exists a set of *end-to-end flows*, denoted as F. Each flow $f \in F$ goes through multiple hops in the network, passing a set of wireless links $L(f)$. A single-hop data transmission in the flow f along a particular wireless link is referred to as a *subflow* of f. Obviously, there may exist multiple subflows along the same wireless link. We use the notation $S(S \subseteq L)$ to represent a set of wireless links in G, such that each of the wireless links in S carries at least one subflow, *i.e.*, the wireless link is not idle.

Based on the protocol model, flows in a wireless ad hoc network contend for shared resources in a location-dependent manner: two subflows contend with each other if either the source or destination of one subflow is within the interference range (d_{int}) of the source or destination of the other.

Formally, we consider a *contention graph* $G_c = (N_c, L_c)$. The vertices of the contention graph $v_i \in N_c$ correspond to the wireless links (*i.e.*, $N_c = S$). There exists an edge between two vertices

if the subflows along these two wireless links contend with each other according to the above protocol model.

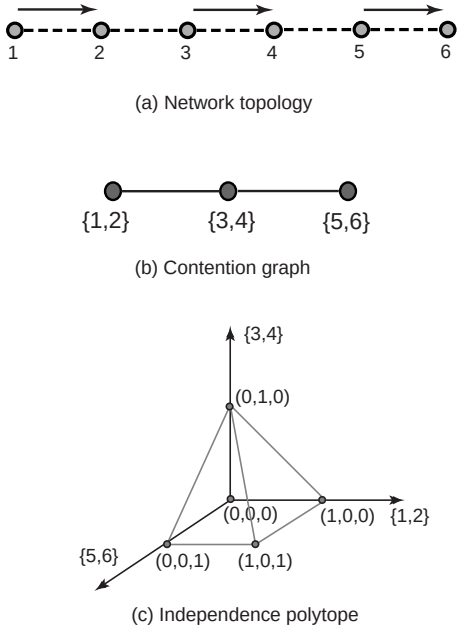

Figure 3.1: Resource model of multihop wireless network

To illustrate these concepts, we show an example in Fig. 3.2.1. Fig. 3.2.1(a) gives the network topology and the traffic used in the example. In this example, the transmission $\{1, 2\}$ and $\{3, 4\}$ contend with each other, also do $\{3, 4\}$ and $\{5, 6\}$. But $\{1, 2\}$ and $\{5, 6\}$ can transmit simultaneously. The contention graph of this wireless network is shown in Fig. 3.2.1(b).

3.2.2 Identifying resource element

Now let us consider an *independent set* $I \subseteq N_c$ of the graph G_c. I can be represented using a $|N_c|$-dimension *independence vector* $\boldsymbol{\iota}_I = (\iota_k, n_k \in N_c)$, defined as follows.

$$\iota_j = \begin{cases} 1 & \text{if } n_k \in I \\ 0 & \text{otherwise} \end{cases}$$

$\boldsymbol{\iota}_I$ can be regarded as a point in a N_c-dimensional *independence space*. In this space, each dimension corresponds to a vertex $n_k \in N_c$.

In the above example, besides the independent sets consisting of each vertex itself (*i.e.*, $\{\{1,2\}\}$, $\{\{3,4\}\}$, $\{\{5,6\}\}$), $\{\{1,2\},\{5,6\}\}$ is also an independent set. Let vertices $\{1,2\}$, $\{3,4\}$, $\{5,6\}$ correspond to the three dimensions of the independence space. Then independence vectors $(1,0,0)$, $(0,1,0)$, $(0,0,1)$ and $(1,0,1)$ correspond to the above independent sets. Fig. 3.2.1(c) show these independence vectors along with a special independence vector – the origin point $(0,0,0)$.

Fig. 3.2.1(c) also shows that a polytope is formed as the convex hull of all points corresponding to each independence vector, or in other words, convex combination of all independence vectors. We call such a polytope the *independent set polytope*, denoted as P_G. Let us consider a $|V_c|$-dimension vector $\boldsymbol{\varrho} = (\varrho_k, n_k \in N_c)$, where ϱ_k is the fraction of time during which link s corresponding to n_k is active. Then $\boldsymbol{\varrho}$ is *schedulable* if there exists a MAC scheduling algorithm that can assign the faction of time indicted by ϱ_k to each wireless link n_k in a conflict free manner. The result of [15] shows that

Lemma 3.2.1. *Vector $\boldsymbol{\varrho} = (\varrho_k, n_k \in N_c)$ is schedulable if and only if it lies within the independent set polytope P_G.*

Reflected in Fig. 3.2.1(c), all points within the polytope P_G is schedulable. To model the resource element from this concept, we consider the *facets* of the polytope P_G[1]. Note that we can get these facets by running any polynomial-time convex hull algorithm[12] on all vertices of the polytope (*i.e.*, all independence vectors). We collect all facets into a set $\boldsymbol{\Theta}$. The plane that a facet $\boldsymbol{\theta}_m \in \boldsymbol{\Theta}$ belongs to can be presented in the following linear form.

$$\sum_{k=1}^{|N_c|} a_{mk}\varrho_k - b_m = 0$$

where a_{mk} and b_m are coefficients of the plane function. Let $\boldsymbol{a} = (a_{mk})_{|\boldsymbol{\Theta}|\times|N_c|}$, then the polytope P_G can be represented in the following vector form.

$$\boldsymbol{a} \cdot \boldsymbol{\varrho} \leq \boldsymbol{b}$$

[1]The facets that lie along the coordination plane are excluded.

where $\boldsymbol{b} = (b_m, \boldsymbol{\theta}_m \in \boldsymbol{\Theta})$. If we scale the independent set polytope P_G by the capacity of the wireless channel C_{chan}, we have that

$$\boldsymbol{a} \cdot \boldsymbol{\varrho} \cdot C_{chan} \leq \boldsymbol{b} \cdot C_{chan}$$

Let *wireless link rate allocation* be $\boldsymbol{y} = (y_s, s \in S)$, where y_s is the rate along wireless link $s \in S$. $\boldsymbol{y}$ is *feasible*, if there exists a MAC scheduling algorithm that can assign rate y_s to each wireless link s in a conflict free manner. Note that $y_s = \varrho_k \cdot C_{chan}$, where $n_k = s$. Thus, by Lemma 3.2.1, we have the following result.

Lemma 3.2.2. *Vector $\boldsymbol{y} = (y_s, s \in S)$ is feasible if and only if it satisfies the following:*

$$\boldsymbol{a} \cdot \boldsymbol{y} \leq C_{chan} \cdot \boldsymbol{b} \tag{3.1}$$

Let $\boldsymbol{A} = (A_{lf})_{|L| \times |F|}$ be the routing matrix defined as follows,

$$A_{lf} = \begin{cases} 1 & \text{if flow } f \text{ passes through wireless link } l \\ 0 & \text{otherwise} \end{cases}$$

Further we define $\boldsymbol{R} = \boldsymbol{a} \cdot \boldsymbol{A}$ and $\boldsymbol{C} = C_{chan} \cdot \boldsymbol{b}$.

Theorem 3.2.1. *Rate allocation vector $\boldsymbol{x} = (x_f, f \in F)$ is feasible, (*i.e.*, there exists a MAC scheduling and an allocation algorithm that assign rate x_f to flow $f \in F$), if and only if it satisfies the following:*

$$\boldsymbol{R} \cdot \boldsymbol{x} \leq \boldsymbol{C} \tag{3.2}$$

Proof. It is easy to see that $\boldsymbol{A} \cdot \boldsymbol{x} = \boldsymbol{y}$. The result straightly follows by Inequality (3.1) in Lemma 3.2.2 and the definition of $\boldsymbol{R}$ and $\boldsymbol{C}$. □

Eq. 3.2 in Theorem 3.2.1 clearly defines the solution space of the resource allocation problem in the multihop wireless networks under the assumption of ideal MAC scheduling. By comparison

of the definitions of R in the abstract network model and the multihop wireless network model, we observe that *each facet $\boldsymbol{\theta}_m \in \boldsymbol{\Theta}$ scaled by C_{chan} can be regarded as a resource element with an independent capacity $C_{chan} \cdot b_m$*.

As an interesting finding, we also notice that the wireline network model is a special case of this formulation. Take the network shown in Fig. 3.2(a) as an example, since all links are independent from each other, any subset of the link set L is an independent set. The resulting independent set polytope (with each dimension normalized by the capacity of its corresponding link) is shown in Fig. 3.2(b). An important property of this polytope is that it is a *cube*. That means for each of its facets, the plane it belongs to only intersects with one axis. Since each axis represents a wireline link, back to Inequality (3.2), this implies that (1) $\boldsymbol{\Theta} = \boldsymbol{I}$, the identity matrix, thus $\boldsymbol{R} = \boldsymbol{A}$, and (2) $b_m = 1$ for any $\boldsymbol{\theta}_m \in \boldsymbol{\Theta}$.

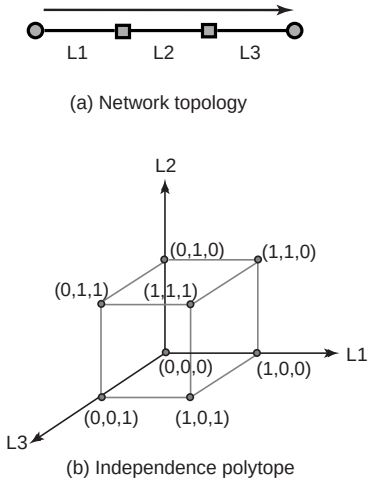

Figure 3.2: Solution space of wireline network.

3.2.3 Approximating resource element

To this end, we have clearly identified the resource elements of a multihop wireless network. However, applying this model to the resource allocation framework can still be difficult, as the problem of finding all independent sets is NP-hard. Besides, this model assumes ideal MAC scheduling. It is difficult to be improved for practical implementations in realistic wireless network

settings, (e.g., with non-ideal MAC algorithm such as IEEE 802.11), because the facets of the independent set polytope of the contention graph lack the intuition to be mapped into any instance in the physical wireless network, not to mention to be implemented via distributed algorithms.

In light of this difficulty, we explore the approximation of resource elements by studying the upper bound of the resource constraint in a multihop wireless network. Here we present a *maximal clique* based approximation. Such an approximation gives a good intuitive explanation on the structure of the resource element in the physical network. Thus it can also facilitate the distributed implementation of resource allocation algorithms.

In a graph, a complete subgraph is referred to as a *clique*. A *maximal clique* is defined as a clique that is not contained in any other cliques[2]. In a contention graph, the vertices in a maximal clique represent a maximal set of mutually contending wireless links, along which at most one subflow may transmit at any given time. Intuitively, each maximal clique in a contention graph represents a maximal distinct contention region, since at most one subflow in the clique can transmit at any time, and adding any other flows into this clique will introduce the possibility of simultaneous transmissions. We denote the set of all maximal cliques in G_c as Q.

Recall that a *rate allocation* $\boldsymbol{y} = (y_s, s \in S)$ is *feasible*, if there exists a collision-free MAC transmission schedule that allocates y_s to s. Based on the above discussions, we have the following results.

Proposition 3.2.1. *Rate allocation* $\boldsymbol{y} = (y_s, s \in S)$ *is feasible, then the following condition is satisfied.*

$$\forall q \in Q_G, \sum_{s \in V(q)} y_s \leq C_{chan} \tag{3.3}$$

where $V(q) \subseteq S$ *is the set of the vertices of the clique* q*.*

Eq. (3.3) gives an upper bound on the rate allocations to the wireless links. Such a bound may

[2]Note that the *maximal clique* has a different definition from the *maximum clique* of a graph, which is the maximal clique with the largest number of vertices. Finding the maximum clique of a graph is a NP-complete problem, while enumerating all the maximal cliques of a graph can be solved in polynomial time [1].

not be tight. Here we discuss two scenarios. First, there may exist no schedules that assign rates to the wireless links to achieve this bound. Such scenario happens when the contention graph has odd holes or odd anti-holes [15]. Second, for some contention graphs, even if there exists a ideal centralized scheduling algorithm that can achieve this bound, the distributed scheduling algorithms that employ carrier sensing multiple access (*e.g.*, IEEE 802.11) can not achieve this bound. Thus we introduce C_q, the *achievable* channel capacity at a clique q. More formally, if $\sum_{s \in V(q)} y_s \leq C_q$ then $\boldsymbol{y} = (y_s, s \in S)$ is feasible. To this end, we observe that a maximal clique q can be regarded as an approximation of a resource element with capacity C_q.

We now proceed to consider the resource constraint of a multihop wireless network using the maximal clique as the approximation of the resource element. We define a clique-flow matrix $\boldsymbol{R} = \{R_{qf}\}$, where $R_{qf} = |V(q) \cap L(f)|$ represents the number of subflows that flow f has in the clique q. If we treat a maximal clique as a resource element, then the clique-flow matrix $\boldsymbol{R}$ represents the "resource usage pattern" of each flow. Let the vector $\boldsymbol{C} = (C_q,\ q \in Q)$ be the vector of achievable channel capacities in each of the cliques. Constraints with respect to rate allocations to end-to-end flows in wireless ad hoc networks are presented in the following proposition.

Proposition 3.2.2. *In a wireless ad hoc network $G = (N, L)$ with a set of flows F, there exists a feasible rate allocation $\boldsymbol{x} = (x_f, f \in F)$, if and only if $\boldsymbol{Rx} \leq \boldsymbol{C}$.*

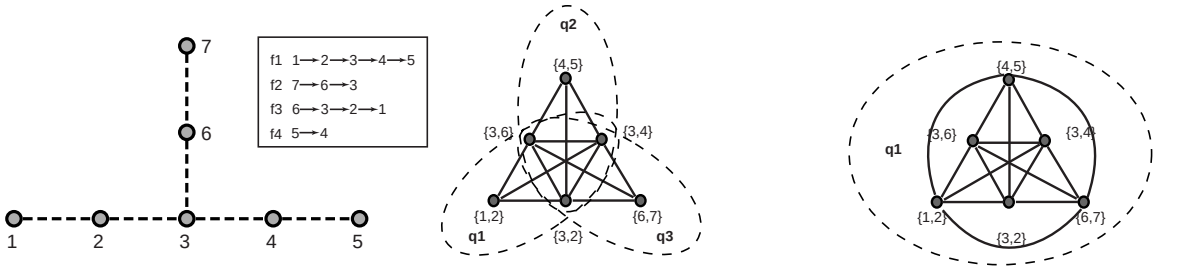

(a) Network topology (b) Wireless link contention graph ($d_{tx} = d_{int}$) (c) Wireless link contention graph ($2d_{tx} = d_{int}$)

Figure 3.3: Approximate resource model of multihop wireless network

We present an example to illustrate the above concepts and notations. Fig. 3.3(a) shows the topology of the network, as well as its ongoing flows. The corresponding contention graph is

shown in Fig. 3.3(b). In this example, there are 4 end-to-end flows $f_1 = \{\{1,2\},\{2,3\},\{3,4\},\{4,5\}\}$, $f_2 = \{\{7,6\},\{6,3\}\}$, $f_3 = \{\{6,3\},\{3,2\},\{2,1\}\}$ and $f_4 = \{\{5,4\}\}$. As such, in Fig. 3.3(b) there are three maximal cliques in the contention graph: $q_1 = \{\{1,2\},\{3,2\},\{3,4\},\{3,6\}\}, q_2 = \{\{3,2\},\{3,4\},\{4,5\},\{3,6\}\}$ and $q_3 = \{\{3,2\},\{3,4\},\{3,6\},\{6,7\}\}$.

We use y_{ij} to denote the aggregated rate of *all* subflows along wireless link $\{i,j\}$. For example, $y_{12} = x_1 + x_3$, $y_{36} = x_2 + x_3$. In each clique, the aggregated rate may not exceed the corresponding channel capacity. That is

$$y_{12} + y_{32} + y_{34} + y_{36} \leq C_1 \tag{3.4}$$

$$y_{32} + y_{34} + y_{45} + y_{36} \leq C_2 \tag{3.5}$$

$$y_{32} + y_{34} + y_{36} + y_{67} \leq C_3 \tag{3.6}$$

When it comes to end-to-end flow rate allocation, the resource constraint imposed by shared wireless channels is as follows.

$$\begin{pmatrix} 3 & 1 & 3 & 0 \\ 3 & 1 & 2 & 1 \\ 2 & 2 & 2 & 0 \end{pmatrix} \boldsymbol{x} \leq \boldsymbol{C}.$$

In summary, the unique characteristics of location-dependent contention in multihop wireless networks imply a fundamentally different resource model compared to the case of wireline networks. In wireline networks, a resource element is a *wireline link*. Its capacity represents the constraint on flows contending for its bandwidth, which is independent from other links. However, in the case of wireless ad hoc networks, the capacity of a wireless link is interrelated with other wireless links in its vicinity. Such a fundamental difference calls for a new treatment with the pricing models in multihop wireless networks and hence a new resource allocation mechanism.

3.3 Distributed Algorithm

Treating resource elements of a multihop wireless network as maximal cliques in its contention graph, we now proceed to study the distributed algorithm for resource allocation. The algorithm needs to answer two questions: (1) how the price is calculated for each resource element; (2) how rate is adjusted for each flow responding to its price. Here we present an algorithm based on the dual method from optimization theory.

3.3.1 Dual problem

Recall that each end-to-end flow $f \in F$ has a *utility function* $U_f(x_f) : \mathfrak{R}_+ \rightarrow \mathfrak{R}_+$, which represents the degree of satisfaction of its corresponding end user. In addition to the assumption A1 and A2 in Section 2.1, we further make the following assumptions about U_f so that the dual method can be employed.

- **A3**. On the interval $I_f = [m_f, M_f]$, the utility function U_f is twice continuously differentiable.
- **A4**. The curvature of U_f is bounded away from zero on I_f: $-U_f''(x_f) \geq 1/\kappa_f > 0$.

Following the problem formulation in the generalized resource allocation framework, we investigate the problem of optimal bandwidth allocation in the sense of maximizing the aggregated utility of all flows,*i.e.*, the following non-linear optimization problem (also called *primal problem*) $\mathbf{P}$:

$$\mathbf{P}: \quad \textbf{maximize} \quad \sum_{f \in F} U_f(x_f) \tag{3.7}$$

$$\textbf{subject to} \quad \boldsymbol{Rx} \leq \boldsymbol{C} \tag{3.8}$$

$$\textbf{over} \quad x_f \in I_f \tag{3.9}$$

Now we proceed to study how the solution to the problem $\mathbf{P}$ may be derived. Recall that by the assumption **A1**, the objective function of $\mathbf{P}$ in Eq. (3.7) is differentiable and strictly concave. In addition, the feasible region of the optimization problem in Inequality (3.8) and (3.9) is convex and compact. By non-linear optimization theory, there exists a maximizing value of argument $\boldsymbol{x}$ for the above optimization problem. Let us consider the Lagrangian form of the optimization problem $\mathbf{P}$:

$$\begin{aligned} L(\boldsymbol{x};\boldsymbol{\mu}) &= \sum_{f\in F} U_f(x_f) + \boldsymbol{\mu}^T(\boldsymbol{C}-\boldsymbol{R}\boldsymbol{x}) \\ &= \sum_{f\in F}(U_f(x_f) - x_f\sum_{q\in Q}\mu_q R_{qf}) + \sum_{q\in Q}\mu_q C_q \end{aligned} \tag{3.10}$$

where $\boldsymbol{\mu} = (\mu_q, q\in Q)$ is a vector of Lagrange multipliers.

Given the global knowledge of utility functions U_f of all flows, problem $\mathbf{P}$ is mathematically tractable using the Lagrangian method. However, in practice, such knowledge is unlikely to be available, while it may also not be feasible to compute and allocate resources in a centralized fashion. In this context, we prefer a decentralized solution where knowledge of utility functions of all flows is not needed. The key to decentralization is to investigate its dual problem, and to decompose the problem via pricing. Let us first consider the dual problem **D** of the primal problem $\mathbf{P}$ as follows.

$$\mathbf{D}: \min_{\boldsymbol{\mu}\geq 0} D(\boldsymbol{\mu}) \tag{3.11}$$

where

$$\begin{aligned} D(\boldsymbol{\mu}) &= \max_{x_f\in I_f} L(\boldsymbol{x};\boldsymbol{\mu}) \\ &= \max_{x_f\in I_f}\sum_{f\in F}(U_f(x_f) - x_f\sum_{q\in Q}\mu_q R_{qf}) + \sum_{q\in Q}\mu_q C_q \\ &= \sum_{f\in F}\max_{x_f\in I_f}(U_f(x_f) - x_f\sum_{q:E(f)\cap V(q)\neq\emptyset}\mu_q R_{qf}) + \sum_{q\in Q}\mu_q C_q \end{aligned} \tag{3.12}$$

Let us also define

$$\lambda_f = \sum_{q:E(f)\cap V(q)\neq\emptyset} \mu_q R_{qf} \tag{3.13}$$

The objective function $D(\boldsymbol{\mu})$ then becomes

$$D(\boldsymbol{\mu}) = \sum_{f\in F} \max_{x_f\in I_f} (U_f(x_f) - \lambda_f x_f) + \sum_{q\in Q} \mu_q C_q \tag{3.14}$$

From the price-based resource allocation framework, the Lagrange multipliers μ_q may be interpreted as the implied cost of a unit flow accessing using the maximal clique q. More straightforwardly, μ_q is the *shadow price of the clique* q. λ_f, on the other hand, may be interpreted as the *shadow price of the flow* f. From Eq. (3.13), we may observe that flow f needs to pay for *all the maximal cliques* that it traverses. For each clique, the price to pay is the product of the number of wireless links that f traverses in this clique and the shadow price of the clique. Alternatively, since

$$\lambda_f = \sum_{q:E(f)\cap V(q)\neq\emptyset} \mu_q R_{qf} = \sum_{s:s\in E(f)} \sum_{q:s\in V(q)} \mu_q \tag{3.15}$$

the shadow price of a flow is also the aggregated price of all its subflows. For each subflow, its price is the aggregated price of all the maximal cliques that it belongs to.

These observations identify a novel pricing model for multihop wireless networks. Here we illustrate this pricing model and compare it with the model for wireline networks with an example. In the example, the wireline network shown in Fig. 3.4(a) has a chain topology consisting of four links, associated with prices μ_1, μ_2, μ_3, μ_4. In this case, the price of the flow f is $\lambda_f = \sum_{l=1}^{4} \mu_l$. In comparison, though the multihop wireless network in Fig. 3.4(b) has the same topology, its maximal cliques $q_1 = \{\{1,2\},\{2,3\},\{3,4\}\}$ and $q_2 = \{\{2,3\},\{3,4\},\{4,5\}\}$ are, in effect, its resource elements. Let the shadow prices of these two cliques be μ_1 and μ_2. The price of flow f that traverses these two cliques is given by $\lambda_f = 3\mu_1 + 3\mu_2$, which is the sum of the product of the number of subflows of f in each clique and the shadow price of this clique. Alternatively, the price can also be written as $\lambda_f = \mu_1 + (\mu_1 + \mu_2) + (\mu_1 + \mu_2) + \mu_2$, which is the sum of the prices of its subflows. The price of each subflow is the aggregated price of all the maximal cliques that it

belongs to.

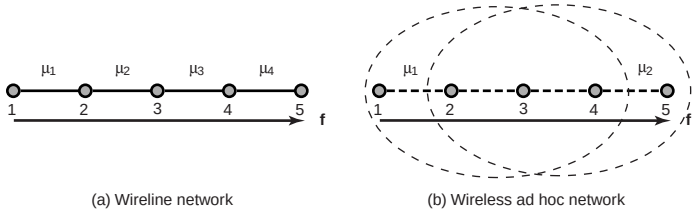

Figure 3.4: Price-based framework: a comparison.

3.3.2 First tier algorithm: per-clique price calculation

Now we proceed to present the distributed two-tier resource allocation algorithm. In the first tier, we design an iterative algorithm that determines per-clique prices and flow rate allocations. In the second tier, we present a decentralized algorithm to construct maximal cliques. Finally, we discuss the implementation choices to integrate these two tiers.

Treating maximal cliques as units of resource allocation, we first present an iterative algorithm that solves the problem **P**. The iterative algorithm we propose applies the gradient projection method to the dual problem **D**. Recall that the objective function $D(\boldsymbol{\mu})$ of the dual problem **D** is

$$D(\boldsymbol{\mu}) = \sum_{f \in F} \max_{x_f \in I_f} (U_f(x_f) - \lambda_f x_f) + \sum_{q \in Q} \mu_q C_q \tag{3.16}$$

Let

$$\phi_f(x_f) = U_f(x_f) - \lambda_f x_f \tag{3.17}$$

As λ_f is the shadow price of the flow f, $\phi_f(x_f)$ may be considered as the *net benefit* of the flow f, which is the difference between its utility and its cost. By assumption A1 and A3, $\phi_f(x_f)$ is strictly concave and twice continuously differentiable. Therefore, a unique maximizer of $\phi_f(x_f)$ exists when

$$\frac{d\phi_f(x_f)}{dx_f} = U_f'(x_f) - \lambda_f = 0 \tag{3.18}$$

We define such a maximizer as follows:

$$x_f(\lambda_f) = \arg\max_{x_f \in I_f} \{\phi_f(x_f)\} \tag{3.19}$$

Obviously:

$$x_f(\lambda_f) = [U_f'^{-1}(\lambda_f)]_{m_f}^{M_f} \tag{3.20}$$

$x_f(\lambda_f)$ is generally referred to as the *demand function*, which reflects the optimal rate for flow f, where its net benefit is maximized with a flow price of λ_f.

We solve the dual problem **D** using the gradient projection method [2]. In this method, $\boldsymbol{\mu}$ is adjusted in the opposite direction to the gradient $\nabla D(\boldsymbol{\mu})$:

$$\mu_q(t+1) = [\mu_q(t) - \gamma \frac{\partial D(\boldsymbol{\mu}(t))}{\partial \mu_q}]^+ \tag{3.21}$$

where γ is the step size. $D(\boldsymbol{\mu})$ is continuously differentiable since U_f is strictly concave [2]. Thus, based on Eq. (3.16), the q-dimension of the gradient is given as follows.

$$\frac{\partial D(\boldsymbol{\mu})}{\partial \mu_q} = C_q - \sum_{f:L(f)\cap N(q)\neq\emptyset} x_f(\lambda_f) R_{qf} \tag{3.22}$$

Eq. (3.22) gives the difference between the resource capacity C_q and its load demand $\sum_{f:L(f)\cap N(q)\neq\emptyset} x_f(\lambda_f) R_{qf}$, which are the rates of all flows that pass this clique multiplied by the number of subflows they have in this clique. Substituting Eq. (3.22) into (3.21), we have

$$\mu_q(t+1) = [\mu_q(t) - \gamma(C_q - \sum_{f:L(f)\cap N(q)\neq\emptyset} x_f(\lambda_f(t)) R_{qf})]^+ \tag{3.23}$$

Eq. (3.23) reflects the law of supply and demand. If the demand for bandwidth at clique q exceeds its supply C_q, the resource constraint is violated. Thus, the clique price μ_q is increased. Otherwise, μ_q is reduced.

We summarize the first-tier iterative algorithm in Table 3.1, where clique q and flow f are considered as abstract entities capable of computing and communicating. In the second tier of the algorithm, details of such entities will be presented.

Clique Price Update (by clique q): At times $t = 1, 2, \ldots$

1 Receive rates $x_f(t)$ from all flows f where $L(f) \cap N(q) \neq \emptyset$

2 Update price

$\mu_q(t+1) = [\mu_q(t) - \gamma(C_q - \sum_{f:L(f)\cap N(q)\neq\emptyset} x_f(t)R_{qf})]^+$

3 Send $\mu_q(t+1)$ to all flows f where $L(f) \cap N(q) \neq \emptyset$

Rate Update (by flow f): At times $t = 1, 2, \ldots$

4 Receive channel prices $\mu_q(t)$ from all cliques q where $L(f) \cap N(q) \neq \emptyset$

5 Calculate

$\lambda_f(t) = \sum_{q:L(f)\cap N(q)\neq\emptyset} \mu_q(t)R_{qf}$

6 Adjust rate

$x_f(t+1) = x_f(\lambda_f(t))$

7 Send $x_f(t+1)$ to all cliques q where $L(f) \cap N(q) \neq \emptyset$.

Table 3.1: First tier: per-clique resource allocation algorithm

We are now in a position to show the properties of this iterative algorithm. Let us define $Y(f) = \sum_{q\in Q} R_{qf}$, which leads to the definition of $\bar{Y} = \max_{f\in F} Y(f)$ as, intuitively speaking, the "length" of the "longest" path. We further define $Z(q) = \sum_{f\in F} R_{qf}$, leading to the definition of $\bar{Z} = \max_{q\in Q} Z(q)$ as the number of subflows at the most "congested" clique. Let $\bar{\kappa} = \max_{f\in F} \kappa_f$, where κ_f is the bound on the curvature of $U_f(\cdot)$ (see assumption **A4**).

Theorem 3.3.1. *Assume that $0 < \gamma < 2/\bar{\kappa}\bar{Y}\bar{Z}$, starting from any initial rates $\boldsymbol{x}(0)(x_f \in I_f)$ and prices $\boldsymbol{\mu}(0) \geq 0$, every limit point $(\boldsymbol{x}^*, \boldsymbol{\mu}^*)$ of the sequence $(\boldsymbol{x}(t), \boldsymbol{\mu}(t))$ generated by the algorithm in Table 3.1 is primal-dual optimal.*

Proof. First, under assumption A1 the dual objective function $D(\boldsymbol{\mu})$ is convex, lower bounded, and continuously differentiable. For any price vector $\boldsymbol{\mu}$ define $\psi_f(\boldsymbol{\mu})$ as

$$\psi_f(\boldsymbol{\mu}) = \begin{cases} \frac{1}{-U_f''((x_f(\boldsymbol{\mu})))} & \text{if } U_f'(M_f) \leq \lambda_f \leq U_f'(m_f) \\ 0 & \text{otherwise} \end{cases} \tag{3.24}$$

where λ_f is defined as in Eq. (3.13), and $x_f(\boldsymbol{\mu}) = x_f(\lambda_f) = x_f(\sum_{q:E(f)\cap V(q)\neq\emptyset} \mu_q R_{qf})$ is defined as in Eq. (3.19). By assumption A4, we have $0 \leq \psi_f(\boldsymbol{\mu}) \leq \kappa_f$. Now we define $\boldsymbol{H}(\boldsymbol{\mu}) = diag(\psi_f(\boldsymbol{\mu}), f \in F)$ be a $|F|\times|F|$ diagonal matrix with diagonal elements $\psi_f(\boldsymbol{\mu})$. From Eq. (3.18) and Eq. (3.22) we further have that the Hessian of D exists and is given by

$$\nabla^2 D(\boldsymbol{\mu}) = \boldsymbol{R}\boldsymbol{H}(\boldsymbol{\mu})\boldsymbol{R}^T \tag{3.25}$$

Now we show that ∇D is Lipschitz with

$$||\nabla D(\boldsymbol{\nu}) - \nabla D(\boldsymbol{\mu})||_2 \leq \bar{\kappa}\bar{Y}\bar{Z}||\boldsymbol{\nu} - \boldsymbol{\mu}||_2 \tag{3.26}$$

for all $\boldsymbol{\nu}, \boldsymbol{\mu} \geq 0$. Given any $\boldsymbol{\nu}, \boldsymbol{\mu} \geq 0$, we have for some $\boldsymbol{\omega}$

$$\nabla D(\boldsymbol{\nu}) - \nabla D(\boldsymbol{\mu}) \leq \nabla^2 D(\boldsymbol{\omega})(\boldsymbol{\nu} - \boldsymbol{\mu}) = \boldsymbol{R}\boldsymbol{H}(\boldsymbol{\omega})\boldsymbol{R}^T(\boldsymbol{\nu} - \boldsymbol{\mu}) \tag{3.27}$$

Hence,

$$||\nabla D(\boldsymbol{\nu}) - \nabla D(\boldsymbol{\mu})||_2 \leq ||\boldsymbol{R}\boldsymbol{H}(\boldsymbol{\omega})\boldsymbol{R}^T||_2 \cdot ||\boldsymbol{\nu} - \boldsymbol{\mu}||_2 \tag{3.28}$$

As $\boldsymbol{R}\boldsymbol{H}(\boldsymbol{\omega})\boldsymbol{R}^T$ is symmetric, $\bar{Y} = \max_{f \in F} \sum_{q \in Q} R_{qf}$, and $\bar{Z} = \max_{q \in Q} \sum_{f \in F} R_{qf}$, we have that

$$\begin{aligned} ||\boldsymbol{R}\boldsymbol{H}(\boldsymbol{\omega})\boldsymbol{R}^T||_2 &\leq ||\boldsymbol{R}\boldsymbol{H}(\boldsymbol{\omega})\boldsymbol{R}^T||_\infty \\ &= \max_q \sum_{q'} [\boldsymbol{R}\boldsymbol{H}(\boldsymbol{\omega})\boldsymbol{R}^T]_{qq'} \\ &= \max_q \sum_{q'} \sum_f \psi_f(\boldsymbol{\omega}) R_{qf} R_{q'f} \\ &\leq \bar{\kappa}\bar{Y}\bar{Z} \end{aligned} \tag{3.29}$$

Thus, the dual objective function D is lower bounded and ∇D is Lipschitz. Then, limit point $\boldsymbol{\mu}^*$ of the sequence $\{\boldsymbol{\mu}(t)\}$ generated by the gradient projection algorithm for the dual problem is dual optimal.

Provided $0 < \gamma < 2/\bar{\kappa}\bar{Y}\bar{Z}$, let $\{\boldsymbol{\mu}(t)\}$ be a subsequence converging to $\boldsymbol{\mu}^*$. Note that $U_f'(x_f)$ is defined on a compact set $[m_f, M_f]$, it is continuous and one-to-one. Thus, its inverse is continuous and $x_f(\boldsymbol{\mu})$ is continuous. Therefore, the subsequence $\{\boldsymbol{x}(t) = \boldsymbol{x}(\boldsymbol{\mu}(t))\}$ converges to the primal optimal rate $\boldsymbol{x}^* = \boldsymbol{x}(\boldsymbol{\mu}^*)$. This establishes the result of Theorem 3.3.1. □

Though there exists a unique maximizer $\boldsymbol{x}^*$ to the problem **P**, there may be multiple dual optimal prices, since only the flow price is constrained at optimum according to $U_f'(x_f^*) = \lambda_f^*$. Theorem 3.3.1 does not guarantee convergence to a unique pair $(\boldsymbol{x}^*, \boldsymbol{\mu}^*)$, though any convergent subsequence leads to the optimal rate allocation $\boldsymbol{x}^*$.

3.3.3 Second tier algorithm: decentralized clique construction

The first tier of the algorithm treats maximal cliques as entities that are able to perform the communication and computation tasks. Obviously, these tasks need to be performed by the network nodes that constitute the maximal clique. As a starting point, a decentralized algorithm to construct maximal cliques is required. Since the existing maximal clique construction algorithms are centralized in nature [1], they can not be directly applied here. Nevertheless, the unique graphical properties of the contention graph may have the potential to facilitate efficient clique construction. Hereafter, we present a decentralized maximal clique construction algorithm that explores the characteristics of contention graphs. In this algorithm, the network topology is decomposed into overlapping subgraphs, and maximal cliques are constructed based only on local topological information within each of the subgraphs. Since only wireless links that are geographically close to each other will form an edge in the contention graph, the communication and computational overhead is significantly reduced.

We first show the implication of topological characteristics of contention graphs when it comes to constructing maximal cliques. Let us denote the maximal clique that contains wireless link $s \in S$ as $q(s)$ (*i.e.*, $s \in N(q)$), and the set of all maximal cliques that contain the wireless link s as $Q(s) = \{q(s)\}$. We now give the subgraph of G on which $Q(s)$ can be constructed. To facilitate discussions, we introduce the following terms.

Definition 3.3.1. (neighbor sets). *The* **wireless link neighbor set** $\mathbb{LN}(l)$ *of a wireless link* $l \in L$ *is defined as* $\mathbb{LN}(l) = \{l' | l \cap l' \neq \emptyset, l' \in L\}$. *Similarly, the* **wireless link** k**-neighbor set** $\mathbb{LN}^k(l)$ *of* l *is defined by induction: (1)* $\mathbb{LN}^1(l) = \mathbb{LN}(l)$*; and (2)* $\mathbb{LN}^k(l) = \mathbb{LN}(\mathbb{LN}^{k-1}(l))$ *for* $k > 1$. *For*

$s \in S \subseteq L$, *we further define* $\mathbb{SN}^k(s) = \mathbb{LN}^k(s) \cap S$.

Theorem 3.3.2. *Let graph* $G_c[N_c(s)]$ *be an induced subgraph of* G_c *with* $N_c(s) = \mathbb{SN}^2(s) \subseteq N_c$. *Then* $G_c[N_c(s)]$ *contains sufficient and necessary topological information to construct* $Q(s)$. *Let graph* $G(s)$ *be* $G(s) = (N(s), L(s))$ *with* $L(s) = \mathbb{SN}^3(s)$ *and* $N(s) = \{i | \exists s$ *such that* $i \in s$ *and* $s \in \mathbb{SN}^2(s)\}$. $G(s)$ *is a subgraph* G, *and* $G(s)$ *contains sufficient and necessary topological information to construct* $G_c[N_c(s)]$.

Proof. By the definitions of the wireless link contention graph and clique, it is obvious that $\cup_{q \in Q(s)} N(q) = \mathbb{SN}^2(s)$. This shows that $G_c[N_c(s)]$ contains sufficient and necessary topological information to construct $Q(s)$. Also, for any pair of $s'', s' \in \mathbb{SN}^2(s)$, we need to know whether they contend with each other to determine whether they are connected in $G_c[N_c(s)]$. Apparently, $\mathbb{LN}^3(s)$ contains all the topological information to construct $G_c[N_c(s)]$. □

For wireless link $s \in S$, one of its vertices will be selected as its *delegation node*, denoted as $n(s)$. The delegation node $n(s)$ constructs all maximal cliques $q \in Q(s)$ by applying the Bierstone algorithm [1] on graph $G_c[N_c(s)]$.

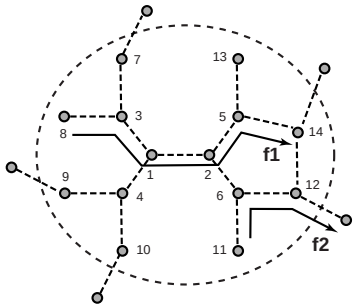

Figure 3.5: Example of decentralized clique construction

We consider an example shown in Fig. 3.5. The set of wireless links $\mathbb{SN}^2(\{1,2\})$ $=\{\{8,3\}, \{3,1\}, \{1,2\}, \{2,5\}, \{5,14\}, \{6,11\}, \{6,12\}\}$ represents all the vertices that appear in $G_c[N_c(\{1,2\})]$. To construct all the maximal cliques $Q(\{1,2\})$, the algorithm also needs to determine which wireless links in $\mathbb{SN}^2(\{1,2\})$ contend with each other. For example, in Fig. 3.5, whether subflow $\{5,14\}$ contends with $\{6,12\}$ needs to be known to determine whether they are within the same

clique. This implies that the knowledge of the wireless link $\{12, 14\}$ needs to be known by the algorithm for correct clique construction. Thus $\mathbb{LN}^3(\{1, 2\}) = \mathbb{SN}^2(\{1, 2\}) \cup \{12, 14\}$ needs to be known. When $d_{int} > d_{tx}$, the network topology graph does not have sufficient information to infer all the interference among wireless links. In this case, the clique construction algorithm only provides an approximation solution. For practical deployment, it will work with the measurement-based bandwidth estimation technique presented in Sec. 3.4, which takes into account the interference among wireless communications.

3.3.4 Two-tier algorithm: integration choices

In the first tier of the algorithm, maximal clique q is considered as an entity that is able to perform the following tasks:

1. obtain the aggregated rate $\sum_{f:L(f)\cap N(q)\neq\emptyset} x_f R_{qf}$ within it;
2. compute the clique-based shadow price μ_q;
3. communicate the price μ_q to the flows that traverse through.

After presenting the decentralized clique construction algorithm, we now proceed to discuss how these tasks are distributed to the network nodes that constitute the maximal clique. There are two implementation choices.

In implementation I, one delegation node in clique q serves as a master that performs the task of price calculation, denoted as $n(q)$. At time t, each delegation node $n(s)$ collects the rate of flow f which passes it (*i.e.*, $s \in L(f)$), computes rate y_s at wireless link s according to $y_s(t) = \sum_{f:s\in L(f)} x_f(t)$ and sends it to the master nodes $n(q)$ of all cliques q which s belongs to (*i.e.*, $s \in V(q)$). The master node $n(q)$ then computes the new price $\mu_q(t + 1)$ of clique q according to

$$\mu_q(t + 1) = [\mu_q(t) - \gamma(C_q - \sum_{s:s\in N(q)} y_s(t))]^+ \tag{3.30}$$

and distributes it to the other delegation nodes $n(s)$ within clique q (*i.e.*, $s \in N(q)$). After obtaining the updated clique price $\mu_q(t+1)$, $n(s)$ computes a per hop price $\lambda_s(t+1)$ according to $\lambda_s(t+1) = \sum_{q:s\in N(q)} \mu_q(t+1)$ for each flow f that satisfies $s \in L(f)$, then sends $\lambda_s(t+1)$ to the source of f.

For flow f, its source node performs the task of rate update. When the source node receives the per hop prices $\lambda_s(t)$, it computes the flow price $\lambda_f(t)$ according to $\lambda_f(t) = \sum_{s:s\in L(f)} \lambda_s(t)$ and adjusts the rate x_f according to $x_f(t+1) = x_f(\lambda_f(t))$. It then notifies $n(s)$ ($s \in L(f)$) of $x_f(t+1)$.

In implementation II, every delegation node in a clique performs price calculation. In particular, it differs from implementation I in the following aspects. At time t each delegation node $n(s)$ broadcasts the rate information y_s to the other delegation nodes $n(s')$ that satisfy $s' \in \mathbb{SN}^2(s)$. As such, each delegation node $n(s)$ can compute the price of clique q ($s \in N(q)$) independently. Let us denote the price of clique q at node $n(s)$ as $\mu_{q(n(s))}$[3]. $\mu_{q(n(s))}$ is calculated as follows:

$$\mu_{q(n(s))}(t+1) = [\mu_{q(n(s))}(t) - \gamma(C_q - \sum_{s:s\in N(q)} y_s(t))]^+ \tag{3.31}$$

Node $n(s)$ then directly computes and communicates $\lambda_s(t+1)$ to the source of f which satisfies $s \in L(f)$.

3.3.5 Towards asynchrony

Our two-tier algorithm assumes that updates at the sources and the relaying nodes are synchronized to occur at times $t = 1, 2, \ldots$. In realistic wireless ad hoc network environments, however, such synchronization is difficult to achieve. In this section, we improve the algorithm to an asynchronous setting, where sending rates and clique prices are updated at different times at different nodes.

First, we briefly introduce the asynchronous model that will be used for our algorithm in the context of implementation I. Let $T = \{0, 1, 2, ...\}$ be the set of time instances at which either rates

[3]In this synchronous setting, given that the initial prices at different delegation nodes of a clique are the same, *i.e.*, $\mu_{q(n(s))}(0) = \mu_q(0)$, it is trivially true that $\mu_{q(n(s))}(t) = \mu_q(t)$. Yet in the asynchronous settings that will be discussed in Sec. 3.3.5, $\mu_{q(n(s))}(t)$ may be different for different nodes $n(s)$.

or prices are updated. In particular, we define

1. $T_q \subseteq T$ — the set of time instances at which master node $n(q)$ updates μ_q;
2. $T_s^\lambda \subseteq T$ — the set of time instances at which delegation node $n(s)$ updates λ_s;
3. $T_f \subseteq T$ — the set of time instances at which the source of flow f updates x_f;
4. $T_s^y \subseteq T$ — the set of time instances at which delegation node $n(s)$ updates y_s.

The asynchronous model further makes the following assumption.

– **A5**. (*Partial Asynchronism*) There exists a positive integer B such that:

1. For every flow f, clique q and wireless link s, the time between consecutive updates is bounded by B for both price and rate updates.
2. One-way communication delay between any two nodes is at most B time units.

This partial asynchronism model is first discussed in [3] and is then adopted by Low *et al.* in the context of wireline networks [26]. Now we improve our two-tier resource allocation algorithm and analyze its convergence under this asynchronous model.

In the asynchronous environment, node $n(q)$, which updates the price $\mu_q(t)$ at time $t \in T_q$, may not have the knowledge of rate information $y_s(t)$. Instead, it only knows a sequence of recent rate updates $y_s((\tau_s^q)^1)$, $y_s((\tau_s^q)^2), \ldots$, that satisfy[4]:

$$t - B \leq (\tau_s^q)^1 \leq (\tau_s^q)^2 \leq ... \leq t \tag{3.32}$$

Thus, node $n(q)$ estimates the rate $\hat{y}_s^q(t)$ by using a weighted average of recent values as follows:

$$\hat{y}_s^q(t) = \sum_{t'=t-B}^{t} \alpha_s^q(t', t) y_s(t') \text{ with } \sum_{t'=t-B}^{t} \alpha_s^q(t', t) = 1 \tag{3.33}$$

Further, node $n(q)$ computes the price of clique q according to the following, which is essentially Eq. (3.23) with the load $\sum_{f:L(f)\cap N(q)\neq\emptyset} x_f(\lambda_f(t))R_{qf}$ replaced by its estimation $\hat{y}_s^q(t)$.

[4]Note that such τ_s^q exists under assumption A5.

$$\mu_q(t+1) = [\mu_q(t) - \gamma(C_q - \sum_{s:s\in N(q)} \hat{y}_s^q(t))]^+ \text{ , } \forall t \in T_q \tag{3.34}$$

At all times $t \notin T_q$, μ_q is unchanged, *i.e.*, $\mu_q(t+1) = \mu_q(t)$.

Similarly, to compute the per hop price $\lambda_s(t)$ at time $t \in T_s^\lambda$, node $n(s)$ estimates the clique price $\hat{\mu}_q^s(t)$ according to

$$\hat{\mu}_q^s(t) = \sum_{t'=t-B}^{t} \alpha_q^s(t',t)\mu_q(t') \text{ with } \sum_{t'=t-B}^{t} \alpha_q^s(t',t) = 1 \tag{3.35}$$

and calculates per hop price according to

$$\lambda_s(t+1) = \sum_{q:s\in N(q)} \hat{\mu}_q^s(t) \text{ , } \forall t \in T_s^\lambda \tag{3.36}$$

At time $t \notin T_s^\lambda$, λ_s is unchanged, *i.e.*, $\lambda_s(t+1) = \lambda_s(t)$.

At time $t \in T_f$, the source of f estimates its flow price according to

$$\hat{\lambda}_f(t) = \sum_{s:s\in L(f)} \hat{\lambda}_s^f(t) \tag{3.37}$$

where

$$\hat{\lambda}_s^f(t) = \sum_{t'=t-B}^{t} \alpha_s^f(t',t)\lambda_s(t') \text{ with } \sum_{t'=t-B}^{t} \alpha_s^f(t',t) = 1 \tag{3.38}$$

and computes its rate according to

$$x_f(t+1) = x_f(\hat{\lambda}_f(t)) \text{ , } \forall t \in T_f \tag{3.39}$$

At time $t \notin T_f$, x_f is unchanged, *i.e.*, $x_f(t+1) = x_f(t)$.

At time $t \in T_s^y$, node $n(s)$ calculates y_s as follows.

$$y_s(t+1) = \sum_{f:s\in L(f)} \hat{x}_f^s(t) \tag{3.40}$$

where

$$\hat{x}_f^s(t) = \sum_{t'=t-B}^{t} \alpha_f^s(t',t) x_f(t') \text{ with } \sum_{t'=t-B}^{t} \alpha_f^s(t',t) = 1 \tag{3.41}$$

At time $t \notin T_s^y$, $y_s(t+1) = y_s(t)$.

In this algorithm, the elements of T can be viewed as the indices of the sequence of physical times at which updates to either prices or rates occur. The sets T_f, T_q, T_s^f, T_s^q as well as the physical times they represent need not be known to any other nodes, since their knowledge is not required in the price and rate computation. Thus, there is no requirement for synchronizing the local clocks at different nodes. We are able to show that, under assumption A5 our resource allocation algorithm converges to global optimality even in asynchronous environments. Our main result is formally presented in the following theorem.

Theorem 3.3.3. *Assume that the step size γ is sufficiently small, then starting from any initial rate $\boldsymbol{x}(0)(x_f \in I_f)$ and prices $\boldsymbol{\mu}(0) \geq 0$, every limit point $(\boldsymbol{x}^*, \boldsymbol{\mu}^*)$ of the sequence $(\boldsymbol{x}(t), \boldsymbol{\mu}(t))$ generated by the asynchronous price-based resource allocation algorithm is primal-dual optimal.*

The proof of of Theorem 3.3.3 follows similar approach as in [3] (Section 7.5) and [26]. The key to the proof is to show that the price adjustment remains in the descent direction. The proof of our case is more complicated, because our two-tier algorithm has two-tier asynchrony: inter-clique asynchrony, where clique price and flow rate updates are asynchronous, and intra-clique asynchrony, where different delegation nodes have different estimations of a clique price.

Define vector $\boldsymbol{\pi}(t)$ as $\boldsymbol{\pi}(t) = \boldsymbol{\mu}(t+1) - \boldsymbol{\mu}(t)$. We first show that the error in rate calculation of flow f is bounded by the successive price change $\boldsymbol{\pi}$.

Lemma 3.3.1. *1. For all t*

$$|U_f'^{-1}(\hat{\lambda}_f(t)) - U_f'^{-1}(\lambda_f(t))| \leq \kappa_f \sum_{t''=t-2B}^{t-1} \sum_{q \in Q} |\pi_q(t'')| R_{qf} \tag{3.42}$$

2. For all t

$$|U_f^{'-1}(\lambda_f(t)) - U_f^{'-1}(\lambda_f(\tau))| \leq \kappa_f \sum_{t'=\tau}^{t-1} \sum_{q \in Q} |\pi_q(t')| R_{qf} \tag{3.43}$$

Proof. First let us define $\overline{\mu}_q(t) = (\mu_q(t''), t'' \in [t-2B, t])$[5] as a sequence of clique q's price at time instances $t-2B, t-2B+1, ..., t$. Further we denote vector $\overline{\boldsymbol{\mu}}(t)$ as $\overline{\boldsymbol{\mu}}(t) = (\overline{\mu}_q(t), q \in Q)$. Now let us define $x_f(\boldsymbol{\epsilon}; \overline{\boldsymbol{\mu}}(t))$ as

$$x_f(\boldsymbol{\epsilon}; \overline{\boldsymbol{\mu}}(t)) = U_f^{'-1}(\sum_{s: s \in E(f)} \sum_{q: s \in V(q)} \sum_{t''=t-2B}^{t} \epsilon_{qt''} \mu_q(t'')) \tag{3.44}$$

By assumption A4, we have that

$$0 \leq |\frac{\partial x_f(\boldsymbol{\epsilon}; \overline{\boldsymbol{\mu}}(t))}{\partial \epsilon_{qt''}}| \leq \kappa_f \mu_q(t'') R_{qf} \tag{3.45}$$

where it exists.

Let us define $\mathbf{1}(t) = (1_{qt''}(t), q \in Q, t'' \in [t-2B, t])$ as

$$1_{qt''}(t) = \begin{cases} 1, & \text{if } V(q) \cap E(f) \neq \emptyset, t'' = t \\ 0, & \text{otherwise} \end{cases}$$

and $\boldsymbol{\epsilon}(t) = (\epsilon_{qt''}(t), q \in Q, t'' \in [t-2B, t])$ as

$$\epsilon_{qt''}(t) = \begin{cases} \alpha_q^s(t'', t) \cdot \sum_{t'=t''}^{min\{t''+B, t\}} \alpha_s^f(t', t) & \text{, if } s \in V(q) \text{ and } s \in E(f) \\ 0, & \text{otherwise} \end{cases}$$

Note that

$$\sum_{t'=t-B}^{t} \alpha_s^f(t') \cdot \sum_{t''=t'-B}^{t'} \alpha_q^s(t'') \mu_q(t'') = \sum_{t''=t-2B}^{} \alpha_q^s(t'') \cdot \mu_q(t'') \sum_{t'=t''}^{min\{t''+B, t\}} \alpha_s^f(t') \tag{3.46}$$

[5] As a convention, we use t' to represent the time instance between $[t-B, t]$; t'' to represent time instance between $[t-2B, t]$; and t''' to represent time instance between $[t-4B, t]$.

and

$$\sum_{t'=t-B}^{t} \alpha_s^f(t') \sum_{t''=t'-B}^{t'} \alpha_q^s(t'') = 1 \tag{3.47}$$

Thus $U_f^{'-1}(\hat{\lambda}_f(t)) = x_f(\epsilon(t); \overline{\boldsymbol{\mu}}(t))$ and $U_f^{'-1}(\lambda_f(t)) = x_f(1(t); \overline{\boldsymbol{\mu}}(t))$, where $x_f(\cdot, \overline{\boldsymbol{\mu}}(t))$ is defined in (3.44). By the mean value theorem, we have for some $\tilde{\epsilon}$,

$$\begin{aligned}
& |U_f^{'-1}(\hat{\lambda}^f(t)) - U_f^{'-1}(\lambda_f(t))| \\
= & \Big| \sum_{q\in Q, t''\in[t-2B,t])} \frac{\partial x_f(\tilde{\epsilon}; \overline{\boldsymbol{\mu}}(t))}{\partial \epsilon_{qt''}} (1_{qt''}(t) - \epsilon_{qt''}(t)) \Big| \\
\leq & \kappa_f \Big| \sum_{q\in Q, t''\in[t-2B,t])} R_{qf} \overline{\mu}_{qt''}(t) (1_{qt''}(t) - \epsilon_{qt''}(t)) \Big| \\
\leq & \kappa_f \sum_{q\in Q} R_{qf} \max_{t-2B\leq t''\leq t} |\mu_q(t) - \mu_q(t'')| \\
\leq & \kappa_f \sum_{t''=t-2B}^{t-1} \sum_{q\in Q} R_{qf} |\pi_q(t'')|
\end{aligned}$$

Further, by the mean value theorem we have that

$$\begin{aligned}
& |U_f^{'-1}(\lambda_f(t)) - U_f^{'-1}(\lambda_f(\tau))| \\
\leq & \kappa_f \sum_{q\in Q} R_{qf} |\mu_q(t) - \mu_q(\tau)| \\
\leq & \kappa_f \sum_{q\in Q} R_{qf} \sum_{t'=\tau}^{t-1} |\pi_q(t')|
\end{aligned}$$

which completes the proof of Lemma 3.3.1. □

The gradient estimation used in our asynchronous algorithm is calculated as

$$\xi_q(t) = C_q - \sum_{s:s\in V(q)} \hat{y}_s^q(t) \tag{3.48}$$

where $\hat{y}_s^q(t)$ is as in Eq. (3.33). We further denote vector $\boldsymbol{\xi}(t)$ as $\boldsymbol{\xi}(t) = (\xi_q(t), q \in Q)$. Next we give the bound of error in gradient estimation in terms of the successive price change $\boldsymbol{\pi}(t)$.

Lemma 3.3.2. *There exists a constant $K_1 > 0$ such that*

$$\|\nabla D(\boldsymbol{\mu}(t)) - \boldsymbol{\xi}(t)\| \le K_1 \sum_{t'''=t-4B}^{t-1} \|\boldsymbol{\pi}(t''')\| \tag{3.49}$$

Proof. First

$$\begin{aligned}
&[\nabla D(\boldsymbol{\mu}(t) - \boldsymbol{\xi}(t)]_q \\
= &\sum_{s:s\in V(q)} \Big(\sum_{t'=t-B}^{t} \alpha_s^q(t',t) \sum_{f:s\in E(f)} \sum_{t''=t'-B}^{t'} \alpha_f^s(t'',t') x_f(t'') - \sum_{f:s\in E(f)} \overline{x}_f(t) \Big)
\end{aligned}$$

where $\overline{x}_f(t)$ is the rate of flow f if its source knows the exact flow price $\lambda_f(t)$. Hence by [3] (Proposition A.2), for some constant $K_1' > 0$ we have

$$\begin{aligned}
&\|\nabla D(\boldsymbol{\mu}(t)) - \boldsymbol{\xi}(t)\| \\
\le\ & K_1' \max_{q\in Q} \sum_{s:s\in V(q)} \Big| \sum_{t'=t-B}^{t} \alpha_s^q(t',t) \sum_{f:s\in E(f)} \sum_{t''=t'-B}^{t'} \alpha_f^s(t'',t') x_f(t'') - \sum_{f:s\in E(f)} \overline{x}_f(t) \Big| \\
\le\ & K_1' \max_{q\in Q} \sum_{s:s\in V(q)} \sum_{f:s\in E(f)} \max_{t-2B\le t''\le t} \Big| x_f(t'') - \overline{x}_f(t) \Big| \\
\le\ & K_1' \max_{q\in Q} \sum_{f:E(f)\cap V(q)\neq\emptyset} R_{qf} \max_{t-2B\le t''\le t} \Big| U_f'^{-1}(\hat{\lambda}^f(t'')) - U_f'^{-1}(\lambda_f(t)) \Big|
\end{aligned}$$

Applying Lemma C.1, we have

$$\begin{aligned}
&\|\nabla D(p(t)) - \boldsymbol{\xi}(t)\| \\
\le\ & K_1' \max_{q\in Q} \sum_{f:E(f)\cap V(q)\neq\emptyset} R_{qf} \max_{t-2B\le t''\le t} |U_f'^{-1}(\lambda_f(t)) - U_f'^{-1}(\lambda_f(t''))| + |U_f'^{-1}(\lambda_f(t'')) - U_f'^{-1}(\hat{\lambda}_f(t''))| \\
\le\ & K_1' \max_{q\in Q} \sum_{f:E(f)\cap V(q)\neq\emptyset} R_{qf} \max_{t-2B\le t''\le t} \kappa_f \Big\{ \sum_{\tau=t''}^{t-1} \sum_{q'\in Q} |\pi_{q'}(\tau)| R_{q'f} + \sum_{\tau=t''-2B}^{t''-1} \sum_{q'\in Q} |\pi_{q'}(\tau)| R_{q'f} \Big\} \\
=\ & K_1' \max_{q\in Q} \sum_{f:E(f)\cap V(q)\neq\emptyset} R_{qf}\kappa_f \max_{t-2B\le t''\le t} \sum_{\tau=t''-2B}^{t-1} \sum_{q'\in Q} |\pi_{q'}(\tau)| R_{q'f} \\
\le\ & K_1' \bar{\kappa} \bar{Z} \bar{Y} \sum_{\tau=t-4B}^{t-1} \|\boldsymbol{\pi}(\tau)\|_1
\end{aligned}$$

Note that all norms are equivalent in finite dimensional vector space [3] (Proposition A.9). Let $K_1 = K_1' \bar{\kappa} \bar{Z} \bar{Y}$, then we complete the proof of Lemma 3.3.2. □

Now we show that $\|\boldsymbol{\pi}(t)\|$ converges to zero in the following lemma.

Lemma 3.3.3. *Provided γ is sufficiently small we have $\|\boldsymbol{\pi}(t)\| \to 0$ as $t \to \infty$.*

Proof. First, by Lemma 5.1 in [3] (Section 7.5), we have that for all t, $\boldsymbol{\xi}^T(t)\boldsymbol{\pi}(t) \leq -(1/\gamma)\|\boldsymbol{\pi}(t)\|^2$. By the descent lemma [3] (Proposition A.32) and Eq. (3.26), we have that there exists K_2 such that

$$\begin{aligned} & D(\boldsymbol{\mu}(t+1)) \\ \leq \; & D(\boldsymbol{\mu}(t)) + \|\nabla D(\boldsymbol{\mu}(t)) - \boldsymbol{\xi}\| \cdot \|\boldsymbol{\pi}(t)\| - \Big(\frac{1}{\gamma} - K_2\Big)\|\boldsymbol{\pi}(t)\|^2 \end{aligned}$$

Applying Lemma C.2, we have

$$\begin{aligned} & D(\boldsymbol{\mu}(t+1)) \\ \leq \; & D(\boldsymbol{\mu}(t)) - \Big(\frac{1}{\gamma} - K_2\Big)\|\boldsymbol{\pi}(t)\|^2 + K_1 \sum_{t'''=t-4B}^{t-1} \|\boldsymbol{\pi}(t)\|^2 \end{aligned} \tag{3.50}$$

Summing (3.50) over all t, we have

$$\begin{aligned} & D(\boldsymbol{\mu}(t+1)) \\ \leq \; & D(\boldsymbol{\mu}(0)) - \Big(\frac{1}{\gamma} - K_2 - (4B+1)K_1\Big) \cdot \sum_{\tau=0}^{t} \|\boldsymbol{\pi}(\tau)\|^2 \end{aligned} \tag{3.51}$$

Choose γ sufficiently small such that $\frac{1}{\gamma} - K_2 - (4B+1)K_1 > 0$. Since $D(\boldsymbol{\mu}(t))$ is lower bounded, letting $t \to \infty$, we must have $\sum_{t=0}^{\infty} \|\boldsymbol{\pi}(t)\|^2 < \infty$, and hence

$$\|\boldsymbol{\pi}(t)\| \to 0 \text{ as } t \to \infty \tag{3.52}$$

□

Summarizing above results, we establish Theorem 3.3.3.

Proof of Theorem 3.3.3

Proof. We first prove that the various errors due to asynchronism all converge to zero. First

$$\begin{aligned}
|\hat{\lambda}_f(t) - \lambda_f(t)| &= |\sum_{s:s\in E(f)} \sum_{t'=t-B}^{t} \alpha_s^f(t',t) \sum_{q:s\in V(q)} \sum_{t''=t'-B}^{t'} \mu_q(t'') - \sum_{s:s\in E(f)} \sum_{q:s\in V(q)} \mu_q(t)| \\
&\leq \max_{t''\in[t-2B,t]} \sum_{q:q\in Q} R_{qf}|\mu_q(t'') - \mu_q(t)| \\
&\leq Y(f) \sum_{t''=t-2B}^{t} \|\boldsymbol{\pi}(t'')\|_1
\end{aligned}$$

which by (3.52) converges to zero as $t \to \infty$. Because $x_f(t)$ and $\overline{x}_f(t)$ are projections of $U_f^{'-1}$ onto $[m_f, M_f]$ and projection is nonexpansive [2] (Proposition 2.1.3), we have

$$\begin{aligned}
|x_f(t) - \overline{x}_f(t)| &\leq |U_f^{'-1}(\hat{\lambda}_f(t)) - U_f^{'-1}(\lambda_f(t))| \\
&\leq Y(f)\kappa_f \sum_{t''=t-2B}^{t-1} \|\boldsymbol{\pi}(t'')\|_1
\end{aligned}$$

Hence, by Eq. (3.52), $|x_f(t) - \overline{x}_f(t)| \to 0$ for all f.

We now show that every limit point of the sequence $\{\boldsymbol{\mu}(t)\}$ generated by the asynchronous algorithm minimizes the dual problem. Let $\boldsymbol{\mu}^*$ be a limit point of $\{\boldsymbol{\mu}(t)\}$. At least one exists, as it is constrained to lie in a compact set, provided γ is sufficiently small. Moreover, since the interval between consecutive updates is bounded (assumption A5), it follows that there exists a sequence of elements of T along which $\boldsymbol{\mu}$ converges. Let $\{t_k\}$ be a subsequence such that $\{\boldsymbol{\mu}(t_k)\}$ converges to $\boldsymbol{\mu}^*$. By Lemma C.2, we have

$$\lim_k \boldsymbol{\xi}(t_k) = \lim_k \nabla D(\boldsymbol{\mu}(t_k)) = \nabla D(\boldsymbol{\mu}^*)$$

Hence

$$[\boldsymbol{\mu}^* - \gamma\nabla D(\boldsymbol{\mu}^*)]^+ - \boldsymbol{\mu}^* = \lim_k [\boldsymbol{\mu}(t_k) - \gamma\boldsymbol{\xi}(t_k)]^+ - \boldsymbol{\mu}(t_k) = \lim_k \boldsymbol{\pi}(t_k) = 0$$

Then by the projection theorem [2] (Proposition 2.1.3) and [3] (Proposition 3.3 in Section 3.3), we have that $\boldsymbol{\mu}^*$ minimizes D over $\boldsymbol{\mu} \geq 0$. By duality $\boldsymbol{x}^* = \boldsymbol{x}(\boldsymbol{\mu}^*)$ is the unique primal optimal

rate. We now show that it is a limit point of $\{\boldsymbol{x}(t)\}$ generated by asynchronous algorithm. Consider a subsequence $\{\boldsymbol{x}(t_m)\}$ of $\{\boldsymbol{x}(t_k)\}$ such that $\{\boldsymbol{x}(t_m)\}$ converges. Since $\|\boldsymbol{x}(t) - \overline{\boldsymbol{x}}(t)\| \to 0$, we have

$$\lim_m \boldsymbol{x}(t_m) = \lim_m \overline{\boldsymbol{x}}(t_m) = \lim_m \boldsymbol{x}(\boldsymbol{\mu}(t_m)) = \boldsymbol{x}(\boldsymbol{\mu}^*)$$

This completes the proof. □

The improvements on implementation II towards asynchrony are similar to implementation I. The only difference is that the communication between delegation nodes and master node of a clique is not required for its price update, as the clique prices are computed independently at delegation nodes. We show via simulation that the asynchronous algorithm under implementation II closely matches the global optimum at equilibrium, if the step size γ is sufficiently small, and the initial prices $\mu_{q(n(s))}(0)$ at different delegation nodes $n(s)$ are the same for a clique q.

To this end, we have presented the distributed algorithm for resource allocation based on the dual method. We first presented the per-clique resource allocation algorithm, then integrated it with the distributed clique construction algorithm. Finally, we improve it towards asynchronous communication.

3.3.6 Improvement for multi-rate wireless network

In wireless networks, the signal strength and noise level of wireless channels vary widely, especially in indoor environments, leading to diverse channel bit error rates (BER). In IEEE 802.11, to reduce the BER, the sender can transmit at a lower data rate by using a more resilient modulation scheme. Four different bit rate levels: 11, 5.5, 2 and 1Mbps, are defined in IEEE 802.11 standard. Many vendors of client adaptors and access points implement automatic bit rate control scheme in which the sender adaptively changes the bit rate based on perceived channel conditions. This leads to a wireless network with *rate diversity*, where competing flows within the interference range transmit at different rates.

This section presents the improvement of our price-based resource allocation algorithm for such multi-rate wireless networks.

Problem formulation

Consider the bit rate of sub-flow s be B_s. Then $\frac{y_s}{B_s}$ is the percentage of the channel time that sub-flow s uses. Let ρ_q be the maximum percentage of channel time used in data transmission (so called maximum channel utilization). Then for each clique q, the following condition needs to be satisfied.

$$\forall q; \sum_{s \in N(q)} \frac{y_s}{B_s} \leq \rho_q \tag{3.53}$$

Let $\boldsymbol{B} = (B_{qs})_{|Q| \times |S|}$ be the bit rate matrix defined as follows:

$$B_{qs} = \begin{cases} \frac{1}{B_s} & \text{if } s \in N(q) \\ 0 & \text{otherwise} \end{cases}$$

Further we define $\boldsymbol{\rho} = (\rho_q, q \in Q)$ as the maximum channel utilization vector. Then Eq. (3.53) can be written in the following form.

$$\boldsymbol{B} \cdot \boldsymbol{y} \leq \boldsymbol{\rho} \tag{3.54}$$

And the channel resource constraint in a multi-rate wireless network is given as follows.

$$\boldsymbol{B} \cdot \boldsymbol{A} \cdot \boldsymbol{x} \leq \boldsymbol{\rho} \tag{3.55}$$

To summarize, the problem of optimal resource allocation in a multi-rate wireless network can be formulated as the following non-linear optimization problem $\mathbf{M}$.

$$\mathbf{M}: \quad \textbf{maximize} \quad \sum_{f \in F} U_f(x_f) \tag{3.56}$$

$$\textbf{subject to} \quad \boldsymbol{BAx} \leq \boldsymbol{\rho} \tag{3.57}$$

$$\textbf{over} \qquad x_f \in I_f \tag{3.58}$$

Algorithm

We solve problem M using a price-based approach, and present the resource allocation algorithm in Table 3.2.

Clique Price Update (by clique q): At times $t = 1, 2, \ldots$
1 Receive rates $x_f(t)$ from all flows f where $L(f) \cap N(q) \neq \emptyset$
2 Update price
$\mu_q(t+1) = [\mu_q(t) - \gamma(\rho_q - \sum_{s:s\in N(q)} \frac{\sum_{f:s\in L(f)} x_f}{B_s})]^+$
3 Send $\mu_q(t+1)$ to all flows f where $L(f) \cap N(q) \neq \emptyset$
Rate Update (by flow f): At times $t = 1, 2, \ldots$
4 Receive channel prices $\mu_q(t)$ from all cliques q where $L(f) \cap N(q) \neq \emptyset$
5 Calculate
$\lambda_f(t) = \sum_{q:L(f)\cap N(q)\neq\emptyset} \sum_{s:s\in N(q)} \frac{\mu_q(t)}{B_s}$
6 Adjust rate
$x_f(t+1) = x_f(\lambda_f(t))$
7 Send $x_f(t+1)$ to all cliques q where $L(f) \cap N(q) \neq \emptyset$.

Table 3.2: Resource allocation algorithm in multi-rate wireless network.

As shown in the table, the improved algorithm considers the rate diversity problem in multi-rate wireless networks. In particular, the prices are adjusted based on the channel time usage, and its difference from maximum channel utilization. And the flow prices take into account the channel bit rate at each hop which the flow travels. And it is intuitive to show that the algorithm converges to the unique global optimal solution of problem M.

3.4 Performance Evaluation

In this section, we present the deployment issues of our price-based resource allocation algorithm over realistic wireless networking environments and evaluate the performance of our algorithm via analysis and under various simulation environments.

In particular, we study our algorithm under three environments. The first environment, referred to as *synsim* for convenience, assumes bounded communication delay and synchronized message updates. The second, referred to as *asynsim* for convenience, considers the asynchronous environments in wireless ad hoc networks. In both environments, we assume that the transmission range is the same as interference range, which are both 250m. We further assume that the MAC layer scheduling is *ideal* in a sense that it can achieve the wireless channel capacity 2Mbps, and the routing algorithm uses shortest path. The third, referred to as *realsim*, considers the realistic wireless environments. *Realsim* adopts two-ray ground reflection model as radio propagation model and uses IEEE 802.11DCF as the MAC protocol. The transmission range in *realsim* is smaller than the interference range, which are 250m and 550m, respectively. The data transmission rate in *realsim* is 1Mbps. To simulate our algorithm under *realsim*, we implement it based on the wireless extensions in the ns-2 simulator. With respect to routing, the ns-2 module of AODV [31] is used in *realsim*. In all simulation environments, utility function $U_f(x_f) = \ln(x_f)$ is used, which enforces proportional fairness.

3.4.1 Deployment issues

The physical and MAC layer reality of wireless ad hoc networks presents several challenges to deploy our price-based resource allocation algorithm. First, the achievable channel bandwidth varies at different contention regions (cliques) depending on the MAC protocol. And it is usually much smaller than the ideal channel capacity and can not be known a priori. Dynamically estimating the achievable channel bandwidth at different contention regions is a critical problem to deploy our algorithm in realistic wireless environments. Second, the two-tier decentralized clique construction and price calculation algorithm requires communication among nodes, which may introduce additional overhead to the network. Designing an efficient communication protocol that still ensures the proper algorithm convergence is also a challenging problem. This problem becomes even more challenging when node mobility is taken into consideration.

To address these challenges, we present two deployment techniques: measurement-based band-

width estimation and lightweight communication protocol. The extensive simulation study shows that with these techniques, our price-based resource allocation algorithm can be efficiently deployed on real wireless environments and provide an effective solution for resource allocation.

Measurement-based bandwidth estimation

The measurement-based bandwidth estimation is based on the approach presented in [38]. It measures the *achievable* bandwidth of each wireless link based on its historic data transmission results.

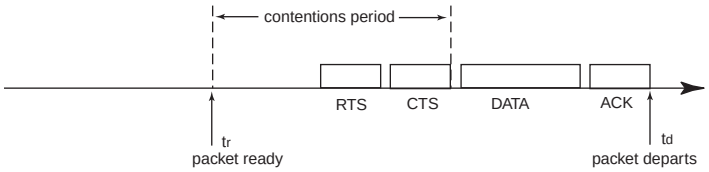

Figure 3.6: Measurement-based bandwidth estimation.

As shown in Fig. 3.6, under IEEE 802.11 MAC protocol, when a packet from a particular wireless link becomes the head-of-line packet (*i.e.,* the first packet waiting to be transmitted), then this packet is *ready*. And we denote this time instance as t_r. When the link layer acknowledgement is received, the packet *departs*. We denote this time instance as t_d. The transmission delay of this packet is then given as $t_d - t_r$, which includes a contention period. The contention period indicates the channel bandwidth used by packet transmissions of other wireless links within the contention region. The achievable bandwidth observed by this wireless link is then calculated as $\frac{z}{t_d - t_r}$, where z is the size of the packet. To achieve more accurate measurement result, we use a window with size w of packets to conduct the bandwidth estimation, *i.e.,* the bandwidth is estimated as $\frac{w \cdot z}{\sum_{i=1}^{w} t_d^i - t_r^i}$. Moreover, packets of different lengths z need to be normalized [38]. We choose not to discuss these details due to the space constraint. The measurement-based bandwidth estimation takes into account the effect of physical layer interference and the inefficiency of MAC protocols, as it is based on the *scheduling result* of packet transmissions. We will show the detailed simulation results on the convergence and evaluate the effect of measurement parameters in Sec. 3.4.2.

Lightweight communication protocol

To calculate the price of each clique, only its load gradient (difference between achievable bandwidth and load) needs to be known. Thus based on its achievable bandwidth and its load, each wireless link calculates its local gradient. Instead of communicating both rate and bandwidth information, only gradient information is sent along with connectivity information to construct cliques and compute their prices.

To achieve low overhead communication, the information is sent via piggybacking. First, the local gradient information of each wireless link is piggybacked onto the data packets of the flows passing by to notify the nodes at their downstreams instantaneously. Second, working with AODV routing protocol, connectivity and local gradient information is also piggybacked onto HELLO packets and are sent at a certain time interval. Based on Theorem 3.3.2, end nodes of subflow s cache the information within $\mathbb{LS}^3(s)$ and transmit information within $\mathbb{LS}^2(s)$ to their neighbor nodes. The prices are also piggybacked onto data packets so that the destination of a flow can notify its source via FEEDBACK packets.

Such protocol provides an asynchronous information update for price calculation and communication. As we have shown in Theorem 3.3.3, the price-based algorithm converges to global optimum in the asynchronous environments. Sec. 3.4.2 presents the simulation results on the convergence and show the impact of HELLO intervals on convergence.

3.4.2 Convergence

We first study the convergence behavior of our price-based resource allocation algorithm under different simulation environments and identify the factors that affect this procedure.

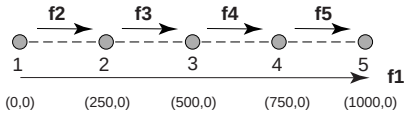

Figure 3.7: 4-hop chain topology

topology (hops)	4	5	6	7	8	9	10
step size (γ)	1	0.8	0.75	0.62	0.6	0.6	0.5
number of iterations to converge	18	23	42	46	55	96	102

Table 3.3: Number of iterations towards convergence

Convergence speed

With appropriately tuned step sizes, we first evaluate how rapidly our algorithm converges to the global optimum. We simulate the algorithm on chain topologies from 4 hops to 10 hops in *synsim*. As an example, the 4-hop chain topology and its traffic pattern is shown in Fig. 3.7. In all the experiments, the initial values of sending rates are 2 Mbps and the initial prices are 2. The results are shown in Table 3.3 along with their corresponding step sizes, which are tuned to ensure the most efficient convergence[6]. From these results, we observe that the best step sizes and the convergence time apparently correspond to the scale of the network. In particular, the larger number of cliques through which the longest flow passes (*i.e.*, $\bar{Y}$), the smaller step sizes and the more iterations are required for convergence.

We have also carried out this experiment with different initial settings of prices and rates. We observe that the algorithm always converges regardless of the initial settings. In particular, the sending rates always converge to a unique optimum regardless of the initial rates, and the prices may converge to different values — all of which are dual optimal — if different initial prices are used. This is because that, at equilibrium, only the flow price λ_f^* is constrained by $U_f'(x_f^*) = \lambda_f^*$, and different price vectors $\boldsymbol{\mu}^*$ may lead to the same value of λ_f^*.

Convergence in asynchronous environments

With *asynsim*, we evaluate the convergence behavior of our algorithm in asynchronous environments. We first show the convergence behavior of implementation I. Recall that in asynchronous models, recent updates are averaged to accommodate delayed and out-of-order messages. In the

[6]The termination criteria in *synsim* are $|x_f(t) - x_f^*| \leq \varepsilon$ for all $f \in F$ and $|\mu_q(t) - \mu_q^*| \leq \varepsilon$ for all $q \in Q$ with $\varepsilon = 10^{-4}$.

simulation, we adopt a moving average method to specify the weight parameters. In particular, let $0 \leq (\tau)^1 \leq (\tau)^2 \leq, ..., \leq (\tau)^m$ be the time instances of the received updates, then α_s^q is specified as

$$\alpha_s^q(t', t) = 1 \quad \text{if} \quad m = 1, t' = (\tau)^1 \tag{3.59}$$

$$\alpha_s^q(t', t) = (1 - \alpha)^{m-j} \cdot \alpha \quad \text{if} \quad m > 1, t' = (\tau)^j, j = 1, 2, ..., m \tag{3.60}$$

α_s^f, α_f^s, and α_q^s are defined in the same way. α is a unified parameter that represents the weight of the history in estimation. When $\alpha = 0$, only the most recently received update is used for estimation. We evaluate the impact of α and step size γ on the convergence. We conduct the experiments on a 4-hop chain topology (Fig. 3.7) using different values of γ and α. The experimental results are shown in Fig. 3.8 and Fig. 3.9, respectively. From the results, we have the following observations. First, at equilibrium, with sufficient small step size ($\gamma \leq 0.05$), independent of the choices of α, rate allocation in asynchronous environments achieves the global optimum as in synchronous settings. This validates the theoretical claim in Theorem 3. Second, the value of the step size that ensures the convergence and optimal rate allocation is much smaller than the synchronous case. For example, as shown in Fig. 3.8, the resource allocation does not converge to the optimum when the step size $\gamma = 0.5$, while in synchronous settings, the algorithm converges to optimum when $\gamma = 1$. Further, the value of α affects the convergence speed, with a larger α leading to a longer convergence time. This means that in implementation I, $\alpha = 0$ can ensure the fastest convergence to the global optimum.

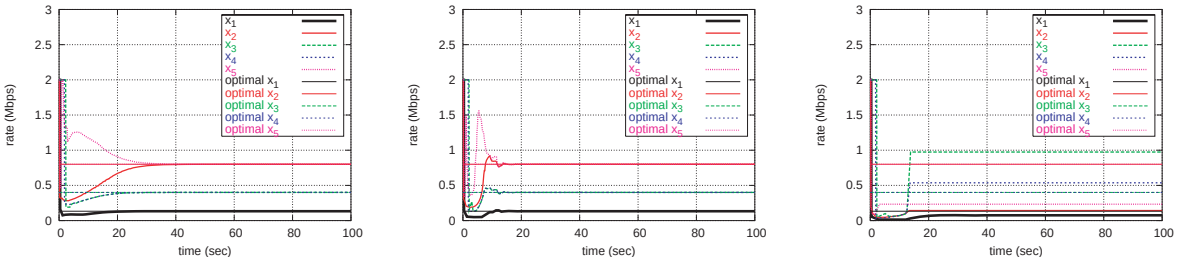

(a) $\gamma = 0.01$ (b) $\gamma = 0.05$ (c) $\gamma = 0.5$

Figure 3.8: Asynchronous experiments of implementation I with different step sizes γ ($\alpha = 0$).

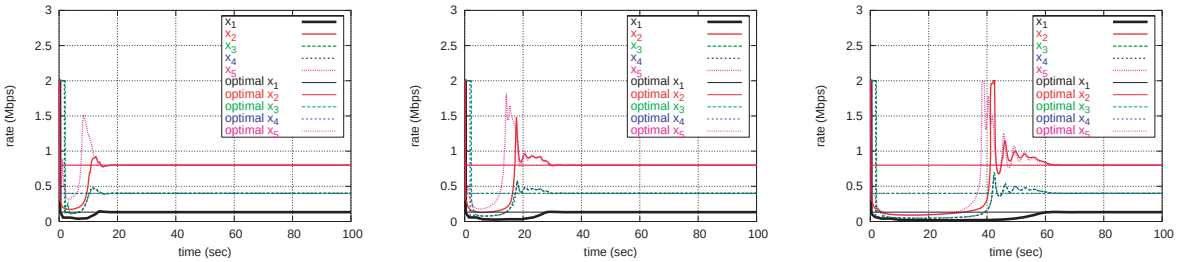

(a) $\alpha = 0.1$ (b) $\alpha = 0.4$ (c) $\alpha = 0.6$

Figure 3.9: Asynchronous experiments of implementation I with different weights α ($\gamma = 0.05$).

We now repeat these experiments using implementation II, with step size $\gamma = 0.05$. The results are shown in Fig. 3.10. From these results, we have the following observations. First, the equilibrium rate allocation closely matches the optimal values. Second, the value of α affects the convergence speed and how close the equilibrium rate allocation matches the optimum. The reason behind this observation can be intuitively explained as follows. In implementation II, different delegation nodes have different rate estimations for clique price calculation, depending on the value of α. Although the clique price changes will converge to zero at each individual node, the difference between clique prices at these nodes does not. Such difference may vary with the value of α. Yet, no matter what value α is set to, the equilibrium rate allocation always closely matches the optimum in the simulations. This is because nodes within a clique have relative small communication delays, hence small rate estimation differences.

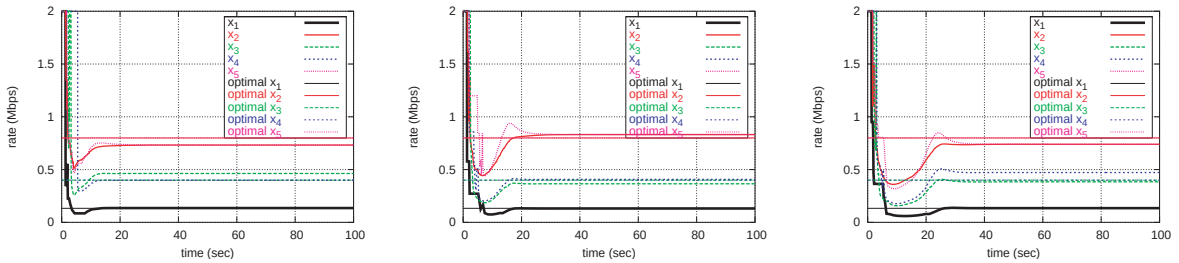

(a) $\alpha = 0.1$ (b) $\alpha = 0.4$ (c) $\alpha = 0.6$

Figure 3.10: Asynchronous experiments with implementation II.

Impact of measurement window size on convergence

Now we study the convergence behavior of our algorithm with bandwidth estimation and evaluate the impact of measurement parameters in *realsim*. We experiment with different measurement window sizes w on the 4-hop chain topology (Fig. 3.7). The results are shown in Fig. 3.11. From the results we have the following observation. The algorithm converges faster in the case of $w = 5$ than the case of $w = 20$, because a smaller measurement window gives faster feedback on the channel condition. On the other hand, too small w results in imprecise measurement. This leads to slight fluctuations at the equilibrium as shown in Fig. 3.11 in the case of $w = 5$. In what follows, we use $w = 20$ as the default measurement window size, because it gives stable and precise measurement results with acceptable convergence speed.

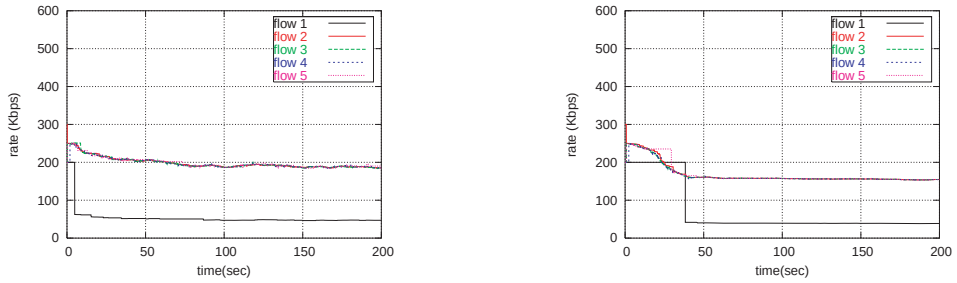

(a) w = 5 (b) w = 20

Figure 3.11: Convergence with bandwidth estimation.

Impact of HELLO interval on convergence

We experiment with different lengths of HELLO intervals and evaluate its impact on convergence. As shown in Fig. 3.12, large HELLO intervals (*e.g.* interval = 20 seconds) increase the convergence time and may cause small fluctuations. The results also show that in a static environment, a HELLO interval of less than 10 seconds can ensure convergence with satisfactory speed and can achieve stability at equilibrium. Obviously, different lengths of HELLO intervals also affect the overhead. Long HELLO intervals can significantly reduce the overhead. In the following simulations, we use 1 second as the default length of the HELLO interval.

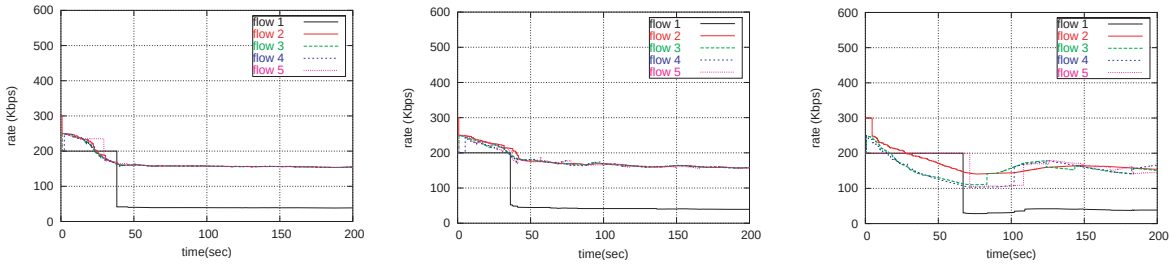

(a) hello interval = 1 second (b) hello interval = 10 seconds (c) hello interval = 20 seconds

Figure 3.12: Convergence under the piggyback-based lightweight communication protocol.

Convergence in random networks

Now we study the convergence behavior of our algorithm with respect to both transmission rate and throughput in a randomly generated wireless network as shown in Fig. 3.13(a). This network consists of 30 nodes deployed over a $600 \times 600\ m^2$ region. In the experiment, 5 flows are established between 5 different pairs of nodes to start at different time instants. Fig. 3.13(b) and (c) plot the instantaneous transmission rate and throughput of each flow respectively. From these results, we have the following observations: (1) our algorithm converges with satisfactory speed even in relatively large scale networks (*e.g.*, 30 node over 600×600 region); (2) our algorithm converges when traffic dynamically joins the network.

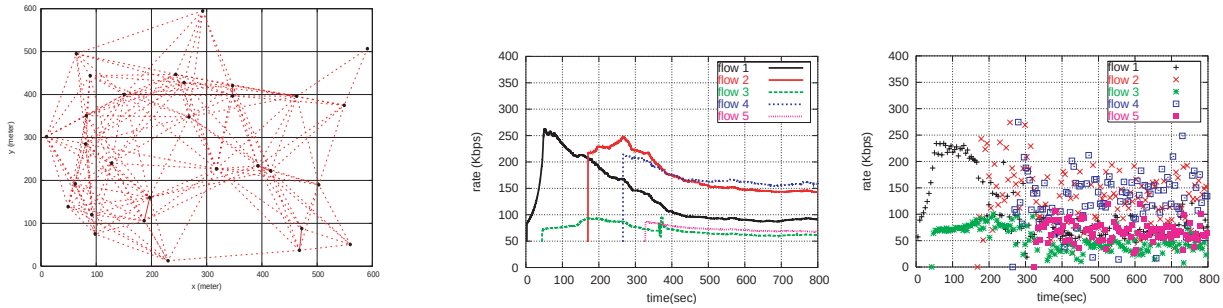

(a) random topology (b) transmission rate (c) throughput

Figure 3.13: Convergence in random networks.

3.4.3 Impact of realistic wireless interference

In the next set of experiments, we are interested in studying the impact of realistic wireless interference on our algorithm.

Special scenarios

First, using *realsim*, we perform our experiments in a set of special network topologies: the *hidden terminal* scenario, the *exposed terminal* scenario, and the *race condition* scenario.

- *Hidden terminal*. Fig. 3.14 shows one example of the hidden terminal scenario, as well as experimental results on the convergence of the transmission rate and the throughput of our algorithm. From the results, we observe that the algorithm performs as expected: at equilibrium, two flows share the resource fairly. The result is obvious because the sending nodes of both flows are able to obtain the information from each other, thus correctly constructing the clique and calculating its price. In contrast, we also show the performance of our algorithm over a different hidden terminal scenario as shown in Fig. 3.15. In this scenario, the sending nodes of the two flows are unable to communicate, though their transmissions still interfere with each other. Thus, each wireless link treats itself as the only link within the clique, though the correct clique construction should consist of both wireless links. In this case, the price of a clique relies on the gradient of one wireless link, which is in turn calculated based on the bandwidth estimation at either node 2 or node 3. Node 2 can sense the interference from node 3, when it sends FEEDBACK packets to node 1. Similarly, node 3 can sense the interference from node 2, when it sends the data packets. But due to their asymmetric traffic loads, their bandwidth estimation results are different. As a result, the rate allocation of these two flows is not fair at equilibrium.

- *Exposed terminal*. Due to the coordination of RTS/CTS at the MAC layer, the sending nodes are able to communicate with each other to exchange necessary load and topology

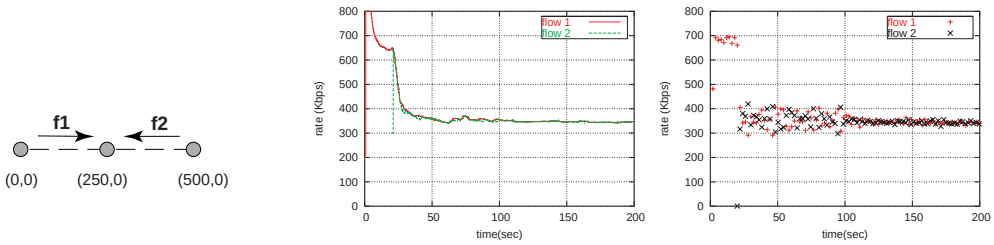

(a) hidden termial topology (b) transmission rate (c) throughput

Figure 3.14: Convergence in the hidden terminal scenario I.

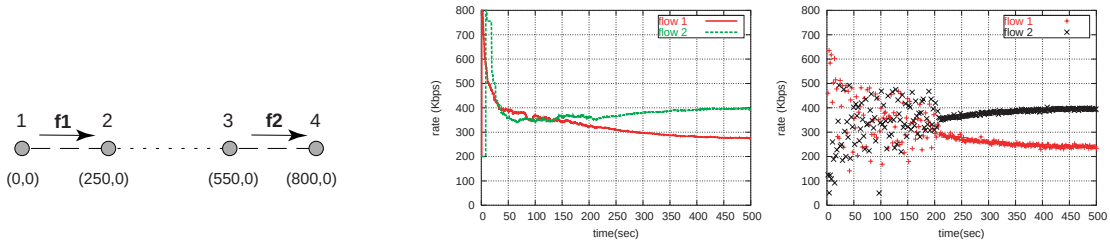

(a) hidden termial topology II (b) transmission rate (c) throughput

Figure 3.15: Convergence in the hidden terminal scenario II.

information. Fig. 3.16 shows that the algorithm performs correctly in the exposed terminal scenario.

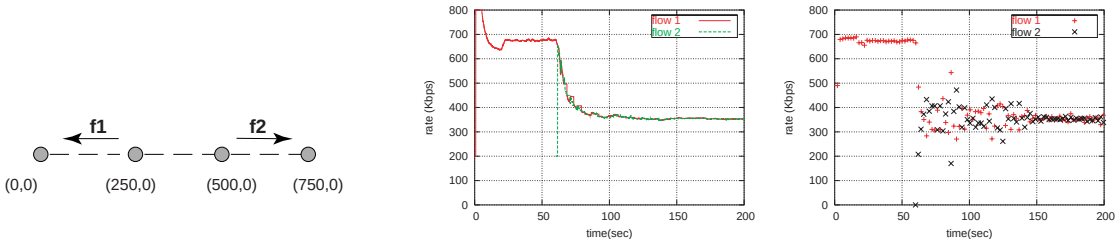

(a) exposed terminal topology (b) transmission rate (c) throughput

Figure 3.16: Convergence in the exposed terminal scenario.

- *Race condition*. The result under the race condition is shown in Fig. 3.17. We observe that the performance of our algorithm under the race condition is different from the hidden terminal scenario in its delayed convergence. This is because flow f_1 is unable to capture the wireless channel at the beginning due to the unawareness of the RTS/CTS signals from the transmission of the other flow and the unfair backoff of IEEE 802.11. Once it gets the chance to transmit, the load change will be detected by flow f_2 via bandwidth estimation, which in

turn leads to the price increase of this contention region and the rate decrease of flow f_2. Via the communication between their receiving nodes, these two flows share the same view of the network condition and the price, thus converge to an equilibrium, where their transmission rates are the same. Although they have approximately the same throughput at equilibrium, slight difference and fluctuation can still be observed on their instantaneous throughput, especially compared with the results in the hidden terminal scenario in Fig. 3.14. This is caused by the imprecise measurement under the race condition: IEEE 802.11 has short-term unfairness in its scheduling even when both flows send at the same rate, which is achievable. This problem is rooted at the MAC protocol, and can not be resolved by our algorithm. However, as we may observe from the results, the long term fairness can be guaranteed at the equilibrium via our price-based algorithm.

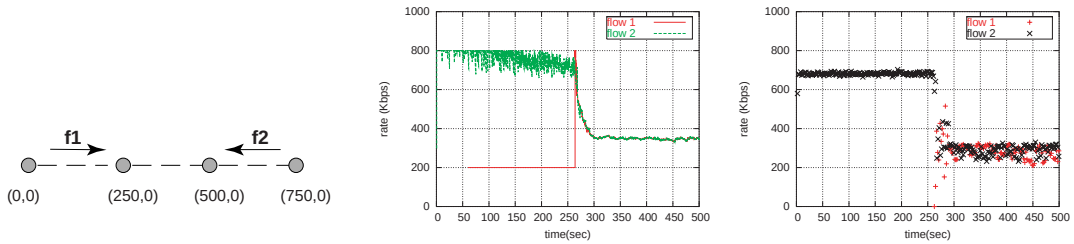

(a) race condition topology (b) transmission rate (c) throughput

Figure 3.17: Convergence in the race condition scenario.

Comparison studies

To further illustrate the meaning of contention region and the impact of interference, we compare the equilibrium resource allocations of an ad hoc network with a wireline network of the same topology and two ad hoc networks with different interference ranges.

First, the rate allocation and the equilibrium prices of the wireline network and the wireless ad hoc network with a 4-hop chain topology are compared under *synsim*. The cliques of the ad hoc network under *synsim* are the same as in Fig. 3.4. The results are listed in Table 3.4. From these results we have the following observations. First, the rate allocated to each flow in the ad hoc network is less than the rate allocated to the corresponding flow in wireline networks.

	x_1	x_2	x_3	x_4	x_5	μ_1	μ_2	μ_3	μ_4
wireline network	0.4	1.6	1.6	1.6	1.6	0.625	0.625	0.625	0.625
ad hoc network	0.133	0.8	0.4	0.4	0.8	1.25	1.25	N/A	N/A

Table 3.4: Rate allocations and equilibrium prices in different networks

The difference lies in their different definitions of contention regions. In the wireline network, a wireline link represents a contention region, whose capacity is the link bandwidth. In the ad hoc network, a wireless link is no longer a contention region. Instead, the set of wireless links, formally represented by a clique, constitutes the contention region, and shares the channel capacity. Thus, with the same capacity of the wireless channel and the wireline link, the throughput of the ad hoc network is lower than that of the wireline network. Second, in the wireline network, the rates of all single-hop flows are the same. In the ad hoc network, the rates of these flows are different. The reason is that, in the wireline network, flows f_2 through f_5 enjoy the same amount of resources; while in the ad hoc network, due to location-dependent contention, f_3 suffers higher contention than f_2. This is also reflected through the prices that f_2 and f_3 need to pay. For f_2, the price is $\lambda_2 = \mu_1$, which equals to 1.25 at equilibrium, while the price for f_3 is $\lambda_3 = \mu_1 + \mu_2$, which equals to 2.5. Third, in both networks, the equilibrium rate allocations for flows with different lengths are different. This is actually the result of proportional fairness. In particular, the longer the flow, the less the rate allocated. This observation is natural from the perspective of maximizing the aggregated utility. When the utility functions of all flows are the same, long flows consume more resources for an unit of utility increase. Hence, the short flows are favored.

To further illustrate the impact of interference, we compare the resource allocation on two ad hoc networks with different interference ranges. The results are shown in Fig. 3.18(b) and (c). We observe that the resource allocations are different for two networks. The reason behind this observation is that different interference ranges lead to different contention regions as shown in Fig. 3.18(a). When the interference range is 550m, the network only consists of one contention region. On the other hand, when interference range is 250m, there are two overlapping contention regions in the network.

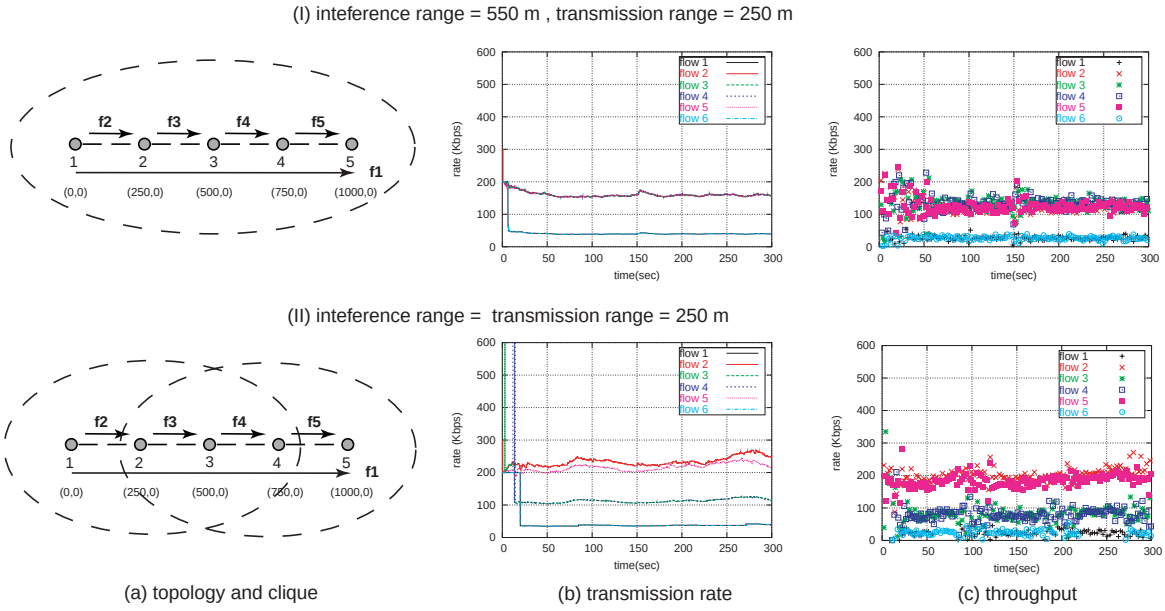

Figure 3.18: Comparison of different interference ranges.

3.4.4 Overhead

Now we proceed to evaluate the overhead of our algorithm via simulation under different mobility degrees. In the simulation, 30 mobile nodes are randomly deployed on a 600×600 m^2 network. They move according to the random waypoint mobility model with an average node speed of 20m/s. The pause time interval is varied in the experiment. For each simulation, the results are averaged over 10 randomly generated mobile scenarios with the same pause time interval.

Fig. 3.19(a) plots the normalized overall packet overhead, which is the ratio between the number of non-data packets and the data packets delivered at each hop. The overall overhead includes the FEEDBACK packets sent by the receiver of each flow, and the AODV routing packets, which include HELLO packets that carry the price calculation information. We compare the overhead of our algorithm with the overhead of the TCP protocol[7] running over AODV. From the results, we observe that our algorithm has lower packet overhead than TCP. This is mainly because our price-based resource allocation algorithm generates fewer FEEDBACK packets than the ACK packets of

[7]TCP is also considered as a form of resource allocation for end-to-end flows in existing literature [20].

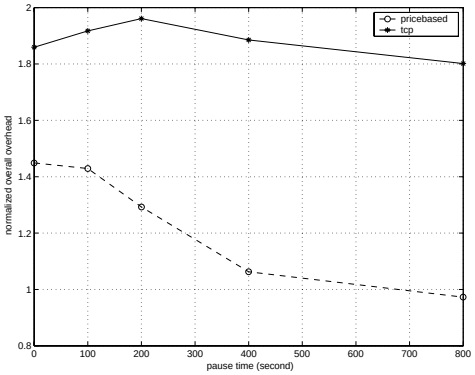

(a) normalized overall packet overhead

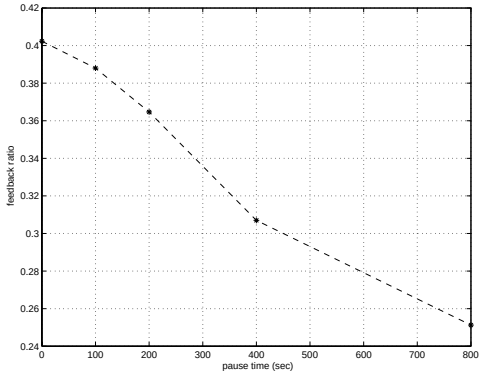

(b) normalized FEEDBACK packet overhead

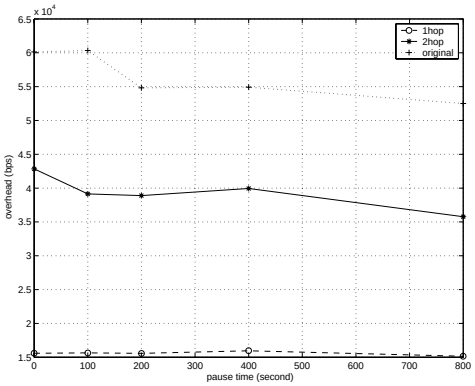

(c) HELLO packet overhead in bits per second

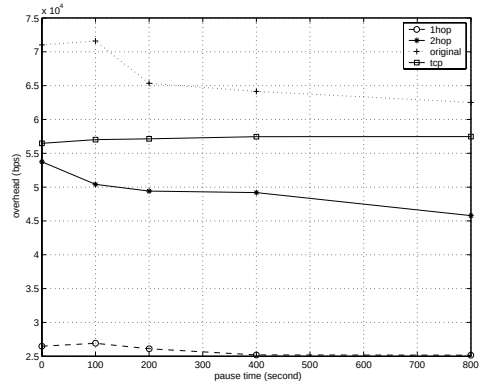

(d) overall overhead in bits per second

Figure 3.19: Overhead.

TCP. Fig. 3.19(b) plots the ratio between the number of FEEDBACK packets sent at the receivers of the flows and the data packets that they receive. We observe that fewer FEEDBACK packets are generated with lower mobility. This is because at the equilibrium where the price is unchanged, no FEEDBACK packet needs to be sent. Moreover, because the lightweight communication protocol uses packet piggybacking as its information delivery method, it does not introduce many additional control packets (AODV packets) at the routing layer into the network.

We proceed to study the overhead of our algorithm in bits per second. From Fig. 3.19(d), we observe that the overhead of our algorithm in bits per second is also comparable to TCP over AODV, although our algorithm uses larger AODV HELLO packets.

3.4.5 k-hop heuristic

To further reduce the overhead, we introduce a set of k-hop heuristic algorithms. In these heuristics, end nodes of subflow s cache the information within $\mathbb{LS}^k(s)$ ($k \leq 3$) and transmit information within $\mathbb{LS}^{k'}(s)$ ($k' = k - 1$) to their neighbor nodes. Based on such partial knowledge of the network topology and load, cliques are constructed, and their prices are computed approximately. We first provide an analytical study of the overhead in k-hop heuristic algorithms. Then we present their simulation results.

As the amount of information depends on the number of neighbors of wireless nodes, we first analyze the expected number of neighbors in a wireless ad hoc network. Let A be the size of the region which is covered by the network being studied. And we assume that the node is uniformly distributed over the region. Then the expected number of neighbors within k ($k < 3$) hops of a wireless node is analyzed as follows.

Consider a wireless node $i \in N$ with transmission range d_{tx}. The probability that it has m neighbors is given in the following probability density function[8]:

[8]Note that when the node is located at the border of the network, the number of its neighbors may be different. For simplicity, we ignore such cases in this analysis.

$$p_{1-hop}(m) = \left(\begin{array}{c} |N|-1 \\ m \end{array} \right) \cdot (\frac{\pi \cdot d_{tx}^2}{A})^m (1 - \frac{\pi \cdot d_{tx}^2}{A})^{|N|-1-m} \tag{3.61}$$

$$p_{2-hop}(m) = \left(\begin{array}{c} |N|-1 \\ m \end{array} \right) \cdot (\frac{\pi \cdot (2 \cdot d_{tx})^2}{A})^m (1 - \frac{\pi \cdot (2 \cdot d_{tx})^2}{A})^{|N|-1-m} \tag{3.62}$$

It is obvious that both satisfy binomial distribution. The expected number of 1-hop neighbors of i is

$$E[1-hop] = \sum_{m=1}^{|N|-1} m \cdot p_{1-hop}(m) = (|N|-1) \cdot \frac{\pi \cdot d_{tx}^2}{A} \tag{3.63}$$

and the expected number of 2-hop neighbors of i is

$$E[2-hop] = \sum_{m=1}^{|N|-1} m \cdot p_{2-hop}(m) = (|N|-1) \cdot \frac{\pi \cdot (2 \cdot d_{tx})^2}{A} \tag{3.64}$$

If the interval of HELLO messages is T_{hello}, and each entry of a wireless link uses b_{nb} bits, then the additional bit overhead of k-hop heuristic algorithms for clique construction and price computation are

- 1-hop heuristic algorithm: $b_{nb} \cdot T_{hello}$;
- 2-hop heuristic algorithm: $(b_{nb} \cdot T_{hello})(1 + E[1-hop])$;
- 3-hop heuristic algorithm (original algorithm): $(b_{nb} \cdot T_{hello})(1 + E[1-hop] + E[2-hop])$;

Now we proceed to study the k-hop heuristic algorithm via simulation. Fig. 3.19(c) shows the overhead in bits per second incurred by HELLO packets when heuristics with different information propagation ranges are used. Fig. 3.19(d) compares the overall overhead in bits per second of the original price-based resource allocation algorithm with its heuristics. From the results, we observe that the 2-hop heuristic has similar overhead as TCP over AODV, while 1-hop heuristic has even smaller overhead in bits per second than TCP.

We further study the performance of these heuristics in terms of rate allocation. First we study the aggregated utilities achieved by different heuristics and compare them with the original algorithm and TCP. In the experiment, we consider wireless ad hoc networks at two scales. At the smaller scale, the networks have 20 nodes deployed over a $500 \times 500\ m^2$. At the larger scale, the networks have 30 nodes deployed over a $600 \times 600\ m^2$ region. For each network scale, 10 topologies are randomly generated. The original algorithm and its heuristics are simulated and compared with TCP over the same topology. The results are shown in Fig. 3.20(a) and Fig. 3.20(b) respectively, corresponding to each network scale.

From these results, we have the following observations. First, the price-based resource allocation algorithm and its heuristics all outperform TCP in terms of aggregated utility. In networks with a smaller scale, the performance of the heuristics closely matches the original algorithm. This observation is because in networks with smaller scales, the hop counts between any two nodes are small. Thus heuristics with smaller information propagation ranges are sufficient to communicate the information for clique construction and price calculation. In some topologies, 1-hop heuristic can provide even better performance than the original algorithm due to its lower overhead. In networks with larger scales, the 2-hop heuristic and the original algorithm give better performance than the 1-hop heuristic owing to more precise clique construction. Moreover, 2-hop heuristic can sometimes outperform the original algorithm due to its lower communication overhead.

Larger aggregated utility indicates more fair resource allocation and better resource utilization. To further understand the results in terms of aggregated utility in Fig. 3.20, we plot in Fig. 3.21 the throughput of each flow from the simulation result of one randomly generated $600 \times 600\ m^2$ network. The result clearly reflects the fairness improvement achieved by our price-based resource allocation algorithms in comparison with TCP.

3.4.6 Impact of mobility

In this section, we study the behavior of our algorithm over mobile ad hoc networks. In particular, we seek to find the threshold of mobility where the convergence speed of the algorithm is not

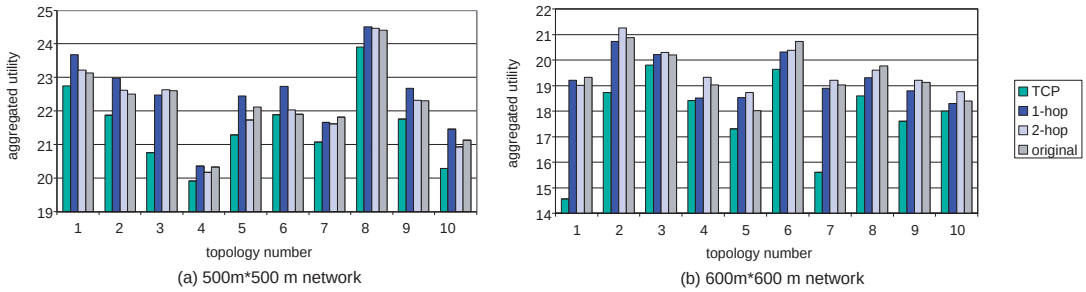

Figure 3.20: Comparison of price-based resource algorithms and TCP over randomly generated networks.

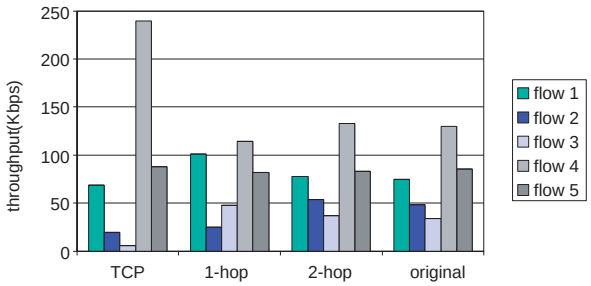

Figure 3.21: Throughput comparison over a randomly generated network with 30 node deployed over a $600 \times 600\ m^2$ region.

fast enough to ensure a sufficient portion of time at equilibrium. We experiment on a specially designed mobile scenario as shown in Fig. 3.22(a). In this mobile scenario, nodes 1 is moving between location $(150, 1000)$ and $(150, 500)$ observing the random waypoint model, and node 2 is moving between $(150, 500)$ and $(150, 0)$. During the simulation, these two nodes will serve as the relaying nodes for flow f_1 in an interwoven fashion. The convergence behavior and the throughput under different node speeds and pause time intervals are plotted in Fig. 3.22. From the figure, we can observe that the new convergence occurs after broken routes are re-established. The results show that the algorithm converges and stays at equilibrium for a large portion of time when the node moves at 10m/s without pause. When the node speed increases to 20m/s, the flow spends approximately the same amount of time during the convergence and at the equilibrium. Further increasing the node speed under this scenario may result in insufficient amount of equilibrium time where resource is optimally allocated. Obviously, if the pause time interval is increased, the algorithm can support higher node speeds. This is illustrated in the figure, when node speeds are

50m/s with the pause time interval as 20 seconds.

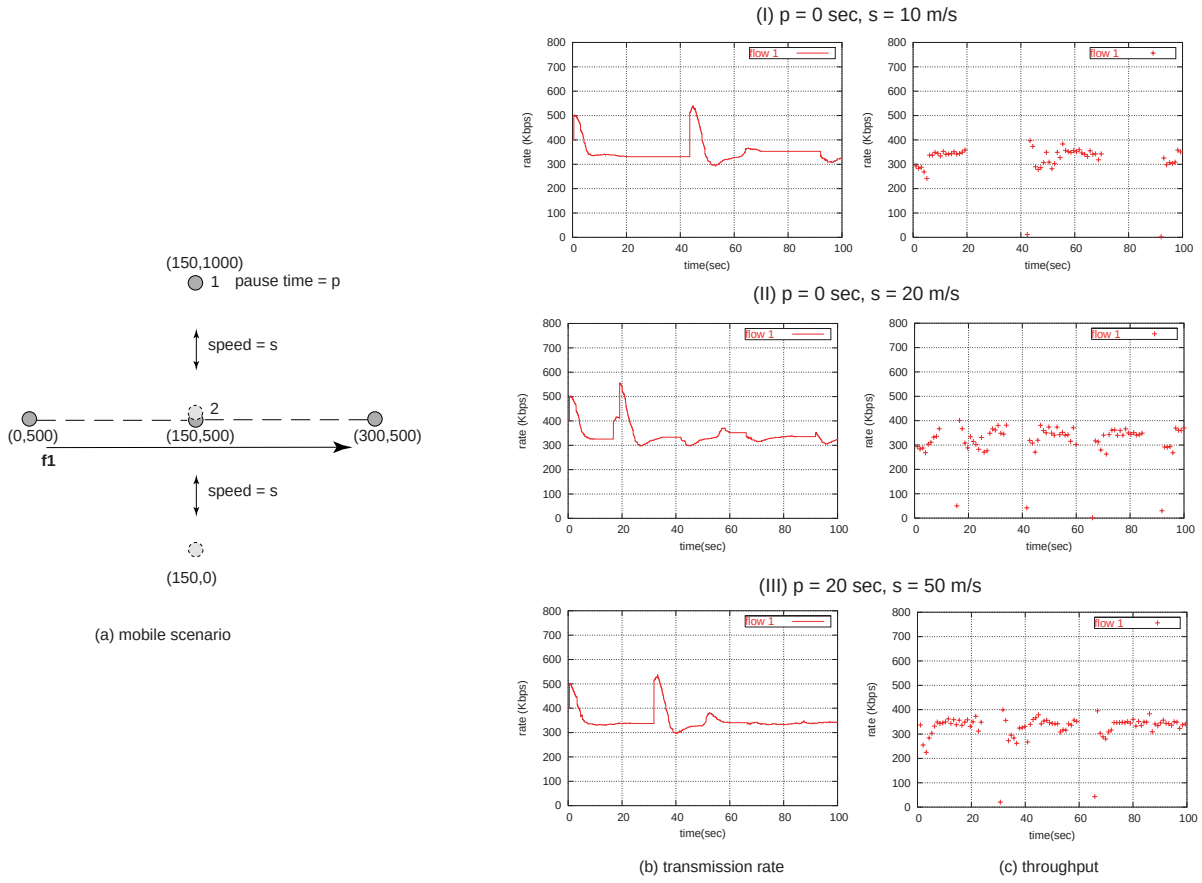

Figure 3.22: Impact of node mobility.

To study the impact of mobility on our algorithm over random networks, we organized the simulated network scenarios into mobility patterns. Each mobility pattern, generated randomly, specifies a sequence of movements. Within each mobility pattern, the mobility index specifies the average node speed and pause time of each mobile scenario. For example, under one mobility pattern, if with index 1 a node takes time t to move from location a to location b, then with index 2, this node will take $2 \times t$ to traverse this distance. Our experiment ranges from mobility index 1, which corresponds to an average node speed of 100m/s and pause time interval of 10 seconds, to mobility index 6, which corresponds to an average node speed of 16.67m/s and pause time interval of 60 seconds. Fig. 3.23(a) plots the aggregated utility of our algorithm with varied mobility indices under 4 different mobility patterns. To better understand the performance indicated by

the aggregated utility, Fig. 3.23(b) plots the throughput of each flow under pattern 1 with varied mobility indices. From these results, we observe that the difference from mobility index 4, which corresponds to an average node speed of 25m/s and pause time interval of 40 seconds, to mobility index 6 is quite small. Moreover, even in highly mobile environments such as the ones indicated by mobility indices smaller than 3, the performance of our algorithm still degrades reasonably with the increased mobility.

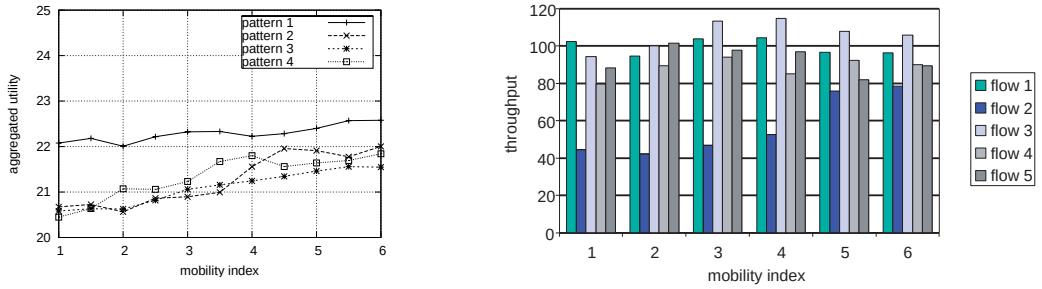

(a) aggregated utility under different patterns

(b) throughput of each flow under pattern 1

Figure 3.23: Impact of node mobility.

3.5 Related Work

We evaluate and highlight our original contributions in light of previous related work.

The problem of optimal and fair resource allocation has been extensively studied in the context of wireline networks. Among these works, pricing has been shown to be an effective approach to achieve distributed solution for rate allocation (*e.g.*, [20, 26, 21, 23, 22, 17, 18]). The role of price in our work is similar to [26], which reflects the relation of the demand and the supply of resources. Nevertheless, the fundamental differences in contention models between ad hoc and wireline networks deserve a fresh treatment to this topic. As we have emphasized, these resource allocation strategies employed in the wireline network may not be applied directly in the context of ad hoc networks due to the unique characteristics of the shared wireless channel. One of the highlights in this work is to propose a new pricing framework for wireless ad hoc networks to address such problems. The essence of our proposal is to define shadow prices for maximal

cliques, rather than wireline links.

A collection of papers have studied the use of pricing in the context of wireless networks (*e.g.*, [14, 16, 9, 37, 36]). In these works, pricing has been used as a mechanism for optimal distributed power control. In comparison, our work is towards different objectives and in different wireless environments. For example, we study rate allocation in multi-hop wireless networks with time-slotted MAC, while most of the work in this group study base-station-based single-hop wireless networks with CDMA. In addition, Liao *et al.* [33] use price as an incentive for service class allocation in wireless LAN. Their solution, however, is applicable in scenarios where centralized management is readily available.

In previous work, fair packet scheduling mechanisms have been proposed [29, 40, 27] and shown to perform effectively in providing fair shares among single-hop flows in wireless ad hoc networks, and in balancing the trade-off between fairness and bandwidth utilization. However, none of the previously proposed algorithms has considered end-to-end flows spanning multiple hops, which reflect the reality in wireless ad hoc networks. While these mechanisms may be sufficient for maintaining basic fairness properties among localized flows, they do not coordinate intra-flow bandwidth allocations between upstream and downstream hops of an end-to-end flow, and thus will not be able to achieve global optimum with respect to bandwidth utilization and fairness. It can be shown that fair resource allocation among single-hop flows may not be optimal for multi-hop flows, due to the unawareness of bottlenecks and lack of coordination among upstream and downstream hops. Due to the complexities of such intra-flow coordinations, we are naturally led to a *price-based* approach, where prices are computed as *signals* to reflect relations between local bandwidth demands and supplies, and are used to coordinate the bandwidth allocations at multiple hops. Finally we argue that our proposed solution for end-to-end flows is complementary to any MAC-layer solutions, and can be implemented based on them.

In recent work, joint rate control and scheduling mechanisms have been proposed [**?**, **?**, 34, 25, 24]. These schemes require the change of the MAC layer protocol to support fair and efficient rate control. In contrast, our solution does not require the support of a particular MAC-layer scheduling

algorithm. Although our pricing model is established based the assumption of an ideal MAC layer scheduling algorithm, it can be extended to be applied with any MAC scheduling algorithm as long as its achievable channel capacity can be estimated. In our system implementation, we illustrate how our solution can be built over IEEE 802.11-based wireless networks.

3.6 Summary

In this chapter, we have presented a novel price-based resource allocation algorithm based on an analytical pricing model that is specifically designed for the unique characteristics of multi-hop wireless ad hoc networks. The original contribution incorporated in the pricing model is the association of shadow prices with the *maximal cliques* in the contention graph model, rather than with individual links as in wireline networks. Based on insights brought forth by such strategies, the algorithms proposed are fully distributed, and arbitrate the contention among end-to-end *multi-hop* flows with respect to fair resource allocation. The validity of our claims is supported by both theoretical studies and extensive simulation results. To the best of our knowledge, there does not exist any previous work that addresses the problem of enforcing fairness among multi-hop flows in wireless ad hoc networks, especially when a price-based approach is utilized to design fully distributed algorithms to achieve this goal.

3.7 Notations

We list all notations introduced in this chapter as follows.

Notation	Definition
$i, j \in N$	node i and j in network node set N
$l \in L$	wireless link l in wireless link set L
$f \in F$	flow f in multi-hop end-to-end flow set F
$s \in S \subseteq E$	wireless link s that carries traffic
$E(f)$	set of wireless links that the flow f traverses
$G = (V, E)$	network topology in the form of a graph
$G_c = (V_c, E_c)$	subflow contention graph
$q \in Q$	maximal clique q in the subflow contention graph
$V(q) \subseteq S$	set of vertices in G_c that the clique q contains
$\boldsymbol{x} = (x_f,\ f \in F)$	vector of rate allocations for flows $f \in F$
$\boldsymbol{C} = (C_q,\ q \in Q)$	vector of achievable channel capacities for cliques $q \in Q$
$\boldsymbol{R} = \{R_{qf}\}$	flow-clique matrix
$U_f(x_f)$, $f \in F$	utility function for flow f
$I_f = [m_f, M_f]$	feasible range of x_f
κ_f	curvature bound of $U_f(x_f)$
$\boldsymbol{\mu} = (\mu_q, q \in Q)$	vector of clique prices
$\lambda_f, f \in F$	price of flow f
$x_f(\lambda_f)$, $f \in F$	demand function of flow f
$q(s)$	maximal clique that contains wireless link $s \in S$
$Q(s) = \{q(s)\}$	set of all maximal cliques that contain wireless link $s \in S$
$\mathbb{LN}^k(e)$	wireless link k-neighbor set of wireless link $e \in E$
y_s	aggregated flow rate at wireless link s
λ_s	aggregated price at wireless link s
$\mu_{q(v(s))}$	price of clique q at node $v(s)$ in implementation II
$T = \{0, 1, 2, ...\}$	set of time instances at which either rates or prices are updated
$T_q \subseteq T$	set of time instances at which master node $v(q)$ updates μ_q
$T_s^\lambda \subseteq T$	set of time instances at which delegation node $v(s)$ updates λ_s
$T_f \subseteq T$	set of time instances at which the source of flow f updates x_f
$T_s^y \subseteq T$	set of time instances at which delegation node $v(s)$ updates y_s
$\hat{\mu}_q^s(t)$	estimation of μ_q at node $v(s)$ at time t
$\hat{\lambda}_s^f(t)$	estimation of λ_s at source of flow f at time t
$\hat{x}_f^s$	estimation of x_f at node $v(s)$ at time t
$\hat{y}_s^q(t)$	estimation of y_s at node $v(q)$ at time t
$\alpha_q^s(t', t)$, $\alpha_s^f(t', t)$, $\alpha_f^s(t', t)$, $\alpha_s^q(t', t)$	estimation weights

Table 3.5: Notations in Chapter 3

Chapter 4

Multi-Resource Allocation and Incentives Arbitration in Multihop Wireless Networks

Cooperation in wireless ad hoc networks has two-fold implications. First, each wireless node does not excessively and greedily inject traffic to the shared wireless channel. Second, intermediate nodes voluntarily relay traffic for upstream nodes towards the destination at the cost of its own private resource. Such an assumption supports almost all existing research when it comes to protocol design in ad hoc networks. We believe that without appropriate incentive mechanisms, the nodes are inherently selfish (unwilling to contribute its private resource to relay traffic) and greedy (unfairly sharing the wireless channel). In this chapter, we present a *price pair* mechanism to arbitrate resource allocation and to provide incentives simultaneously such that cooperation is promoted and the desired global optimal network operating point is reached by convergence with a fully decentralized self-optimizing algorithm. Such desired network-wide global optimum is characterized with the concept of Nash bargaining solution, which not only provides the Pareto optimal point for the network, but is also consistent with the fairness axioms of game theory. We simulate the price pair mechanism and report encouraging results to support and validate our theoretical claims.

4.1 Overview

In wireless ad hoc networks, nodes are both *greedy* when it comes to sharing public resource (wireless channel), and *selfish* when it comes to contributing private resource (such as battery energy). In other words, the network may fail to function at all in realistic scenarios once neither assumption holds.

The only way to solve these problems is to design appropriate incentive mechanisms to not

only encourage cooperative behavior of selfish nodes, but also curb unfair and excessive resource usage when sharing a common resource pool, such as a shared channel. Such designs of incentives should optimize towards a clearly specified objective, which is a desired optimal operating point of the wireless network. At such an optimal point, resources are shared fairly, and the levels of cooperation are adequate for all necessary data communications and network functions. This chapter exactly targets this critical issue in multi-hop wireless networks.

Our original contributions are two-fold. First, we clearly characterize the desired network-wide optimal operating point using a game theoretic framework, based on the concept of Nash Bargaining Solution (NBS). NBS naturally encapsulates two favorable properties: (1) Pareto efficiency in terms of resource usage; and (2) a set of fairness axioms with respect to resource allocations. Using this framework, the problem of finding the desired globally optimal operating point may be formulated as a non-linear optimization problem. Second, we propose a decentralized algorithm that uses a *price pair* mechanism to arbitrate incentives. With a pair of prices, localized self-optimization by individual nodes naturally converges to globally optimal network operating points. Within the price pair, the *channel price* regulates greedy usage of the shared wireless channel, while the *relay price* encourages traffic relaying. Effectively, our price pair mechanism transforms non-cooperative behavior in wireless ad hoc networks to a *cooperative game*, whose optimal operating points demonstrate more advantageous properties than the usual Nash Equilibrium in typical non-cooperative environments.

The essence of our work is to integrate the mechanisms that use pricing as signals to (1) fairly allocate resources; and (2) adequately incentivize cooperative behavior. Though there exists previous work towards either one of these objectives, we are not aware of existing work that integrates both prices into a coherent framework. Such integration becomes more complicated if we consider the unique channel contention characteristics in wireless ad hoc networks, where the traffic flows contend in multiple *contention cliques*. Considerations of such unique complications in ad hoc networks are beyond all of the existing work in the area of pricing or incentives.

The remainder of this chapter is organized as follows. Sec. 4.2 presents some preliminaries

before formal treatment of this topic. Sec. 4.3 defines the desired network operating points using the concept of Nash Bargaining Solution. We present the distributed algorithm in Sec. 4.5. We show simulation results in Sec. 4.7, present related work in Sec. 4.8 and finally summarize the chapter in Sec. 4.9.

4.2 Network Model and Resource Constraints

4.2.1 Characterizing wireless ad hoc networks

We consider a wireless ad hoc network which consists of a set of nodes $\mathcal{N} = \{1, 2, ..., N\}$. In this network, only nodes that are within the transmission range of each other can communicate directly and form a *wireless link*. We model such a network as a bidirectional graph $\mathcal{G}_N = (\mathcal{N}, \mathcal{L})$, where $\mathcal{L} = \{1, 2, ..., L\}$ is the set of wireless links.

In such a network, a wireless node $i \in \mathcal{N}$ may establish an end-to-end flow, or simply *flow*, f_i with rate x_i to another node. Flow f_i is assumed to be elastic: it requires a minimum rate of x_i^m and a maximum rate of x_i^M, *i.e.*, $x_i^m \leq x_i \leq x_i^M$. In general, f_i flows through multiple hops in the network, passing a set of wireless links. We use this set of wireless links to represent f_i, *i.e.*, $f_i \subset \mathcal{L}$. We denote the set of relaying nodes for flow f_i as $R(f_i)$, and the destination of f_i as $D(f_i)$. For simplicity of exposition, we further define $H(f_i) = R(f_i) \cup \{D(f_i), i\}$ as the set of nodes f_i traverses, and $K(f_i) = H(f_i) - \{i\}$. A single-hop data transmission along a particular wireless link is referred to as a *subflow*, and is a part of a flow. Several subflows from different flows along the same wireless link form an *aggregated subflow*.

In such a network, nodes compete for two types of resources: shared wireless channel and individual nodes' relaying cost (such as energy). The availability of these resources constrains the solution space of resource allocations. We proceed to analyze the characteristics of both types of resources.

From previous discussion in Chapter 3, constraint with respect to rate allocations to end-to-end

flows in wireless ad hoc networks is $\boldsymbol{Rx} \leq \boldsymbol{C}$.

Relaying traffic for upstream nodes apparently incurs cost, since localized resources need to be consumed, such as energy, CPU cycle, and memory space. Without loss of generality, we use energy levels on each node as an example to characterize such costs of relays. Given a minimum expected lifetime in the network, each node j has a budget on its energy consumption rate, denoted as E_j. Here, we consider two types of energy consumption related to packet transmission: (1) e^r as the energy consumed for receiving a unit flow; (2) e^s as the energy consumed for transmitting a unit flow. Then the energy consumption at node j is $x_j e^s + \sum_{i:j \in R(f_i)} x_i(e^r + e^s) + \sum_{i:j=D(f_i)} x_i e^r$. As the energy consumption rate can not exceed the energy budget, we have the following relation:

$$x_j e^s + \sum_{i:j \in R(f_i)} x_i(e^r + e^s) + \sum_{i:j=D(f_i)} x_i e^r \leq E_i \tag{4.1}$$

We now proceed to define a $N \times N$ matrix $\boldsymbol{B}$ as follows.

$$B_{ji} = \begin{cases} e^s & \text{if } j = i \\ e^r + e^s & \text{if node } j \text{ forwards packets for flow } f_i, \\ & \textit{i.e.}, j \in R(f_i) \\ e^r & \text{if node } j \text{ is the destination of flow } f_i, \\ & \textit{i.e.}, j = D(f_i) \\ 0 & \text{otherwise} \end{cases} \tag{4.2}$$

$\boldsymbol{B}$ specifies the relaying relation among nodes in the ad hoc network. To summarize, the local constraint on energy can be formalized as follows:

$$\boldsymbol{B} \cdot \boldsymbol{x} \leq \boldsymbol{E} \tag{4.3}$$

where $\boldsymbol{E} = (E_j, j \in \mathcal{N})$ is the energy consumption budget vector.

Here we illustrate the above concepts using an example. The network topology and the flows in the example are shown in Fig. 4.1(a). The corresponding subflow contention graph is shown in Fig. 4.1(b). In this example, there are three maximal cliques in the contention graph: $q_1 =$

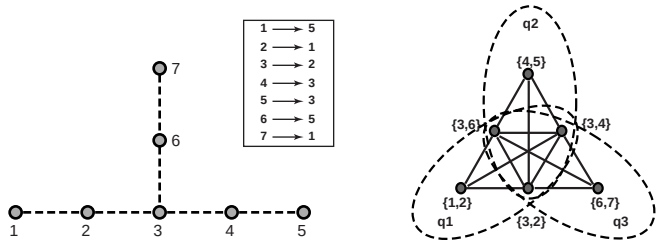

(a) Network topology (b) Subflow contention graph

Figure 4.1: Example of wireless ad hoc network and its subflow contention graph

$\{\{1,2\},\{3,2\},\{3,4\},\{3,6\}\}, q_2 = \{\{3,2\},\{3,4\},\{4,5\},\{3,6\}\}$ and $q_3 = \{\{3,2\},\{3,4\},\{3,6\},\{6,7\}\}$. Let us use y_{ij} to denote the aggregated rate of *all* subflows along node i and j. For example, $y_{12} = x_1 + x_2 + x_7$, $y_{23} = x_1 + x_3 + x_7$, $y_{36} = x_6 + x_7$. In each clique, the aggregated rate can not exceed the channel capacity, *i.e.*,

$$y_{12} + y_{32} + y_{34} + y_{36} \leq C_1 \tag{4.4}$$

$$y_{32} + y_{34} + y_{45} + y_{36} \leq C_2 \tag{4.5}$$

$$y_{32} + y_{34} + y_{36} + y_{67} \leq C_3 \tag{4.6}$$

When it comes to end-to-end flow rate allocation, the resource constraint imposed by shared wireless channel is as follows:

$$\begin{pmatrix} 3 & 1 & 1 & 1 & 1 & 2 & 3 \\ 3 & 0 & 1 & 1 & 2 & 3 & 2 \\ 2 & 0 & 1 & 1 & 1 & 2 & 3 \end{pmatrix} \boldsymbol{x} \leq \boldsymbol{C}.$$

In this example, let the energy consumed for receiving $e^r = 1$, for transmitting $e^s = 2$. Then the energy constraint is as follows:

$$\begin{pmatrix} 2 & 1 & 0 & 0 & 0 & 0 & 1 \\ 3 & 2 & 1 & 0 & 0 & 0 & 3 \\ 3 & 0 & 2 & 1 & 1 & 3 & 3 \\ 3 & 0 & 0 & 2 & 3 & 3 & 0 \\ 1 & 0 & 0 & 0 & 2 & 1 & 0 \\ 0 & 0 & 0 & 0 & 0 & 2 & 3 \\ 0 & 0 & 0 & 0 & 0 & 0 & 2 \end{pmatrix} \boldsymbol{x} \leq \boldsymbol{E}.$$

4.3 Problem Formulation

In this section, we characterize the desired network-wide optimal operating point using a game theoretic framework, based on the concept of Nash Bargaining Solution (NBS). NBS naturally encapsulates two favorable properties: (1) Pareto efficiency in terms of resource usage; and (2) a set of fairness axioms with respect to resource allocations. Using this framework, the problem of finding the desired globally optimal operating point may be formulated as a non-linear optimization problem. We show how such a global optimization problem may be decomposed into localized greedy optimization problems via a price pair.

4.3.1 Nash Bargaining Solution: a game theoretical formulation

We present the basic concepts and results of Nash bargaining solutions (NBS) from game theory [30] and show how it can characterize and formulate the desired network operation point, towards which our price pair mechanism should converge.

The basic setting of the problem is as follows: The set of nodes $\mathcal{N}$ in the wireless ad hoc network $\mathcal{G}_N$ constitutes a set of players in the game. They compete for the use of a fixed amount of resources (wireless channel and costs of relays such as energy). The rate allocation $\boldsymbol{x} = (x_i, i \in \mathcal{N})$ is the utility vector of all players in the game. Let $S \subset \Re^N$ be the set of all feasible utility

vectors. We assume that S is a non-empty convex closed and bounded set. Further, we denote the initial agreement point of the game as $\boldsymbol{x}^*$, which is the guaranteed utilities of players without any cooperation in order to enter the game.

In such a problem setting, a *bargaining problem* is any $(S, \boldsymbol{x}^*)$ where $\{\boldsymbol{x} \in S | \boldsymbol{x} \geq \boldsymbol{x}^*\} \neq \emptyset$. In other words, a bargaining problem is actually a set of rate allocations $\boldsymbol{x}$ that is acceptable to all players. Let $\mathfrak{B} = \{(S, \boldsymbol{x}^*)\}$ denote the set of all bargaining problems. It then follows that a *bargaining solution* is any function $\varphi : \mathfrak{B} \rightarrow \mathfrak{R}^N$, so that $\forall (S, \boldsymbol{x}^*) \in \mathfrak{B}$, $\varphi(S, \boldsymbol{x}^*) \in S$. A bargaining solution actually specifies finding a rate allocation within all acceptable allocations. A natural question about the bargaining solution is how such a function φ is to be defined. There are two reasonable properties desired for a bargaining solution: (1) efficient use of resources; and (2) fair allocation among all players. These two conditions are precisely encapsulated by the concept of *Nash Bargaining Solution* defined as follows.

Definition 4.3.1 (Nash Bargaining Solution). A bargaining solution $\varphi : \mathfrak{B} \rightarrow \mathfrak{R}^N$ is a *Nash Bargaining Solution* (NBS), if $\bar{\boldsymbol{x}} = \varphi(S, \boldsymbol{x}^*)$ satisfies the *Nash Axioms* A1-A6.

A1 (Individual rationality) $\bar{\boldsymbol{x}} \geq \boldsymbol{x}^*$;

A2 (Feasibility) $\bar{\boldsymbol{x}} \in S$;

A3 (Pareto optimality) If $\forall \boldsymbol{x} \in S, \boldsymbol{x} \geq \bar{\boldsymbol{x}}$, then $\boldsymbol{x} = \bar{\boldsymbol{x}}$;

A4 (Independence of irrelevant alternatives) If $\bar{\boldsymbol{x}} \in T \subset S$ and $\bar{\boldsymbol{x}} = \varphi(S, \boldsymbol{x}^*)$, then $\bar{\boldsymbol{x}} = \varphi(T, \boldsymbol{x}^*)$;

A5 (Independence of linear transformation) Let T be obtained from S by the linear transformation $\phi(\boldsymbol{x})$ with

$$\phi(\boldsymbol{x})_i = a_i x_i + b_i, a_i, b_i > 0, i = 1, 2, ..., N. \tag{4.7}$$

Then if $\varphi(S, \boldsymbol{x}^*) = \bar{\boldsymbol{x}}$, then $\varphi(T, \phi(x^*)) = \phi(\bar{\boldsymbol{x}})$;

A6 (Symmetry) Suppose S is symmetric with respect to a subset $J \subseteq \{1, 2, ..., N\}$ of indices, then φ is symmetry, which means that if $\boldsymbol{x} \in S$ and for $i, j \in J$, $x_i^* = x_j^*$, then $\bar{x}_i = \bar{x}_j$.

The above axioms encapsulate both the concept of Pareto optimality (A3) and the concept of fairness (A4-A6). Pareto optimality means that there is no other point which gives strict superior utility for all the players simultaneously. The definition of Pareto optimality reflects the condition of efficient use of resources, where there are no "idle" resources in the network. Axioms A4-A6 represent the axioms of fairness. The independence of irrelevant alternatives axiom (A4) states that, if a bargaining solution $\bar{\boldsymbol{x}}$ to a problem on an enlarged feasible set S can be found on a restricted domain T, then it is also the bargaining solution to the problem on the restricted set. The independence of linear transformation axiom (A5) states that the bargaining solution is scale invariant, *i.e.*, the bargaining solution is unchanged if the utility is changed using a positive linear transformation. The symmetry axiom (A6) states that the bargaining point does not depend on the specific labels, *i.e.*, players with the same initial points and objectives will realize the same utility.

The existing work in game theory [30] and its application in wireline communication networks [42] establish the following results for NBS.

Theorem 4.3.1. *There exists a unique function φ defined on all bargaining problems $(S, \boldsymbol{x}^*)$ that satisfies axioms A1-A6,* i.e., *a unique Nash Bargaining Solution (NBS) exists. Moreover, the unique solution $\bar{\boldsymbol{x}}$ is a unique vector that solves the following maximization problems:*

$$\mathbf{N_1} : \max_{\boldsymbol{x}} \prod_{i \in \mathcal{N}} (\bar{x}_i - x_i^*); \tag{4.8}$$

Equivalently,

$$\mathbf{N_2} : \max_{\boldsymbol{x}} \sum_{i \in \mathcal{N}} \ln(\bar{x}_i - x_i^*). \tag{4.9}$$

Above concepts are illustrated in Fig. 4.2, where the utility space of a two-player game is plotted. In the example, two players are competing for a unit resource. The initial agreement point $\boldsymbol{x}^* = (0, 0)$, and the NBS $\bar{\boldsymbol{x}} = (1/2, 1/2)$.

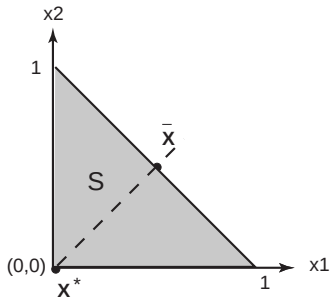

Figure 4.2: Example of Nash bargaining solution

4.3.2 Network operating points: optimal and fair rate allocations

We assume that each player involved in the game can be guaranteed with its minimum rate vector $\boldsymbol{x}^m$. Thus, the minimum rate vector $\boldsymbol{x}^m$ can be regarded as an initial agreement point of the game $\boldsymbol{x}^*$. From the discussions in Sec. 4.3.1, it is clear that the NBS formulates the desired network operation point, which is fair to all nodes while efficient from the network's point of view. Thus, the problem of finding the globally optimal resource allocation is transformed to solving the NBS of its corresponding game, which is the solution of the following nonlinear optimization problem by Theorem 4.3.1.

$$\mathbf{P}: \quad \textbf{maximize} \quad \sum_{i\in\mathcal{N}} \ln(x_i - x_i^m) \tag{4.10}$$

$$\textbf{subject to} \quad \boldsymbol{A}\cdot\boldsymbol{x} \leq \boldsymbol{C} \tag{4.11}$$

$$\boldsymbol{B}\cdot\boldsymbol{x} \leq \boldsymbol{E} \tag{4.12}$$

$$\textbf{over} \quad \boldsymbol{x}^m \leq \boldsymbol{x} \leq \boldsymbol{x}^M \tag{4.13}$$

The objective function in Eq. (4.10) of the optimization problem corresponds to the optimization problem whose solution is NBS. The constraints of the optimization problem Eq. (4.11) and Eq. (4.12) are the constraints from the shared wireless channel and costs of relays, respectively, as discussed in Sec. 4.2.

Note that the objective function $\sum_{i\in\mathcal{N}} \ln(x_i - x_i^m)$ is strictly concave. In addition, the feasible

region of the optimization problem is non-empty, convex, and compact. By non-linear optimization theory, there exists a maximizing value of argument $\boldsymbol{x}$ for the above optimization problem. Let us consider the Lagrangian form of the optimization problem **P**:

$$\begin{aligned} & L(\boldsymbol{x}, \boldsymbol{\mu}^{\alpha}, \boldsymbol{\mu}^{\beta}) \\ = & \sum_{i \in \mathcal{N}} \ln(x_i - x_i^m) + \boldsymbol{\mu}^{\alpha}(\boldsymbol{C} - \boldsymbol{A}\boldsymbol{x}) + \boldsymbol{\mu}^{\beta}(\boldsymbol{E} - \boldsymbol{B}\boldsymbol{x}) \end{aligned} \tag{4.14}$$

where $\boldsymbol{\mu}^{\alpha} = (\mu_q^{\alpha}, q \in \mathcal{Q})$, $\boldsymbol{\mu}^{\beta} = (\mu_j^{\beta}, j \in \mathcal{N})$ are two vectors of Lagrange multipliers. The first-order Kuhn-Tucker conditions are necessary and sufficient for optimality of problem **P**. Thus, for $i \in \mathcal{N}$, the following conditions hold:

$$\frac{1}{x_i - x_i^m} - \sum_{q \in \mathcal{Q}} \mu_q^{\alpha} A_{qi} - \sum_{j \in \mathcal{N}} \mu_j^{\beta} B_{ji} = 0 \tag{4.15}$$

$$\boldsymbol{\mu}^{\alpha}(\boldsymbol{C} - \boldsymbol{A}\boldsymbol{x}) = 0; \boldsymbol{\mu}^{\alpha} \geq 0 \tag{4.16}$$

$$\boldsymbol{\mu}^{\beta}(\boldsymbol{E} - \boldsymbol{B}\boldsymbol{x}) = 0; \boldsymbol{\mu}^{\beta} \geq 0 \tag{4.17}$$

$$\boldsymbol{x}^m \leq \boldsymbol{x} \leq \boldsymbol{x}^M \tag{4.18}$$

In the Lagrangian form shown in Eq. (4.14), the Lagrange multipliers μ_q^{α} can be regarded as the implied cost of unit flow accessing the channel at the maximal clique q. In other words, μ_q^{α} is the *shadow price* of clique q, called *channel price*. This price corresponds to the shared channel resource constraint. The Lagrange multipliers μ_j^{β} can be regarded as the implied relay cost of unit flow at node j. In other words, μ_j^{β} is the *shadow price* of relay at node j, called *relay price*. This pair of prices $(\boldsymbol{\mu}^{\alpha}, \boldsymbol{\mu}^{\beta})$ will be used as incentives so that localized self-optimizing decision can implement the global optimum. In particular, the price $\boldsymbol{\mu}^{\alpha}$ will signal a "charge" (contrary to incentives) to the shared channel usage and regulate the greedy behavior, while the price $\boldsymbol{\mu}^{\beta}$ will provide incentives to traffic relays at intermediate nodes and regulate the selfish behavior of

wireless nodes.

Let us denote

$$\lambda_i^{\alpha} = \sum_{q \in \mathcal{Q}} \mu_q^{\alpha} A_{qi} \tag{4.19}$$

$$\lambda_i^{\beta} = \sum_{j \in \mathcal{N}} \mu_j^{\beta} B_{ji} \tag{4.20}$$

Clearly,

$$\lambda_i^{\alpha} = \sum_{q: f_i \cap q \neq \emptyset} \mu_q^{\alpha} A_{qi} \tag{4.21}$$

$$= \sum_{l: l \in f_i} \sum_{q: l \in q} \mu_q^{\alpha} \tag{4.22}$$

$$\lambda_i^{\beta} = \sum_{j \in H(f_i)} \mu_j^{\beta} B_{ji} \tag{4.23}$$

$$= \mu_i^{\beta} e^s + \sum_{j \in R(f_i)} \mu_j^{\beta} (e^s + e^r) + \mu_{D(f_i)}^{\beta} e^r \tag{4.24}$$

Then λ_i^{α} and λ_i^{β} are the prices for node i, which is the source of flow f_i, for accessing shared channels and relay services, respectively. For channel usage, node i needs to pay for *all the maximal cliques* that it traverses. For each clique, the price to pay is the product of the number of wireless links that f_i traverses in this clique and the shadow price of this clique as in Eq. (4.21). Alternatively, the price of flow f_i is the aggregated price of all its subflows. For each subflow, its price is *the aggregated price of the maximal cliques* that it belongs to as in Eq. (4.22). Note that such a pricing policy for end-to-end flows is fundamentally different from the pricing models in wireline networks, where a flow's price is the aggregation of the link prices which it traverses. Such difference is rooted at the nature of the shared medium — the interference and spatial reuse of wireless channel in an ad hoc network. For traffic relay services, node i needs to pay for the relay costs of all relaying nodes of f_i, including itself and the destination. Using flow f_1 as an

example, the channel price model is illustrated in Fig. 4.3(a) and the relay price model is illustrated in Fig. 4.3(b). The channel price for f_1 is $\lambda_1^\alpha = 3\mu_1^\alpha + 3\mu_2^\alpha + 2\mu_3^\alpha$; and the relay price $\lambda_1^\beta = 2\mu_1^\beta + 3\mu_2^\beta + 3\mu_3^\beta + 3\mu_4^\beta + \mu_5^\beta$.

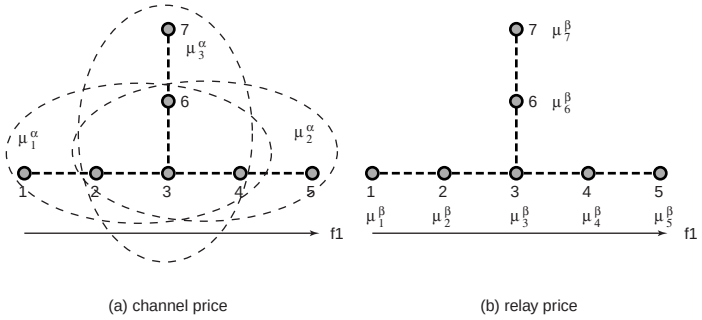

Figure 4.3: An example of the price pair mechanism

To summarize, we have the following results with respect to the globally optimal network operating point.

Theorem 4.3.2. *There exists a unique solution to problem* **P** *(*i.e.*, unique NBS), which is characterized as follows: There exist two vectors* $\boldsymbol{\mu}^\alpha = (\mu_q^\alpha, q \in \mathcal{Q})$, $\boldsymbol{\mu}^\beta = (\mu_j^\beta, j \in \mathcal{N})$ *such that*

$$x_i = [\frac{1}{\lambda_i^\alpha + \lambda_i^\beta} + x_i^m]_{x_i^m}^{x_i^M}, \text{ for } i \in \mathcal{N} \tag{4.25}$$

$$\boldsymbol{\mu}^\alpha(\boldsymbol{C} - \boldsymbol{A}\boldsymbol{x}) = 0; \boldsymbol{\mu}^\alpha \geq 0 \tag{4.26}$$

$$\boldsymbol{\mu}^\beta(\boldsymbol{E} - \boldsymbol{B}\boldsymbol{x}) = 0; \boldsymbol{\mu}^\beta \geq 0 \tag{4.27}$$

where $[z]_a^b = \max\{\min\{z, b\}, a\}$.

4.3.3 Local strategies: self-optimizing decisions

With the understanding of the global optimal point, we now study how this point can be achieved in a distributed manner by localized self-optimizing decisions at each individual node. The key to this goal is to use the pair of prices $(\boldsymbol{\mu}^\alpha, \boldsymbol{\mu}^\beta)$ as signals to coordinate the distributed decisions.

First, we study the conditions that the prices need to satisfy in order to incentivize local node decisions so that they could implement the global network optimum. Let us consider the following problems:

Channel$(\boldsymbol{A}, \boldsymbol{C}; \boldsymbol{\mu}^{\alpha})$:

$$\textbf{maximize} \quad \sum_{i \in \mathcal{N}} \lambda_i^{\alpha} x_i \tag{4.28}$$

$$\textbf{subject to} \quad \boldsymbol{A}\boldsymbol{x} \leq \boldsymbol{C} \tag{4.29}$$

$$\textbf{over} \quad \boldsymbol{x}^m \leq \boldsymbol{x} \leq \boldsymbol{x}^M \tag{4.30}$$

where λ_i^{α} is a function of $\boldsymbol{\mu}^{\alpha}$, as defined in Eq. (4.19). Problem *Channel*$(\boldsymbol{A}, \boldsymbol{C}; \boldsymbol{\mu}^{\alpha})$ maximizes the total revenue of channel based on charging λ_i^{α} per unit of bandwidth to user i subject to the channel capacity constraint.

Relay$(\boldsymbol{B}, \boldsymbol{E}; \boldsymbol{\mu}^{\beta})$:

$$\textbf{maximize} \quad \sum_{i \in \mathcal{N}} \lambda_i^{\beta} x_i \tag{4.31}$$

$$\textbf{subject to} \quad \boldsymbol{B}\boldsymbol{x} \leq \boldsymbol{E} \tag{4.32}$$

$$\textbf{over} \quad \boldsymbol{x}^m \leq \boldsymbol{x} \leq \boldsymbol{x}^M \tag{4.33}$$

where λ_i^{β} is a function of $\boldsymbol{\mu}^{\beta}$, as defined in Eq. (4.20). Problem *Relay*$(\boldsymbol{B}, \boldsymbol{E}; \boldsymbol{\mu}^{\beta})$ maximizes the total relay revenue of all nodes subject to the relay cost constraint at each individual node.

Now let us consider a local self-optimizing decision at each node i which corresponds to the following problem:

Node$_i(\lambda_i^{\alpha}, \lambda_i^{\beta}, \mu_i^{\beta})$:

$$\textbf{maximize} \quad \ln(x_i - x_i^m) - \lambda_i^{\alpha} x_i - \lambda_i^{\beta} x_i + \mu_i^{\beta} E_i \tag{4.34}$$

$$\textbf{over} \qquad x_i^m \leq x_i \leq x_i^M \tag{4.35}$$

The relationship between localized node decision and the global optimal network operating point is then given as follows.

Theorem 4.3.3. *There exist vectors $\boldsymbol{\mu}^\alpha$, $\boldsymbol{\mu}^\beta$ and $\boldsymbol{x}$ such that*

1. *x_i is the unique solution to* Node$_i(\lambda_i^\alpha, \lambda_i^\beta, \mu_i^\beta)$*;*
2. *$\boldsymbol{x}$ solves* Channel$(\boldsymbol{A}, \boldsymbol{C}; \boldsymbol{\mu}^\alpha)$ *;*
3. *$\boldsymbol{x}$ solves* Relay$(\boldsymbol{B}, \boldsymbol{E}; \boldsymbol{\mu}^\beta)$*;*

Then $\boldsymbol{x}$ also solves problem **P**.

4.4 Proof of Theorem 4.3.3

Proof. As the objective function Eq. (4.34) of *Node*$_i(\lambda_i^\alpha, \lambda_i^\beta, \mu_i^\beta)$ is strict concave, the problem *Node*$_i(\lambda_i^\alpha, \lambda_i^\beta, \mu_i^\beta)$ has a unique solution given by,

$$x_i = [\frac{1}{\lambda_i^\alpha + \lambda_i^\beta} + x_i^m]_{x_i^m}^{x_i^M} \tag{4.36}$$

As the Lagrangian form for the *Channel*$(\boldsymbol{A}, \boldsymbol{C}; \boldsymbol{\mu}^\alpha)$ problem is

$$\begin{aligned} & L(\boldsymbol{x}, \boldsymbol{\mu}^\alpha, \boldsymbol{p}^\alpha) \\ = & \sum_{i \in \mathcal{N}} \lambda_i^\alpha x_i + \boldsymbol{p}^\alpha (\boldsymbol{C} - \boldsymbol{A}\boldsymbol{x}) \end{aligned} \tag{4.37}$$

at the optimum of $L(\boldsymbol{x}, \boldsymbol{\mu}^\alpha, \boldsymbol{p}^\alpha)$ the following conditions hold:

$$(\boldsymbol{\mu}^\alpha - \boldsymbol{p}^\alpha)\boldsymbol{A}\boldsymbol{x} = 0 \tag{4.38}$$

$$\boldsymbol{p}^\alpha (\boldsymbol{C} - \boldsymbol{A}\boldsymbol{x}) = 0 \tag{4.39}$$

Similarly, as the Lagrangian form for the *Relay*$(\boldsymbol{B}, \boldsymbol{E}; \boldsymbol{\mu}^\beta)$ problem is

$$\begin{aligned} & L(\boldsymbol{x}, \boldsymbol{\mu}^\beta, \boldsymbol{p}^\beta) \\ = & \sum_{i \in \mathcal{N}} \lambda_i^\beta x_i + \boldsymbol{p}^\beta (\boldsymbol{E} - \boldsymbol{B}\boldsymbol{x}) \end{aligned} \tag{4.40}$$

at the optimum of $L(\boldsymbol{x}, \boldsymbol{\mu}^\beta, \boldsymbol{p}^\beta)$ the following conditions hold:

$$(\boldsymbol{\mu}^\beta - \boldsymbol{p}^\beta)\boldsymbol{B}\boldsymbol{x} = 0 \tag{4.41}$$

$$\boldsymbol{p}^\beta (\boldsymbol{E} - \boldsymbol{B}\boldsymbol{x}) = 0 \tag{4.42}$$

The triple $(\boldsymbol{\mu}^\alpha, \boldsymbol{\mu}^\beta, \boldsymbol{x})$ which satisfies conditions Eq. (4.26), and Eq. (4.27) identifies a tuple $(\boldsymbol{p}^\alpha, \boldsymbol{x})$ that satisfies condition Eq. (4.38) and Eq. (4.39) with $\boldsymbol{p}^\alpha = \boldsymbol{\mu}^\alpha$, Thus it identifies a solution for *Channel*$(\boldsymbol{A}, \boldsymbol{C}; \boldsymbol{\mu}^\alpha)$ problem. Similarly, the triple $(\boldsymbol{\mu}^\alpha, \boldsymbol{\mu}^\beta, \boldsymbol{x})$ also identifies a tuple $(\boldsymbol{p}^\beta, \boldsymbol{x})$ that satisfies condition Eq. (4.41) and Eq. (4.42) with $\boldsymbol{p}^\beta = \boldsymbol{\mu}^\beta$, Thus it identifies a solution for *Relay*$(\boldsymbol{A}, \boldsymbol{C}; \boldsymbol{\mu}^\beta)$ problem. Moreover, note that Eq. (4.25) is the same as Eq. (4.36), which means it is also a solution to *Node*$_i(\lambda_i^\alpha, \lambda_i^\beta, \mu_i^\beta)$.

Conversely, we can construct a triple $(\boldsymbol{\mu}^\alpha, \boldsymbol{\mu}^\beta, \boldsymbol{x})$ with $\boldsymbol{\mu}^\alpha = \boldsymbol{p}^\alpha$ and $\boldsymbol{\mu}^\beta = \boldsymbol{p}^\beta$. Thus if x_i solves *Node*$_i(\lambda_i^\alpha, \lambda_i^\beta, \mu_i^\beta)$, *Channel*$(\boldsymbol{A}, \boldsymbol{C}; \boldsymbol{\mu}^\alpha)$ and *Relay*$(\boldsymbol{B}, \boldsymbol{E}; \boldsymbol{\mu}^\beta)$, then it satisfies Eq. (4.36), Eq. (4.38), Eq. (4.38), Eq. (4.41), and Eq. (4.42), which lead to Eq. (4.25), Eq. (4.26), and Eq. (4.27), thus identifying a solution to **P**. □

Let us denote

$$\Phi(x_i) = \ln(x_i - x_i^m) - \lambda_i^\alpha x_i - \lambda_i^\beta x_i + \mu_i^\beta E_i \tag{4.43}$$

Now we show that $\Phi(x_i)$ reflects the "net benefit" of node i and problem *Node*$_i(\lambda_i^\alpha, \lambda_i^\beta, \mu_i^\beta)$ maximizes the node i's net benefit. This claim is based on the following two observations. First, node i does not pay its relay cost to itself from a local point of view, while the flow relay price λ_i^β, which is defined from a global point of view, contains the price of relay for itself. Thus from a *local* point

of view, the cost of node i is:

$$\lambda_i^{\alpha} x_i + \sum_{j \in K(f_i)} B_{ji} = (\lambda_i^{\alpha} + \lambda_i^{\beta}) x_i - \mu_i^{\beta} e^s x_i \tag{4.44}$$

And the revenue of node i is:

$$\sum_{j:i \in K(f_j)} \mu_i^{\beta} B_{ij} x_j = \mu_i^{\beta} \sum_{j:i \in H(f_j)} B_{ij} x_j - \mu_i^{\beta} e^s x_i \tag{4.45}$$

Second, from Theorem 4.3.3 we have

$$\mu_i^{\beta} = 0 \text{ , if } \sum_{j:i \in H(f_j)} B_{ij} x_j < E_i \tag{4.46}$$

$$\mu_i^{\beta} > 0 \text{ , if } \sum_{j:i \in H(f_j)} B_{ij} x_j = E_i \tag{4.47}$$

Thus it is clear that $\Phi(x_i)$ reflects the "net benefit" of node i, which is the difference between utility, revenue and cost.

4.5 Algorithm

Although the global problem **P** can be mathematically solvable in a centralized fashion, it is impractical for realistic operations in wireless ad hoc networks. In this section, we present a distributed iterative algorithm for price calculation and resource arbitration. We show that the iterative algorithm converges to the global optimum, and maximizes the local net benefit at each node simultaneously.

4.5.1 Dual problem

In order to achieve a distributed solution, we first look at the dual problem of **P** as follows.

$$\mathbf{D}: \min_{\boldsymbol{\mu}^{\alpha}, \boldsymbol{\mu}^{\beta} \geq \mathbf{0}} D(\boldsymbol{\mu}^{\alpha}, \boldsymbol{\mu}^{\beta}) \tag{4.48}$$

where

$$\begin{aligned} & D(\boldsymbol{\mu}^{\alpha}, \boldsymbol{\mu}^{\beta}) \\ = & \max_{\boldsymbol{x}} L(\boldsymbol{x}, \boldsymbol{\mu}^{\alpha}, \boldsymbol{\mu}^{\beta}) \\ = & \max_{\boldsymbol{x}} \sum_{i \in \mathcal{N}} \underbrace{(\ln(x_i - x_i^m) - (\lambda_i^{\alpha} + \lambda_i^{\beta}) x_i + \mu_i^{\beta} E_i)}_{\Phi(x_i)} \\ & + \sum_{q \in \mathcal{Q}} \mu_q^{\alpha} C_q \end{aligned}$$

Note that $\Phi(x_i)$ is node i's "net benefit". By the separation nature of Lagrangian form, maximizing $L(\boldsymbol{x}, \boldsymbol{\mu}^{\alpha}, \boldsymbol{\mu}^{\beta})$ can be decomposed into separately maximizing $\Phi(x_i)$ for each node $i \in \mathcal{N}$ (Sec. 3.4.2 in [3]). We now have

$$D(\boldsymbol{\mu}^{\alpha}, \boldsymbol{\mu}^{\beta}) = \sum_{i \in \mathcal{N}} \max_{x_i^m \le x_i \le x_i^M} \{\Phi(x_i)\} + \sum_{q \in \mathcal{Q}} \mu_q^{\alpha} c_q \tag{4.49}$$

As $\Phi(\cdot)$ is strictly concave and twice continuously differentiable, a unique maximizer of $\Phi(x_i)$ exists when

$$\frac{d\Phi(x_i)}{dx_i} = \frac{1}{x_i - x_i^m} - (\lambda_i^{\alpha} + \lambda_i^{\beta}) = 0$$

We define the maximizer as follows:

$$x_i(\lambda_i^{\alpha}, \lambda_i^{\beta}) = \arg \max_{x_i^m \le x_i \le x_i^M} \{\Phi(x_i)\} \tag{4.50}$$

Note that $x_i(\lambda_i^{\alpha}, \lambda_i^{\beta})$ is usually called demand function, which reflects the optimal rate for node i with channel price as λ_i^{α} and relay price as λ_i^{β}.

4.5.2 Distributed algorithm

We solve the dual problem $\mathbf{D}$ using the gradient projection method [3]. In this method, $\boldsymbol{\mu}^{\alpha}$ and $\boldsymbol{\mu}^{\beta}$ are adjusted in the opposite direction to the gradient $\nabla D(\boldsymbol{\mu}^{\alpha}, \boldsymbol{\mu}^{\beta})$:

$$\mu_q^\alpha(t+1) = [\mu_q^\alpha(t) - \gamma \frac{\partial D(\boldsymbol{\mu}^\alpha(t), \boldsymbol{\mu}^\beta(t))}{\partial \mu_q^\alpha}]^+ \quad (4.51)$$

$$\mu_j^\beta(t+1) = [\mu_j^\beta(t) - \gamma \frac{\partial D(\boldsymbol{\mu}^\beta(t), \boldsymbol{\mu}^\beta(t))}{\partial \mu_j^\beta}]^+ \quad (4.52)$$

where γ is the stepsize. $D(\boldsymbol{\mu}^\alpha, \boldsymbol{\mu}^\beta)$ is continuously differentiable since $\ln(\cdot)$ is strictly concave [3]. Thus, it follows that

$$\frac{\partial D(\boldsymbol{\mu}^\alpha, \boldsymbol{\mu}^\beta)}{\partial \mu_q^\alpha} = C_q - \sum_{i: f_i \cap q \neq \emptyset} x_i(\lambda_i^\alpha, \lambda_i^\beta) A_{qi} \quad (4.53)$$

$$\frac{\partial D(\boldsymbol{\mu}^\alpha, \boldsymbol{\mu}^\beta)}{\partial \mu_j^\beta} = E_j - \sum_{i: j \in H(f_i)} x_i(\lambda_i^\alpha, \lambda_i^\beta) B_{ji} \quad (4.54)$$

Substituting Eq. (4.53) into (4.51) and (4.54) into (4.52), we have

$$\mu_q^\alpha(t+1) = [\mu_q^\alpha(t) + \gamma(\sum_{i: f_i \cap q \neq \emptyset} x_i(\lambda_i^\alpha(t), \lambda_i^\beta(t)) A_{qi} - C_q)]^+ \quad (4.55)$$

$$\mu_j^\beta(t+1) = [\mu_j^\beta(t) + \gamma(\sum_{i: j \in H(f_i)} x_i(\lambda_i^\alpha(t), \lambda_i^\beta(t)) B_{ji} - E_j)]^+ \quad (4.56)$$

Eq. (4.55) and Eq. (4.56) reflect the law of supply and demand. If the demand for bandwidth at clique q exceeds its supply C_q, the channel constraint is violated. Thus, the channel price μ_q^α is raised. Otherwise, μ_q^α is reduced. Similarly, in Eq. (4.56), if the demand for energy at node j exceeds its budget E_j, the energy constraint is violated. Thus, the relay price μ_j^β is raised. Otherwise, μ_j^β is reduced.

We summarize our algorithm in Table 4.1, where clique q and node i are deemed as entities capable of computing and communicating.

Clique Price Update (by clique q): At times $t = 1, 2, \ldots$

1 Receive rates $x_i(t)$ from all flows f_i where $f_i \cap q \neq \emptyset$

2 Update price

$\mu_q^\alpha(t+1) = [\mu_q^\alpha(t) + \gamma(\sum_{f_i \cap q \neq \emptyset} x_i(t) A_{qi} - C_q)]^+$

3 Send $\mu_q^\alpha(t+1)$ to all flows f_i where $f_i \cap q \neq \emptyset$

Relay Price Update (by node j): At times $t = 1, 2, \ldots$

1 Receive rates $x_i(t)$ from all flows f_i where $j \in H(f_i)$

2 Update price

$\mu_j^\beta(t+1) = [\mu_j^\beta(t) + \gamma(\sum_{i:j \in H(f_i)} x_i(t) B_{ji} - E_j)]^+$

3 Send $\mu_j^\beta(t+1)$ to all flows f_i where $j \in H(f_i)$

Rate Update (by node i): At times $t = 1, 2, \ldots$

1 Receive channel prices $\mu_q^\alpha(t)$ from q where $f_i \cap q \neq \emptyset$

2 Receive relay prices $\mu_j^\beta(t)$ from j where $j \in H(f_i)$

3 Calculate

$\lambda_i^\alpha = \sum_{q: f_i \cap q \neq \emptyset} \mu_q^\alpha A_{qi}$

$\lambda_i^\beta = \sum_{j: j \in H(f_i)} \mu_j^\beta B_{ji}$

5 Adjust rate

$x_i(t+1) = x_i(\lambda_i^\alpha, \lambda_i^\beta)$

4 Send $x_i(t+1)$ to corresponding cliques.

Table 4.1: Distributed algorithm

We now show the property of this distributed iterative algorithm. Let us define $Y(i) = \sum_q A_{qi} + \sum_j B_{ji}$, and $\bar{Y} = \max_{i\in\mathcal{N}} Y(i)$. Further, we define $U(q) = \sum_{i\in\mathcal{N}} A_{qi}$ and $\bar{U} = \max_{q\in\mathcal{Q}} U(q)$; $V(j) = \sum_{i\in\mathcal{N}} B_{ji}$ and $\bar{V} = \max_{j\in\mathcal{N}} V(j)$; $\bar{Z} = \max\{\bar{U}, \bar{V}\}$. Let $\kappa_i = (x_i^M - x_i^m)^2$ and $\bar{\kappa} = \max_{i\in\mathcal{N}} \kappa_i$.

Theorem 4.5.1. ***(Global convergence and optimality)****. Suppose $0 < \gamma < 2/\bar{\kappa}\bar{Y}\bar{Z}$. Starting from any initial rates $\boldsymbol{x}^m \le \boldsymbol{x}(0) \le \boldsymbol{x}^M$, and prices $\boldsymbol{\mu}^\alpha(0) \ge 0$ and $\boldsymbol{\mu}^\beta(0) \ge 0$, every accumulation point $(\boldsymbol{x}^*, \boldsymbol{\mu}^{\alpha*}, \boldsymbol{\mu}^{\beta*})$ of the sequence $(\boldsymbol{x}(t), \boldsymbol{\mu}^\alpha(t), \boldsymbol{\mu}^\beta(t))$ generated by the algorithm in Table 4.1 is primal-dual optimal.*

4.6 Proof of Theorem 4.5.1

Proof. First, the dual objective function $D(\mu)$ is convex, lower bounded, and continuously differentiable.

For any price vector $(\boldsymbol{\mu}^\alpha, \boldsymbol{\mu}^\beta)$ define $\psi_i(\boldsymbol{\mu}^\alpha, \boldsymbol{\mu}^\beta)$ as

$$\psi_i(\boldsymbol{\mu}^\alpha, \boldsymbol{\mu}^\beta) = \begin{cases} (x_i(\lambda_i^\alpha, \lambda_i^\beta) - x_i^m)^2 & \text{if } \frac{1}{x_i^M} \le \lambda_i^\alpha + \lambda_i^\beta \le \frac{1}{x_i^m} \\ 0 & \text{otherwise} \end{cases}$$

where λ_i^α and λ_i^β are defined as in (4.19), (4.20) and x_i is defined as in (3.19).

Now we define $\boldsymbol{H}(\boldsymbol{\mu}^\alpha, \boldsymbol{\mu}^\beta) = diag(\psi_f(\boldsymbol{\mu}^\alpha, \boldsymbol{\mu}^\beta), i \in \mathcal{N})$ be a $|\mathcal{N}| \times |\mathcal{N}|$ diagonal matrix with diagonal elements $\psi_i(\boldsymbol{\mu}^\alpha, \boldsymbol{\mu}^\beta)$. Note that $0 \le \psi_i(\boldsymbol{\mu}^\alpha, \boldsymbol{\mu}^\beta) \le \kappa_i$.

Let $\frac{\partial \boldsymbol{x}}{\partial \boldsymbol{\mu}^\alpha}(\boldsymbol{\mu}^\alpha, \boldsymbol{\mu}^\beta)$ denote the $|\mathcal{N}| \times |\mathcal{Q}|$ Jacobian matrix whose (i, q) element is $(\frac{\partial x_i(\boldsymbol{\mu}^\alpha, \boldsymbol{\mu}^\beta)}{\partial \mu_q^\alpha})$, where

$$\frac{\partial x_i(\boldsymbol{\mu}^\alpha, \boldsymbol{\mu}^\beta)}{\partial \mu_q^\alpha} = \tag{4.57}$$

$$\begin{cases} -A_{qi}(x_i(\lambda_i^\alpha, \lambda_i^\beta) - x_i^m)^2 & \text{if } \frac{1}{x_i^M} \leq \lambda_i^\alpha + \lambda_i^\beta \leq \frac{1}{x_i^m} \\ 0 & \text{otherwise} \end{cases}$$

Let $\frac{\partial \boldsymbol{x}}{\partial \boldsymbol{\mu}^\beta}(\boldsymbol{\mu}^\alpha, \boldsymbol{\mu}^\beta)$ denote the $|\mathcal{N}| \times |\mathcal{N}|$ Jacobian matrix whose (i, j) element is $(\frac{\partial x_i(\boldsymbol{\mu}^\alpha, \boldsymbol{\mu}^\beta)}{\partial \mu_j^\beta})$, where

$$\frac{\partial x_i(\boldsymbol{\mu}^\alpha, \boldsymbol{\mu}^\beta)}{\partial \mu_j^\beta} = \tag{4.58}$$
$$\begin{cases} -B_{ji}(x_i(\lambda_i^\alpha, \lambda_i^\beta) - x_i^m)^2 & \text{if } \frac{1}{x_i^M} \leq \lambda_i^\alpha + \lambda_i^\beta \leq \frac{1}{x_i^m} \\ 0 & \text{otherwise} \end{cases}$$

From (4.53), (4.54) we have,

$$\nabla_{\boldsymbol{\mu}^\alpha} D(\boldsymbol{\mu}^\alpha, \boldsymbol{\mu}^\beta) = \boldsymbol{C} - \boldsymbol{A}\boldsymbol{x}(\lambda_i^\alpha, \lambda_i^\beta) \tag{4.59}$$

$$\nabla_{\boldsymbol{\mu}^\beta} D(\boldsymbol{\mu}^\alpha, \boldsymbol{\mu}^\beta) = \boldsymbol{E} - \boldsymbol{B}\boldsymbol{x}(\lambda_i^\alpha, \lambda_i^\beta) \tag{4.60}$$

Using (4.57), we have

$$[\frac{\partial \boldsymbol{x}}{\partial \boldsymbol{\mu}^\alpha}(\boldsymbol{\mu}^\alpha, \boldsymbol{\mu}^\beta)] = -\boldsymbol{H}(\boldsymbol{\mu}^\alpha, \boldsymbol{\mu}^\beta)\boldsymbol{A}^T \tag{4.61}$$

$$[\frac{\partial \boldsymbol{x}}{\partial \boldsymbol{\mu}^\beta}(\boldsymbol{\mu}^\alpha, \boldsymbol{\mu}^\beta)] = -\boldsymbol{H}(\boldsymbol{\mu}^\alpha, \boldsymbol{\mu}^\beta)\boldsymbol{B}^T \tag{4.62}$$

Thus the Hessian of D is given as follows.

$$\nabla^2_{\boldsymbol{\mu}^\alpha \boldsymbol{\mu}^\alpha} D(\boldsymbol{\mu}^\alpha, \boldsymbol{\mu}^\beta) = \boldsymbol{A}\boldsymbol{H}(\boldsymbol{\mu}^\alpha, \boldsymbol{\mu}^\beta)\boldsymbol{A}^T \tag{4.63}$$

$$\nabla^2_{\boldsymbol{\mu}^\beta \boldsymbol{\mu}^\beta} D(\boldsymbol{\mu}^\alpha, \boldsymbol{\mu}^\beta) = \boldsymbol{B}\boldsymbol{H}(\boldsymbol{\mu}^\alpha, \boldsymbol{\mu}^\beta)\boldsymbol{B}^T \tag{4.64}$$

$$\nabla^2_{\boldsymbol{\mu}^\alpha \boldsymbol{\mu}^\beta} D(\boldsymbol{\mu}^\alpha, \boldsymbol{\mu}^\beta) = \boldsymbol{A}\boldsymbol{H}(\boldsymbol{\mu}^\alpha, \boldsymbol{\mu}^\beta)\boldsymbol{B}^T \tag{4.65}$$

$$\nabla^2_{\boldsymbol{\mu}^\beta \boldsymbol{\mu}^\alpha} D(\boldsymbol{\mu}^\alpha, \boldsymbol{\mu}^\beta) = \boldsymbol{B}\boldsymbol{H}(\boldsymbol{\mu}^\alpha, \boldsymbol{\mu}^\beta)\boldsymbol{A}^T \tag{4.66}$$

Now we show that ∇D is Lipschitz with

$$||\nabla D(\boldsymbol{\nu}) - \nabla D(\boldsymbol{\mu})||_2 \leq \bar{\kappa}\bar{Y}\bar{Z}||\boldsymbol{\nu} - \boldsymbol{\mu}||_2 \tag{4.67}$$

for all $\boldsymbol{\mu}, \boldsymbol{\nu} \geq 0$.

First, given any $\boldsymbol{\mu}, \boldsymbol{\nu} \geq 0$, using Taylor theorem we have

$$\nabla D(\boldsymbol{\nu}) - \nabla D(\boldsymbol{\mu}) = \nabla^2 D(\boldsymbol{\omega})(\boldsymbol{\nu} - \boldsymbol{\mu}) = \tag{4.68}$$

for some $\boldsymbol{\omega} = t\boldsymbol{\mu} + (1-t)\boldsymbol{\nu} \geq 0$, $t \in [0, 1]$.

Hence,

$$||\nabla D(\boldsymbol{\nu}) - \nabla D(\boldsymbol{\mu})||_2 \leq ||\nabla^2 D(\boldsymbol{\omega})||_2 \cdot ||\boldsymbol{\nu} - \boldsymbol{\mu}||_2 \tag{4.69}$$

Now we show that $||\nabla^2 D(\boldsymbol{\omega})||_2 \leq \kappa\bar{Y}\bar{Z}$.

First

$$||\nabla^2 D(\boldsymbol{\omega})||_2^2 \leq ||\nabla^2 D(\boldsymbol{\omega})||_\infty \cdot ||\nabla^2 D(\boldsymbol{\omega})||_1 \tag{4.70}$$

Since $\nabla^2 D(\boldsymbol{\omega})$ is symmetric, we have

$$||\nabla^2 D(\boldsymbol{\omega})||_\infty = ||\nabla^2 D(\boldsymbol{\omega})||_1 \tag{4.71}$$

Hence,

$$||\nabla^2 D(\boldsymbol{\omega})||_2 \leq ||\nabla^2 D(\boldsymbol{\omega})||_\infty = \max_r \sum_{r'} [\nabla^2 D(\boldsymbol{\omega})]_{rr'} \tag{4.72}$$

Actually,

$$[\nabla^2 D(\boldsymbol{\omega})]_{rr'} =$$

$$\begin{cases} \sum_i \psi_i(\boldsymbol{\omega}) A_{ri} A_{r'i} & \text{if} \quad r, r' \in [0, Q-1] \\ \sum_i \psi_i(\boldsymbol{\omega}) A_{ri} B_{(r'-Q)i} & \text{if} \quad r \in [0, Q-1], \\ & \qquad r' \in [Q, Q+N-1] \\ \sum_i \psi_i(\boldsymbol{\omega}) B_{(r-Q)f} A_{r'i} & \text{if} \quad r \in [Q, Q+N-1], \\ & \qquad r' \in [0, N-1] \\ \sum_i \psi_i(\boldsymbol{\omega}) B_{(r-Q)f} B_{(r'-Q)i} & \text{if} \quad r, r' \in [Q, Q+N-1] \end{cases}$$

Now we have,

$$\sum_{r'} [\nabla^2 D(\boldsymbol{\omega})]_{rr'} =$$
$$\begin{cases} \sum_i \left[\begin{array}{l} \psi_i(\boldsymbol{\omega}) A_{ri} (\sum_{r'=0}^{Q-1} A_{r'i} \\ + \sum_{r'=0}^{N-1} B_{r'i}) \end{array} \right] & \text{if } r \in [0, Q-1] \\ \sum_i \left[\begin{array}{l} \psi_i(\boldsymbol{\omega}) B_{(r-L)i} (\sum_{r'=0}^{Q-1} A_{r'i} \\ + \sum_{r'=0}^{N-1} B_{r'i}) \end{array} \right] & \text{if } r \in \left[\begin{array}{l} Q, Q+ \\ N-1 \end{array} \right] \end{cases}$$

As $Y(i) = \sum_q A_{qi} + \sum_j B_{ji}$, and $\bar{Y} = \max_{i \in \mathcal{N}} Y(i)$, we have

$$\sum_{r'} [\nabla^2 D(\boldsymbol{\omega})]_{rr'} \leq \begin{cases} \bar{Y} \sum_i \psi_i(\boldsymbol{\omega}) A_{ri} & \text{if } r \in [0, Q-1] \\ \bar{Y} \sum_i \psi_i(\boldsymbol{\omega}) B_{(r-L)i} & \text{if } r \in [Q, Q+N-1] \end{cases} \tag{4.73}$$

Also because $U(q) = \sum_{i \in \mathcal{N}} A_{qi}$ and $\bar{U} = \max_{q \in \mathcal{Q}} U(q)$; $V(j) = \sum_{i \in \mathcal{N}} B_{ji}$ and $\bar{V} = \max_{j \in \mathcal{N}} V(j)$; $\bar{Z} = \max\{\bar{U}, \bar{V}\}$; $\bar{\kappa} = \max_{i \in \mathcal{N}} \kappa_i$, we have

$$\max_r \sum_{r'} [\nabla^2 D(\boldsymbol{\omega})]_{rr'} \leq \bar{\kappa} \bar{Y} \bar{Z}. \tag{4.74}$$

Since the dual objective function D is lower bounded and ∇D is Lipschitz, then any accumulation point $(\mu^{\alpha *}, \mu^{\beta *})$ of the sequence $(\mu^{\alpha}(t), \mu^{\beta}(t))$ generated by the gradient projection algorithm for the dual problem is dual optimal. Provided that $0 < \gamma < 2/\bar{\kappa} \bar{Y} \bar{Z}$, then let $(\mu^{\alpha}(t), \mu^{\beta}(t))$ be a

subsequence converging to $(\mu^{\alpha*}, \mu^{\beta*})$. Note that $x(\mu^{\alpha}, \mu^{\beta})$ is continuous. Thus, the subsequence $\{x(t)\}$ converges to the primal optimal rate x^*. □

Though there exists a unique maximizer $\boldsymbol{x}^*$ to the problem **P**, there may be multiple dual optimal prices, since only the flow price is constrained at optimality according to $U_f'(x_f^*) = \lambda_i^{\alpha*} + \lambda_i^{\beta*}$. Theorem 4.5.1 does not guarantee convergence to a unique vector $(\boldsymbol{x}^*, \boldsymbol{\mu}^{\alpha*}, \boldsymbol{\mu}^{\beta*})$, though any convergent subsequence leads to the optimal rate allocation $\boldsymbol{x}^*$.

4.6.1 Implementation issues

In the above iterative algorithm, a maximal clique is regarded as a network element that can carry out certain network functions. In particular, it assumes that a maximal clique q can perform the following tasks for price calculation and resource allocation: (1) obtain the aggregated bandwidth demand within the clique q; (2) calculate the per-clique shadow price μ_q^{α}; and (3) notify the price μ_q^{α} to the flows that pass through it. However, a maximal clique is only a concept defined based on subflow contention graph. To deploy the algorithm in an actual ad hoc network, the above tasks of a maximal clique need to be carried out by the nodes that constitute the clique in a distributed fashion.

The price pair based self-optimizing algorithm needs the support from a virtual credit system to enforce the pricing signal. As this paper mainly focuses on how to calculate the incentive price, the design of such a virtual credit system is beyond the scope of this paper. Interesting readers are referred to [5] [6] for these issues.

4.7 Simulation Results

We illustrate our price pair mechanism and the distributed algorithm via simulation. The network used in the simulation has 20 nodes deployed on a 600×600 square meter region as shown in Fig. 4.4. Such a network has 10 cliques that represent maximal contending regions in the wireless

channel as shown in Table 4.3. Each node sets up a connection with a randomly selected destination and delivers traffic via shortest path routing. The flows and their routes are shown in Table 4.2. We use uniform achievable channel capacities $C_q = 1$Mbps for all cliques q in the simulation. The default initial energy level for all nodes is 432 Joules. The transmission energy consumption is 2×10^{-7}J/bit and the receiving energy consumption is 10^{-7}J/bit. The network is expected to last 2 hours with a energy budget of 0.06J/sec for each node. The minimum and maximum rate requirement of flows are $\boldsymbol{x}_i^m = 0$Mbps and $\boldsymbol{x}_i^M = 1$Mbps for all flows f_i.

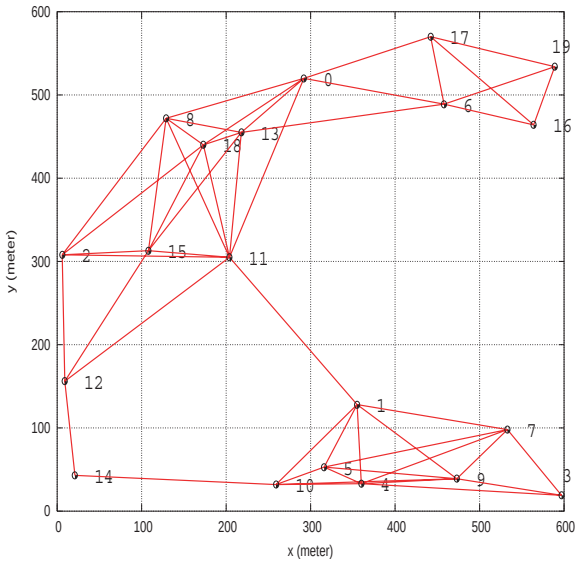

Figure 4.4: Random topology used in the simulation

4.7.1 Convergence

We first show the convergence behavior of our iterative algorithm. In the simulation, the initial values are $x_i(0) = 0$ Kbps, $\mu_q^{\alpha}(0) = \mu_j^{\beta}(0) = 0.01$ for all i, q, j. The step size that ensures the convergence is set to $\gamma = 10^{-6}$. As shown in Fig. 4.5, the algorithm converges to a global network equilibrium within about 300 iterations. At the equilibrium point, the optimal resource allocation and prices are listed in Table 4.4. We observe that node 1, 10, 11 and 17 are the bottleneck relaying nodes and clique 1 is the bottleneck channel resource. They, therefore, have positive prices. We have also experimented with different sets of initial values for the rates and prices, and the results

Flow ID	Route
0	$0 \rightarrow 8 \rightarrow 15$
1	$1 \rightarrow 10$
2	$2 \rightarrow 8 \rightarrow 0 \rightarrow 6 \rightarrow 19$
3	$3 \rightarrow 4 \rightarrow 1 \rightarrow 11$
4	$4 \rightarrow 1 \rightarrow 11 \rightarrow 0 \rightarrow 6$
5	$5 \rightarrow 1 \rightarrow 11 \rightarrow 0 \rightarrow 17$
6	$6 \rightarrow 0 \rightarrow 11 \rightarrow 12 \rightarrow 14$
7	$7 \rightarrow 1 \rightarrow 10$
8	$8 \rightarrow 13$
9	$9 \rightarrow 10$
10	$10 \rightarrow 14 \rightarrow 12$
11	$11 \rightarrow 1$
12	$12 \rightarrow 11$
13	$13 \rightarrow 18$
14	$14 \rightarrow 12 \rightarrow 11$
15	$15 \rightarrow 11$
16	$16 \rightarrow 6 \rightarrow 0 \rightarrow 11 \rightarrow 1 \rightarrow 4$
17	$17 \rightarrow 19$
18	$18 \rightarrow 0 \rightarrow 6$
19	$19 \rightarrow 6 \rightarrow 0 \rightarrow 11 \rightarrow 1 \rightarrow 4$

Table 4.2: Flows and their routes

Clique ID	Subflows in the clique
0	$(0,6),(0,8),(0,11),(0,17),(0,18),(6,16),(6,19)$ $(17,19)$
1	$(0,6),(0,8),(0,11),(0,17),(0,18),(1,11),(2,8)$ $(8,13),(8,15),(11,12),(11,15),(13,18)$
2	$(0,6),(0,8),(0,11),(0,17),(0,18),(6,16),(6,19)$ $(8,13),(13,18)$
3	$(0,11),(1,11),(2,8),(8,15),(11,12),(11,15)$ $(12,14)$
4	$(0,11),(1,10),(1,11),(11,12),(11,15),(12,14)$
5	$(1,10),(1,11),(10,14),(11,12),(12,14)$
6	$(1,10),(1,11),(9,10),(10,14),(12,14)$
7	$(0,11),(1,4),(1,5),(1,7),(1,10),(1,11),(11,12)$ $(11,15)$
8	$(1,4),(1,5),(1,7),(1,10),(1,11),(10,14),(11,12)$
9	$(1,4),(1,5),(1,7),(1,10),(1,11),(3,4),(9,10)$ $(10,14)$

Table 4.3: Maximal Cliques

have been coherent with our illustrated example.

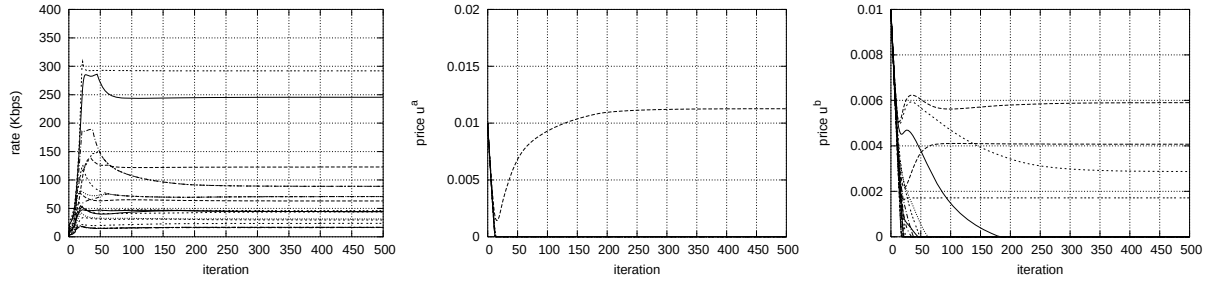

(a) Flow Rates x_i ($i \in \mathcal{N}$) (b) Channel Price μ_q^α ($q \in \mathcal{Q}$) ($j \in \mathcal{N}$) (c) Relay Price μ_j^β

Figure 4.5: Convergence of the algorithm on the network shown in Fig. 4.1

4.7.2 Impact of resource capacity

We further illustrate the roles and interactions of the channel and relay prices, by repeating the simulation with different values of energy budget $\boldsymbol{E}$ and channel capacity $\boldsymbol{C}$. In the experiment, the energy budgets of two bottleneck nodes 1 and 11 are changed to $E_1 = E_{11} = 0.1$J/sec. The convergence behavior and the equilibrium results are shown in Fig. 4.6 and Table 4.5 respectively. We observe that the relay prices at node 1 and 11 have been decreasing, since more energy is available at these two nodes, causing less competition with respect to energy. At the same time, we also observe that the channel price has increased, since the decreasing relay cost increases the rate demand and causes more competition for the channel.

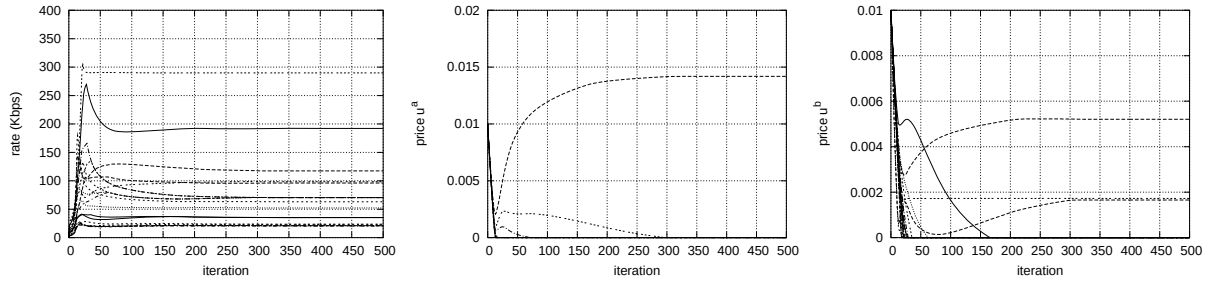

(a) Flow Rates x_i ($i \in \mathcal{N}$) (b) Channel Price μ_q^α ($q \in \mathcal{Q}$) ($j \in \mathcal{N}$) (c) Relay Price μ_j^β

Figure 4.6: Convergence when more energy is available at node 11 and 1.

Node/Flow ID	Flow rate (Kbps)	Relay price	Clique ID	Channel price
0	39.03	0	0	0.000000
1	162.03	0.005898	1	0.011267
2	26.02	0	2	0.000000
3	35.02	0	3	0.000000
4	19.89	0	4	0.000000
5	19.49	0	5	0.000000
6	24.04	0	6	0.000000
7	91.26	0	7	0.000000
8	78.07	0	8	0.000000
9	189.37	0	9	0.000000
10	150.01	0.004073		
11	52.68	0.002871		
12	72.99	0		
13	78.07	0		
14	66.28	0		
15	72.99	0		
16	19.89	0		
17	490.25	0.001713		
18	39.03	0		
19	19.89	0		

Table 4.4: Equilibrium rates and prices

Node/Flow ID	Flow rate (Kbps)	Relay price	Clique ID	Channel price
0	35.24	0.000000	0	0.000000
1	117.45	0.001654	1	0.014187
2	23.49	0.000000	2	0.000000
3	52.21	0.000000	3	0.000000
4	21.04	0.000000	4	0.000000
5	20.30	0.000000	5	0.000000
6	23.49	0.000000	6	0.000000
7	98.34	0.000000	7	0.000000
8	70.48	0.000000	8	0.000000
9	192.10	0.000000	9	0.000000
10	96.05	0.005206		
11	63.12	0.000000		
12	70.48	0.000000		
13	70.48	0.000000		
14	70.48	0.000000		
15	70.48	0.000000		
16	21.04	0.000000		
17	289.84	0.001725		
18	35.24	0.000000		
19	21.04	0.000000		

Table 4.5: Equilibrium rates and prices when more energy is available at node 11 and 1.

We now show two special cases where the role of one price in the price pair can implicitly be assumed by the other. In the first case, $E_i = 0.04$J/sec for all i. The result is plotted in Fig. 4.7. From the figure, we observe that the channel prices eventually converge to 0, with the increase of relay prices. It shows that in this scenario, the energy constraints are the dominant factors in the network. Thus, when the relay prices give adequate incentives to these energy constrained nodes to relay appropriate amount of traffic, the wireless channel is naturally shared among all nodes in a fair manner. In the second case, we show a scenario where the shared wireless channel capacity is the dominant factor. In this experiment, the energy budget is set to be sufficiently large: $E_i = 0.2$J/sec for all i. As shown in Fig. 4.8, we can observe that the channel prices play a dominant role in arbitrating resource contention among different nodes.

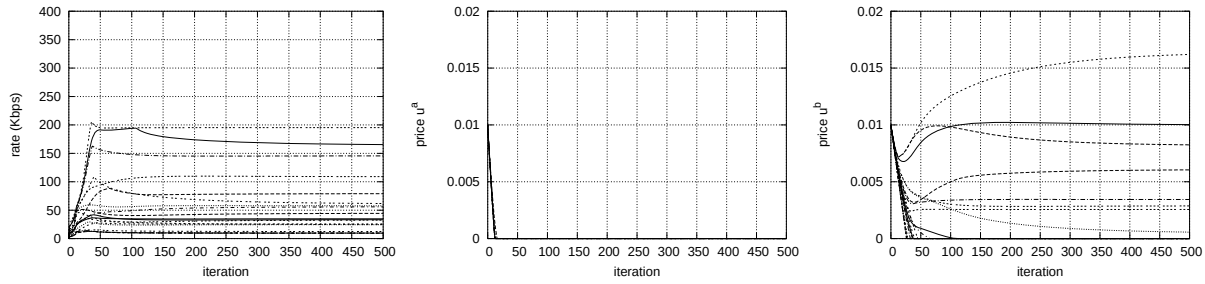

(a) Flow Rates x_i ($i \in \mathcal{N}$) (b) Channel Price μ_q^α ($q \in \mathcal{Q}$) ($j \in \mathcal{N}$) (c) Relay Price μ_j^β

Figure 4.7: Energy is dominant factor

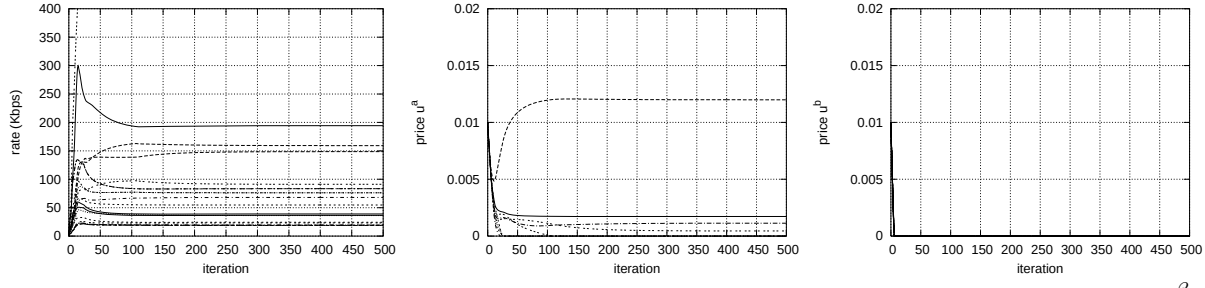

(a) Flow Rates x_i ($i \in \mathcal{N}$) (b) Channel Price μ_q^α ($q \in \mathcal{Q}$) ($j \in \mathcal{N}$) (c) Relay Price μ_j^β

Figure 4.8: Channel is dominant factor

4.7.3 Network performance with incentives

We now show the performance of the network as the price pair is used as incentives. In particular, we compare the case where all nodes follow the incentive signals with the case where there exist nodes that deviate from the signals. In the latter case, the node with ID 3 deviates from the price pair signal by increasing its transmission rate by 60 Kbps. Table 4.6 shows the results of such a comparison, including the following performance metrics:

- *Throughput* – the average transmission rate of a flow over the network operation time;
- *Cost* – the total cost (price $\times$ rate) over the network operation time, *i.e.*, $cost_i = \sum_t (\lambda_i^{\alpha}(t) + \lambda_i^{\beta}(t)) \times x_i(t)$;
- *Revenue* – the total revenue of a node from relaying, *i.e.*, $revenue_i = \sum_t \mu_i^{\beta}(t) \times \sum_j x_i(t) B_{ij}$;
- *Remaining energy* – the remaining energy at the end of network operation.

From the results, we have the following observations. First, from a single node point of view, though node 3 has a higher throughput when deviating from the incentive signals, it is also charged with a much higher cost, which leads to a decrease of net benefit (utility from throughput + revenue - cost) by 20233.08. Second, from the point of view of the entire network, the total utility of the network decreases from 78.27 to 77.31; the total remaining energy decreases from 3839.91J to 3701.55J. We can draw the conclusion that, a node that deviates from the price-pair incentive signal does not only cause the entire network to operate at a suboptimal point, but also decreases the net benefit of itself – which is unacceptable for a rational node.

To summarize our results of performance evaluations, when using price pairs as incentives, the localized distributed algorithm at each node correctly converges to network operating points that are optimal, for the benefits of both individual nodes and the entire network.

	Follow incentives				Deviate incentives			
ID	Throughput	Cost	Revenue	Remaining energy	Throughput	Cost	Revenue	Remaining energy
0	44.37	7197.57	209.89	15.27	43.68	7197.58	138.41	45.77
1	63.00	7197.49	25440.83	0.41	39.07	7197.92	47161.32	0.00
2	29.58	7197.30	1.49	389.40	29.12	7197.32	1.48	390.05
3	31.40	7197.33	1.81	386.77	81.35	27443.76	14.20	314.84
4	16.60	7197.52	5.75	316.34	13.35	7197.71	33.37	217.79
5	16.14	7197.55	1.12	408.75	13.06	7197.74	0.99	413.18
6	23.49	7197.21	12.81	218.69	23.75	7197.19	11.51	236.12
7	45.91	7197.29	2.70	365.87	27.37	7197.77	2.17	392.57
8	89.21	7197.66	37.43	143.78	87.66	7197.68	36.08	148.47
9	245.19	7196.72	16.07	78.91	266.37	7196.65	18.40	48.42
10	122.52	7196.42	17545.82	0.59	133.15	7196.34	16141.22	0.62
11	43.59	7197.66	12586.52	0.71	36.36	7197.80	11148.97	0.74
12	70.68	7197.37	45.18	38.77	71.38	7197.34	39.57	27.98
13	89.41	7197.71	21.75	239.01	87.85	7197.72	19.99	242.36
14	70.59	7196.80	14.16	48.77	71.30	7196.79	15.67	24.60
15	70.80	7197.61	8.86	298.08	71.49	7197.59	8.07	297.59
16	16.60	7197.38	0.95	408.09	13.35	7197.57	0.85	412.76
17	291.35	7196.76	7391.43	0.82	292.89	7196.75	7352.58	0.82
18	44.31	7197.50	7.64	303.80	43.66	7197.52	7.52	305.86
19	16.59	7197.38	7.37	177.02	13.35	7197.57	7.18	180.91

Table 4.6: Comparison of Network Performance

4.8 Related Work

The problem of optimal and fair resource allocation has been extensively studied in the context of wireline networks. Among these works, pricing has been shown to be an effective approach to achieve distributed solution for flow control [20] [26] and service differentiation [10]. Simultaneously, game theory is applied to model resource sharing among multiple users, e.g., [42][7].

The main difference that distinguishes our work from the existing works is rooted in the unique characteristics of resource models of ad hoc network. First, the allocation mechanism needs to consider two types of resources, namely, the shared channel and the private resource such as energy. Second, due to the location dependent contention and spatial reuse of the shared channel resource, the channel price is associated with a maximal clique in the subflow contention graph, rather than a wireline link. This presents a different pricing policy for end-to-end flows.

Incentives in wireless networks have stimulated much research interests. (e.g., in the context of ad hoc networks [5][39][41] and in wireless LAN [33]). In particular, the works in [5] [6] present

virtual credit based mechanisms to stimulate cooperation in ad hoc networks, where virtual credits (so called nuglets) are awarded for packet forwarding. Some approaches [4] [43] use a reputation based mechanism where selfish or misbehaving nodes are identified, isolated or punished. Our work distinguishes from the existing works in that, it does not only promote cooperation in packet forwarding, more importantly, it studies at what level of cooperation the network operates at its optimal point, and how to achieve such cooperation using pricing as incentives. Auction-based approach [8] has also been employed for incentives in ad hoc networks. The essential idea of this approach is that each relay node operates as a market, the users of the network put bids for their packets and will be charged accordingly, when the packets are forwarded. As an important approach of mechanism design, auction has been shown to have several important properties such as truthful bidding, social welfare maximization in single market. However, directly applying this approach to ad hoc network environments, where relaying nodes constitute multiple networked markets, these properties no longer hold. For example, user pay-off and social welfare are no longer maximized. And how much they deviate from the optimum is not clear. Our approach instead can be shown to achieve both user self optimization and global social welfare optimum (*i.e.*, Nash Bargaining Solution).

Noncooperative game theory has been used to model the relaying behavior among nodes in ad hoc networks in [39] [41]. By designing appropriate game strategies and analyzing the Nash Equilibrium of the corresponding relaying game, these works show the existence of a network operating point where node cooperation is promoted. In our work, Nash bargaining solution is used to characterize the global network operating point, which usually demonstrates more advantageous properties, such as Pareto optimality and fairness, than the usual Nash Equilibrium in a noncooperative game.

There are also previous works that address the issue of resource allocation [32] and use a price-based approach [11]. However, the ad hoc network models in these works do not consider the shared nature of the wireless channel, and thus their solutions are not able to capture the unique issues in wireless ad hoc networks. Moreover, the price-based distributed algorithm presented in

[32] only converges to a network optimum when its utility function takes certain a special form, and such a utility function does not satisfy the fairness axiom.

4.9 Summary

This chapter presents a price pair mechanism that both regulates greedy behaviors and incentivizes selfish users in ad hoc networks. A pair of prices is the centerpiece of this mechanism: (1) the channel price that reflects the unique characteristics of location dependent contention in ad hoc networks, and regulates the usage of shared wireless channel; (2) the relay price that gives incentives to reach the adequate level of cooperation with respect to traffic relay. By using such a price pair as a signal, the decentralized self-optimizing decisions at each individual node converges to the global network optimal operation point. Simulation results are also presented to validate our theoretical claims. We believe that we have reached an important milestone that integrates pricing and incentives strategies for channel access and traffic relays into the same coherent framework, which is a problem that has not been addressed previously before this work, especially when the objective is to converge to a desirable optimal operating point for the entire wireless ad hoc network.

4.10 Notations

Table I shows a summary of important notations introduced in this chapter.

Notation	Definition
$i, j \in \mathcal{N} = \{1, ..., N\}$	Network nodes
$f_i, R(f_i), D(f_i)$	The flow from source node i, f_i's relaying nodes and destination
$H(f_i)$	$R(f_i) \cup \{D(f_i), i\}$
$K(f_i)$	$H(f_i) - \{i\}$
$l \in \mathcal{L} = \{1, ..., L\}$	Wireless links
$q \in \mathcal{Q} = \{1, ..., Q\}$	Maximal cliques
$\boldsymbol{x} = (x_i, i \in \mathcal{N})$	Rate allocation vector
$\boldsymbol{x}^m, \boldsymbol{x}^M$	Minimum (or maximum) rate vector
$\boldsymbol{C} = (C_q, q \in \mathcal{Q})$	Clique capacity vector
$\boldsymbol{E} = (E_j, j \in \mathcal{N})$	Energy budget vector
$\boldsymbol{A} = (A_{qi})_{Q \times N}$	Channel constraint matrix
$\boldsymbol{B} = (B_{ji})_{N \times N}$	Energy constraint matrix

Table 4.7: Notations in Chapter 4

Chapter 5

Software Architecture and System Implementation

This chapter presents the software architecture and system implementation of our price-based resource allocation algorithm.

5.1 Software Architecture

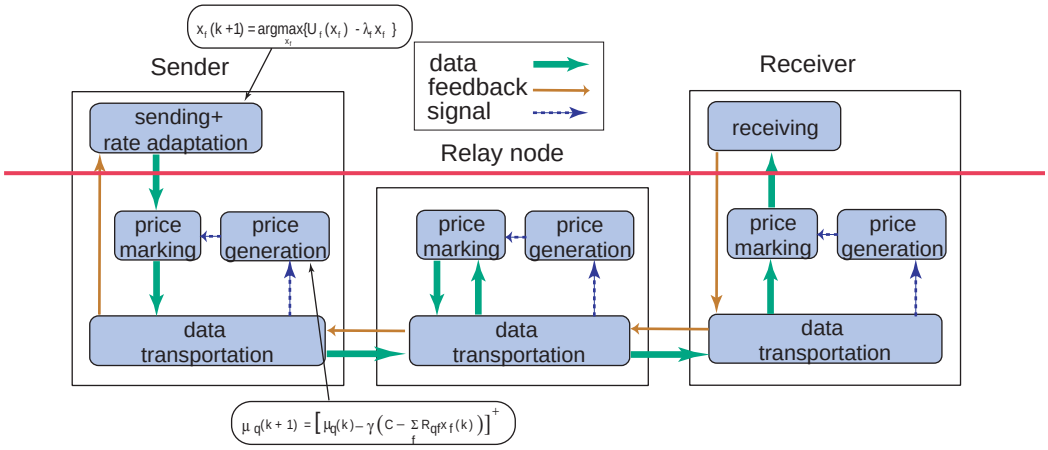

Figure 5.1: Overview of software architecture.

From Sec. 3.3, we know that the price-based resource allocation algorithm can be decomposed into two parts, *i.e.*, *price generation* and *rate adaptation*, which can be implemented at different network entities and different levels of the network stack. As shown in Fig. 5.1, the *price generation* sub-algorithm needs to be implemented at all hosts that participate in the data delivery of the network. While the *rate adaptation* sub-algorithm only needs to reside on the end hosts which are the source or the destination of the data delivery. Thus *price generation* can be implemented at the network level, while *rate adaptation* can be part of the transportation layer or at the application

level. To realize the price-based resource allocation, these two parts of the algorithm communicate via data delivery, feedback message, and internal control signals. As shown in Fig. 5.1, data packets are sent from the sender, and are marked with prices at each relaying node. The prices are aggregated along the path of data delivery. Once the data packets arrive at the receiver, the aggregated price information are retrieved from data packets and are sent back to the sender via feedback packets. Upon receiving the feedback packets, the sender adjusts its sending rate based on the received price information via *rate adaptation* algorithm.

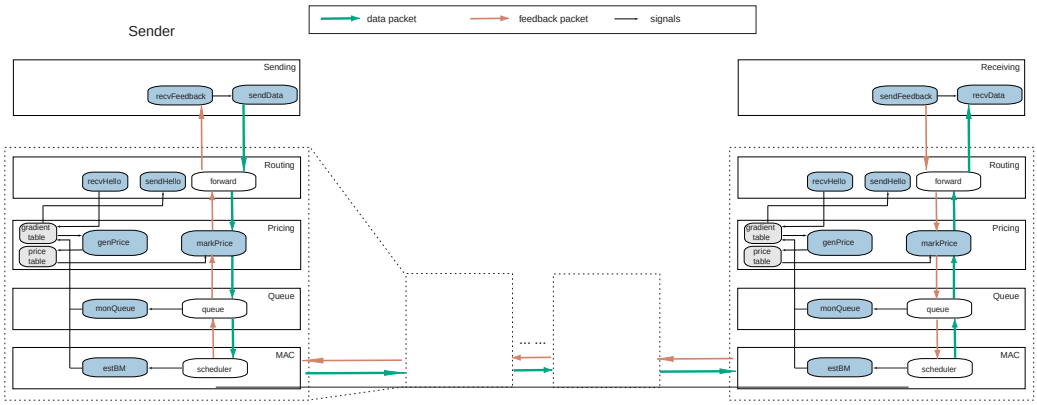

Figure 5.2: Details of software architecture.

Fig. 5.2 shows a detailed software architecture of the price-based resource allocation algorithm. In this figure, *rate adaptation* is implemented at both sender and receiver via four modules, which are responsible for sending(or receiving) data(or feedback) packets, respectively. *price generation* is implemented as several components at different levels. At the MAC level, the bandwidth estimator measures the local achievable bandwidth to each neighboring node. At the interface queue level, the monitor observes the backlogged traffic to each neighboring node. Working with the bandwidth estimator, the monitor generates the local gradient (difference between packet arrival rate and departure rate) for each wireless link between the node itself and its neighbors. At the routing level, HELLO messages communicate the local gradient information to its neighbors. The local gradient information, together with the gradient information received from HELLO messages, is maintained in a gradient cache table. The changes at the gradient cache table trigger the price update component, which reads the gradient information and calculates the clique prices.

These clique prices are maintained at a price cache table. When the price marking component receives data packets from the forwarding component, it calculates the per-hop price based on the information provided by price cache table, and adds it to the aggregated price from the upstream hops.

5.2 System Implementation

Based on the presented architecture, we implement the price-based resource allocation algorithm over Linux system with kernel version $2.6.*$[1], and wireless card driver $orinoco\_cs$. For better portability and extensibility, our system implementation aims to minimize the changes to the kernel. In particular, we implement the bandwidth estimator and the queue monitor as two kernel modules, while implement the rate adaptation and routing module in the user space.

5.2.1 Data structure

Two important data structures that are used to implement the price-based algorithm are:

- *gradient table*. Each entry in gradient table represents the difference between the traffic load and the achievable bandwidth of a wireless link. Each node maintains a gradient table which contains the information for wireless links within its k-hop neighborhood, where k is the parameter of the heuristic algorithm in Sec. 3.4.4.

```
typedef struct {
    in_addr_t src;
    in_addr_t dest;
    float grad;
    int hop;    // hop counts from this wireless link to me
    struct timeval grad_timestamp;
```

[1] In particular, version $2.6.5$ and $2.6.9$ are tested.

```
    struct timeval topo_timestamp;
} grad_entry_t;
```

- *price table.* Each entry in the price table maintains the information for clique construction and clique-based price computation.

```
typedef struct {
    unsigned int clique_ID;
    grad_entry_t **grad_info;   //gradient information
    int num_grad;
    double clique_price;
    struct timeval clique_timestamp;
    unsigned int is_master; //Am I a master node of this clique?
} price_entry_t;
```

Based on these two data structures, individual modules of the system are implemented as follows.

5.2.2 Router

Router is the most important module in the system. It is implemented in the user space. It consists of three threads, *recvHello*, *sendHello*, and *forward*. *sendHello* is controlled by a timer and sends HELLO messages periodically to the broadcast address in the subnet. The HELLO message contains the gradient information of wireless links that involve $k-1$ hop neighbors. *recvHello* module retrieves the gradient information from the HELLO message and updates the gradient table. *genPrice* is called when the gradient table is updated. *forward* module receives data and FEEDBACK packets, and forwards them according to the routing table. It marks the price onto the data packet based on its next hop. If the node is the final destination of the received packet, *forward* module will send it up to the *recvData* or *recvFeedback* module via internal socket.

5.2.3 Queue monitor

Queue monitor (*queueMon*) is implemented as a kernel module. It monitors the instantaneous queue length and provides such information to the user space. To get the instantaneous queue length, this module hooks two kernel queue management routines with our functions. In particular, it first retrieves the wireless device handler[2], and its queue discipline member *qdisc*. Then it replaces the function *enqueue* and *dequeue* of *qdisc* with two new functions that monitor the queue length and its changes. To provide the information of queue length to the user space, this module uses an *inode* device/file *queuelen*. Each entry in the *queuelen* device/file has a structure as follows. The module also hooks up two new file handlers *dread* and *dwrite*, which operate over the system memory instead of disk file. This approach provides low-overhead kernel and user space communication.

```
struct queue_len_entry {
    int qlen;
    __u32 dest;
    struct timeval tv;
};
```

5.2.4 Bandwidth estimator

When the queue length is short and close to zero, *queueMon* may not provide accurate local gradient information. In this case, the price-based resource allocation system uses *estBM* [35], to estimate the local achievable bandwidth of each wireless link. In particular, it monitors the historical data transmission and estimates the future achievable bandwidth with a moving window. The basic idea of its operation is illustrated in Fig. 5.3.

Under the IEEE 802.11 MAC protocol, at time t_r, when a packet from a particular wireless link becomes the head-of-line packet (*i.e.*, the first packet waiting to be transmitted), we claim

[2]The wireless adaptor device in the Linux system is usually configured to "eth1".

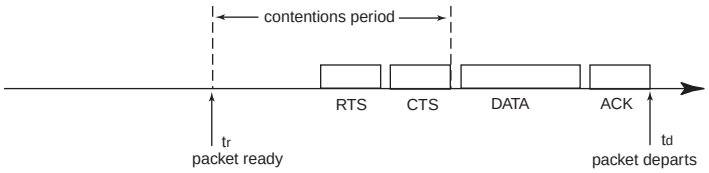

Figure 5.3: Measurement-based bandwidth estimation.

that the packet is *ready*. At time t_d, when the link layer acknowledgment is received, the packet *departs*. The transmission delay of this packet is then given as $t_d - t_r$, which includes a contention period. The contention period indicates the channel bandwidth used by packet transmissions of other wireless links within the contention region. The achievable bandwidth observed by this wireless link is then calculated as $\frac{z}{t_d - t_r}$, where z is the size of the packet. To achieve more accurate measurement results, we use a window of w packets to conduct the bandwidth estimation, *i.e.*, the bandwidth is estimated as $\frac{w \cdot z}{\sum_{i=1}^{w} t_d^i - t_r^i}$. The measurement-based bandwidth estimation takes into account the effect of physical layer interference and the inefficiency of MAC protocols, as it is based on the *scheduling results* of packet transmissions. *estBM* is implemented as a part of the wireless adaptor driver *orinoco_cs*, which is also a kernel module at the device level. To communicate the measurement results, similar approach is used as *queueMon*.

5.2.5 Data bit rate monitor

Information of data bit rate is used to calculate the price in multi-rate wireless networks. In order to get the channel bit rate, we use the wireless tool package *iwlib* developed by HP Lab. In particular, function *iw_sockets_open* returns a raw socket descriptor to the wireless driver at the kernel. And function *iw_print_bitrate* is used to get the instantaneous channel bit rate used by the current wireless adaptor.

5.3 Experiment Results

We deploy our system over IBM laptops (T41, T42, G41), with IEEE 802.11b-based Orinoco wireless adaptor. The wireless adaptors operate in *ad-hoc demo* mode using channel 6 in the experiments. The default algorithm parameters are: *moving average parameter* $\alpha = 0.1$, *step size* $\gamma = 0.0001$, and *HELLO message interval* 1 second. The default channel bit rate is 11Mbps.

Scenario 1

In the first set of experiments, we study the basic behavior of our algorithm. The experiment result in a single hop network is shown in Fig. 5.4 (b).

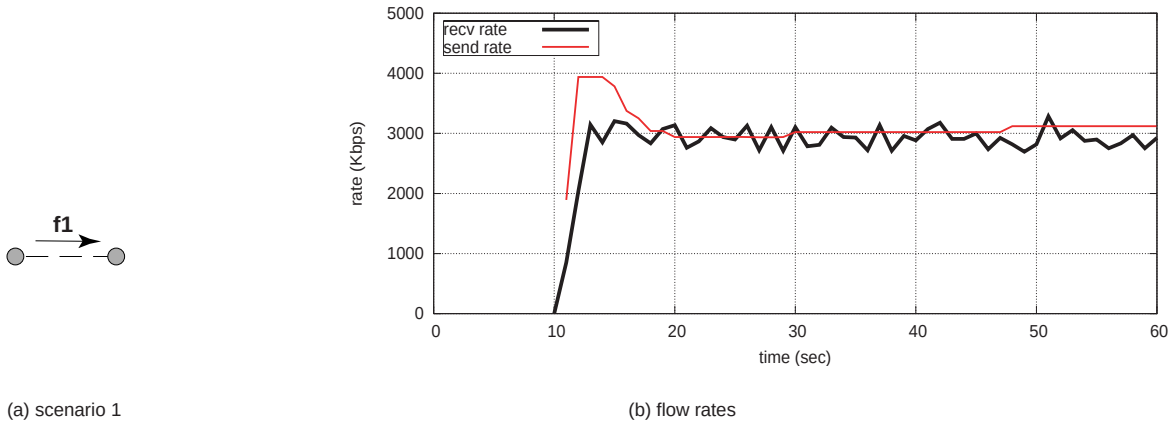

Figure 5.4: Single scenario.

In the multihop wireless network as shown in Fig. 5.5 (a), one flow travels 3 hops in the network. Its instantaneous sending rates and receiving rates are plotted in Fig. 5.5 (b).

From the figures, we have the following observations: (1) the instantaneous sending rate and receiving rate converges within 10 seconds; (2) the sending rate and the receiving rate closely matches at the equilibrium, which leads to very low loss rate;

Scenario 2

The network setup of the second experiment is shown in Fig. 5.6 (a). 4 wireless nodes in the network are all within the transmission range of each other. In this experiment, two flows start to

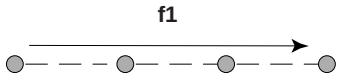

(a) scenario 3

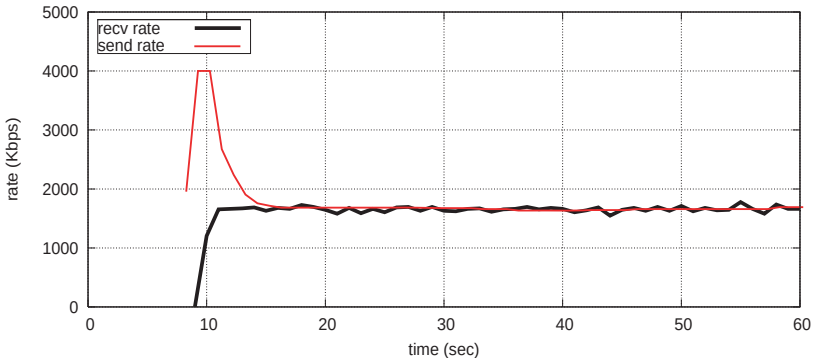

(a) flow rates

Figure 5.5: Multihop scenario.

transmit at different time instances. The experiment result is shown in Fig. 5.6 (b).

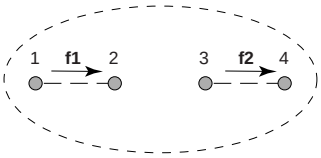

(a) scenario 2

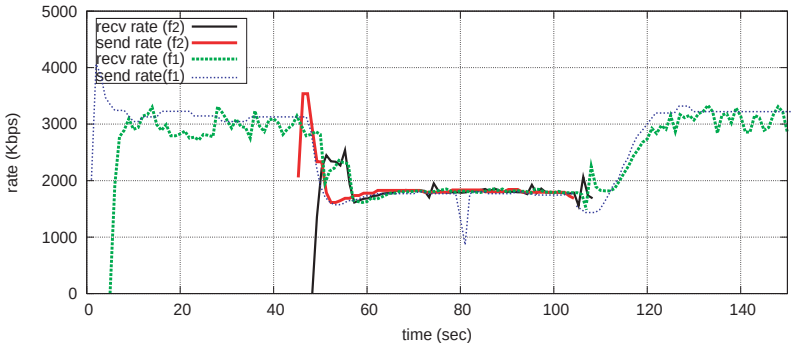

(b) flow rates

Figure 5.6: Scenario 2.

This result shows that: (1) the instantaneous sending rate and receiving rate converges even when traffic dynamically joins and departs the network. The time for convergence is within 10 seconds; (2) At equilibrium, the sending rates and throughput of both flows closely match, which means both flows share the wireless channel fairly.

Race condition

Now we perform our experiments in a special network topology: the *race condition* scenario as shown in Fig. 5.7 (a). In this scenario, node 1 and 4 are out of transmission range. They establish

two flows to node 2 and 3 respectively at different time instances. The instantaneous sending and receiving rates of these two flows are plotted in Fig. 5.7 (b).

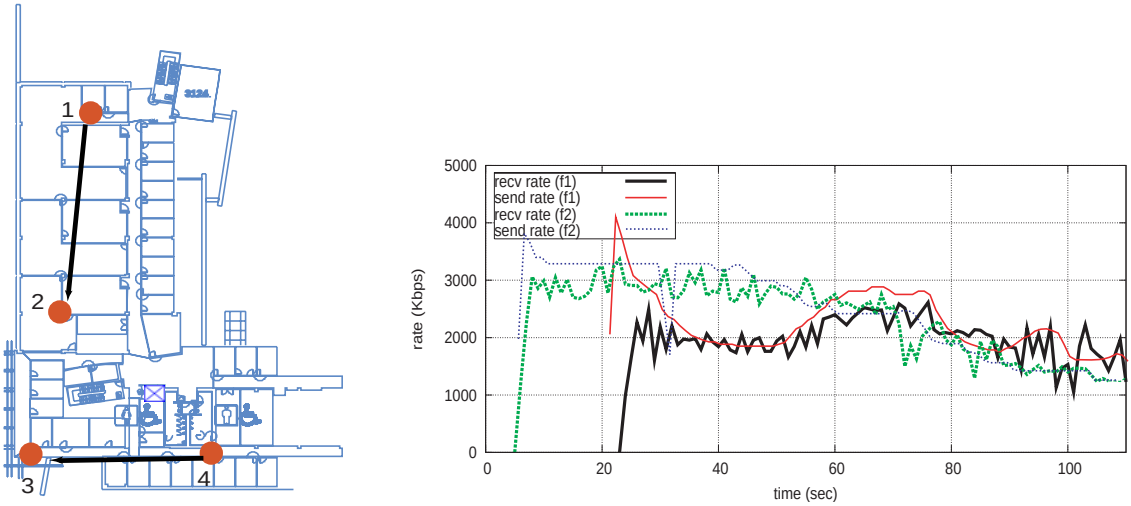

(a) race condition network setup

(b) flow rates

Figure 5.7: Race condition.

From the figure, we observe that the performance of our algorithm under the race condition suffers delayed convergence. This is because flow f_2 may capture the wireless channel at the beginning due to the unawareness of the RTS/CTS signals from the transmission of the other flow and the unfair backoff of IEEE 802.11. Once the gradient and price information is delivered by HELLO messages between node 1 and 4, these two flows share the same view of the network condition, thus converge to an equilibrium, where their transmission rates are the same. Although they have approximately the same throughput at equilibrium, slight difference and fluctuation can still be observed on their instantaneous throughput. This is caused by the unpredicted delay in the delivery of HELLO messages due to the possible channel capture situation. However, as we may observe from the results, the long term fairness can be guaranteed at the equilibrium via our price-based algorithm.

Multi-rate scenario

We proceed to evaluate the performance of our algorithm in multi-rate wireless networks. The first experiment is conducted on a simple topology as in Fig. 5.4 (a). In the experiment, we manually set the bit rate of the wireless node *fixed* at different levels (in the sequence of 2M, 1M, 11M, and 5.5Mbps). The instantaneous sending and receiving rates of this flow is shown in Fig. 5.8. From the result, we see that our algorithm quickly adapts to the channel bit rate adjustment, and converges to the new equilibrium rate allocations within 10 seconds. In the second experiment, we set the channel bit rate of the wireless node to *automatic adaptation* mode. In this mode, the channel bit rate will be automatically adjusted based on the channel condition. In the experiment, we move the wireless node to create a dynamic channel condition, so that the bit rate will be adjusted accordingly. The result is plotted in Fig. 5.9. From the figure, we have similar observation that our algorithm quickly responds to the channel bit rate changes.

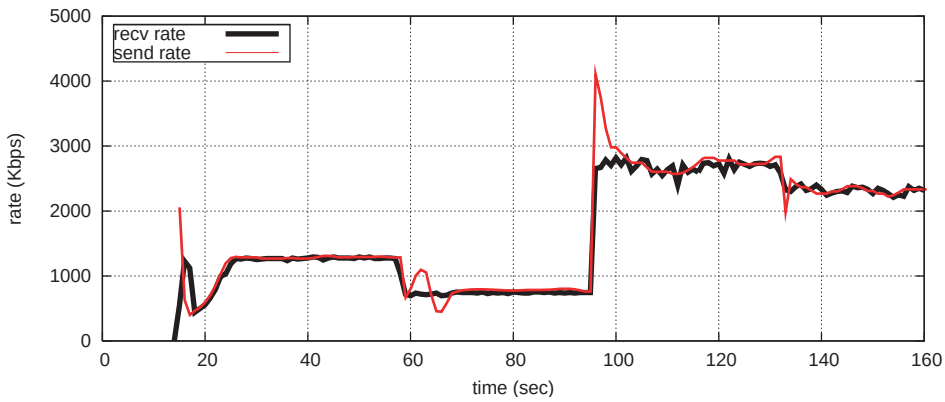

Figure 5.8: Multi-rate scenario 1.

Now we experiment on the network as shown in Fig. 5.6 (a). In this experiment, the channel bit rate of node 1 is fixed at 11Mbps, while the bit rate of node 3 is adjusted manually in the sequence of 11M, 5.5M, and 2Mbps. The experiment result is shown in Fig. 5.10. From the result, we have the following observations: (1) the sending and receiving rates of both flows converge within 10 second after the bit rate adjustment of node 3; (2) At equilibrium, when both node 1 and 3 have the same channel bit rate, these two flows share the same throughput. When their bit rates are differ-

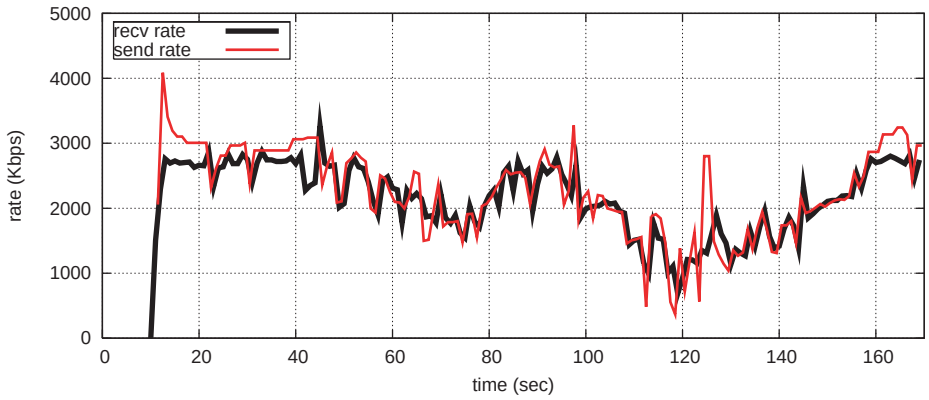

Figure 5.9: Multi-rate scenario (mobile).

ent, the throughput of these two flows are different. Moreover, their throughput ratio follows the ratio of the bit rates. This is a significant different result from the TCP performance in multi-rate wireless networks. As shown in Fig. 5.11, the throughput of both TCP flows are affected by the bit rate adjustment of node 3, even though the bit rate of flow 1 remains to be 11bps. This behavior is also called "performance anomaly" [28]. And it would significantly decrease the aggregated performance of the wireless network. Our experiment shows that our price-based resource allocation algorithm addresses this problem, improves the channel resource utilization, and provides proportional fair rate allocation to the contending flows in multi-rate wireless networks.

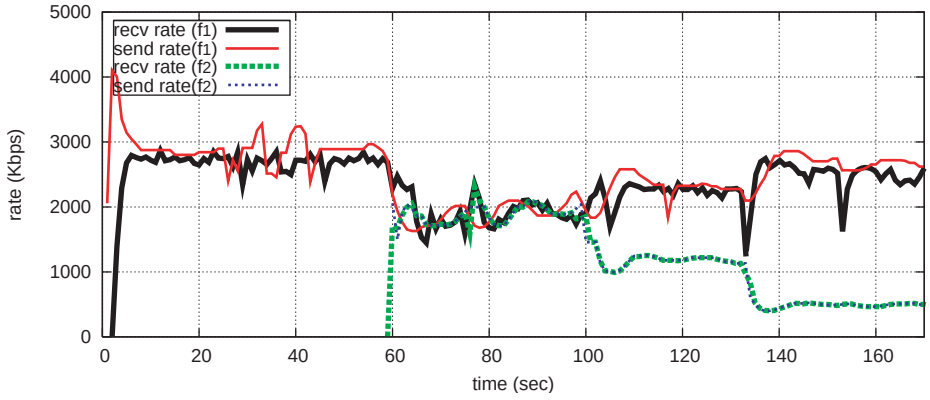

Figure 5.10: Multi-rate scenario 2.

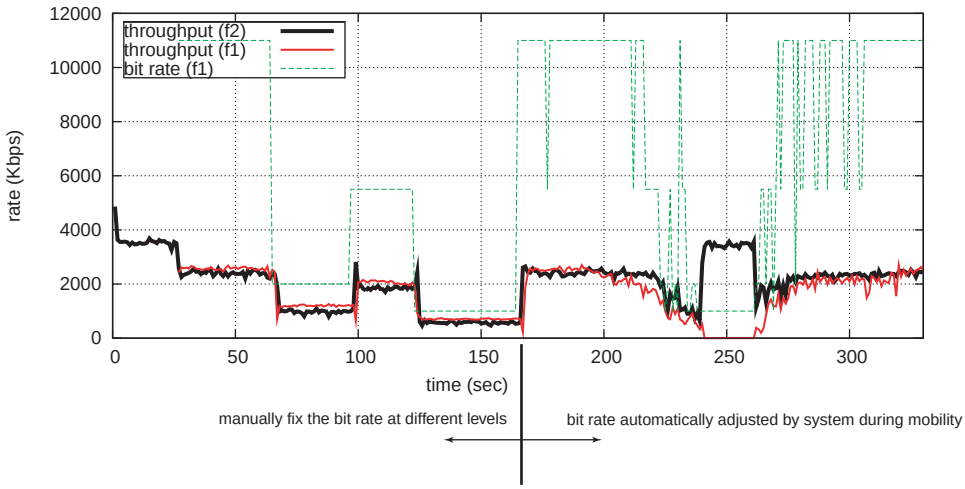

Figure 5.11: TCP performance in multi-rate wireless network.

5.4 Limitations of Price-based Resource Allocation in Wireless Networks

With the lessons learnt from real system implementation and performance evaluation, we now reach the stage to evaluate the limitations of our price-based resource allocation algorithm. In what follows, we present these limitations from three aspects, namely theoretical model, algorithm design, and system implementation.

- *Model Limitation*. Our clique-based pricing model is derived under the IEEE 802.11-style protocol model [13]. This model hides the complexity of wireless communication at the physical layer, and presents a simplified interface for algorithms and protocols at the higher layers. Inevitably, many characteristics of wireless communication in reality are not precisely revealed. For example, the interference between wireless communications is modelled as a binary state $(0, 1)$ in protocol model using interference range (*i.e.*, if either the source or the destination of wireless communications are within interference range, they form an edge in the contention graph). In reality, the interference effect can spread over a continuous space between 0 and 1 based on the location of the communicating nodes. Also the IEEE 802.11 protocol model shows that the contention graph of a multi-hop wireless network is

a bidirectional graph. In reality, the asymmetric traffic of data and acknowledgement frame in IEEE 802.11 may lead to a directional contention graph. Such simplifications in network modelling may result in inaccuracy in the resource constraint in our optimization problem. Our online measurement-based capacity estimation in the system design partially addresses this problem.

- *Algorithm Limitation*. The price-based resource allocation algorithm is an iterative algorithm. It can only converge to the equilibrium point where resource is optimally allocated, when the lifetime of the flow is long enough. For short-time flows, the algorithm may operate at a sub-optimal state.

- *Implementation Limitation*. To implement the price-based resource allocation algorithm, message communication among nodes is required to provide traffic load estimation and price signal feedback. Such message deliveries introduce overhead to the wireless network. Moreover, the maximal clique is an approximation of the maximal contention region of wireless communication. Its achievable capacity C_q depends on the number of active nodes within the contention region and is estimated online using queue monitor and bandwidth estimator. The imprecision and possible fluctuation in the measurement will affect the channel utilization and the stability of our algorithm.

The evaluation of our system limitations helps us to understand the best application scenarios for our price-based resource allocation system. In particular, our algorithm best fits static or semi-static wireless networks such wireless mesh networks. Further, the algorithm performs the best when the lifetime of the flow is more than 10sec.

Chapter 6

Concluding Remarks and Future Directions

6.1 Concluding Remarks

We conclude the main contributions of this dissertation as follows.

- We presented a novel price-based resource allocation framework based on an analytical pricing model that is specifically designed for the unique characteristics of multi-hop wireless ad hoc networks. The original contribution incorporated in the pricing model is the association of shadow prices with the *maximal cliques* in the contention graph model, rather than with individual links as in wireline networks. Based on insights brought forth by such strategies, the algorithms proposed are fully distributed, and arbitrate the contention among end-to-end *multi-hop* flows with respect to fair resource allocation. The frequently used fairness models, such as weighted proportional or max-min fairness, may be straightforwardly supported by assigning their corresponding utility functions in the pricing model. The validity of our claims is supported by both theoretical studies and extensive experiment results.

- We presented a price pair mechanism that both regulates greedy behaviors and incentivizes selfish users in ad hoc networks. A pair of prices is the centerpiece of this mechanism: (1) the channel price that reflects the unique characteristics of location dependent contention in ad hoc networks, and regulates the usage of shared wireless channel; (2) the relay price that gives incentives to reach the adequate level of cooperation with respect to traffic relay. By using such a price pair as a signal, the decentralized self-optimizing decisions at each individual node converge to the global network optimal operation point. Simulation results are

also presented to validate our theoretical claims. We believe that we have reached an important milestone that integrates pricing and incentives strategies for channel access and traffic relays into the same coherent framework, which is a problem that has not been addressed previously before this work, especially when the objective is to converge to a desirable optimal operating point for the entire wireless ad hoc network.

6.2 Future Directions

My future research plan will go along both theoretical and experimental fronts of research directions. Theoretically, I will continue to explore decentralized resource allocation algorithms for wireless networks. In particular, I will explore the following problems and approaches.

- *Integrated resource allocation mechanisms*. The price-based resource allocation algorithm presented in this dissertation provides a rate control mechanism for elastic traffic whose utility function is increasing, and continuously differentiable. In the future, I would like to study resource allocation algorithms that consider both elastic traffic and non-elastic traffic, such as multimedia and real-time traffic simultaneously. The goal is to provide an integrated rate control and admission control mechanism which achieves aggregated utility maximization.

- *Revenue maximization resource allocation*. This dissertation has focused on the optimal resource allocation in a sense that the social welfare is maximized. In network settings such as Wi-Fi hotspot, the service provider may be more interested in a resource allocation mechanism where its revenue is maximized. I would like to study the revenue maximizing pricing strategies under various resource allocation mechanisms (*e.g.*, service differentiation, admission control, and rate control) in the future.

Along the experimental front, I would like to further investigate the following issues.

- *Channel-energy resource coordination*. This dissertation has presented the system implementation for wireless channel resource allocation and the theoretical modeling of channel-

energy price-pair coordination. In the future, I would like to engage in the research of system design for coordinated channel-energy resource allocation using a price-pair approach. In particular, I would like to explore the impact of multiple system parameters, such as CPU frequency, network adaptor power level and sleeping cycle, on the price generation.

- *Cross-layer design for coordinated resource adaptation*. Mobile applications built over wireless networks face severely constrained resources and highly dynamic environments. They usually exhibit application-specific adaptability by tuning performance based on resource availability. On the other hand, similar adaptation can be performed at system devices as well (e.g. wireless adaptor transmission range and schedule, and CPU frequency). This requires mobile systems to be capable of capturing and supporting adaptation at multiple layers (application, middleware, and OS) in a flexible yet coordinated fashion, so that if viewed globally, these adaptations lead to fair and efficient resource sharing in dynamic mobile computing environments. This dissertation has indicated that to achieve such goals, cross-layer efforts are required. Moving forward, I would like to explore the system model and software architecture to support such efforts. In particular, I am interested in applying control theory and optimization theory to enable stable distributed adaptation where resource can be optimally utilized.

References

[1] J. G. Augustson and J. Minker. An analysis of some graph theoretical cluster techniques. *Journal of ACM*, 17(4):571–586, 1970.

[2] D. Bertsekas. *Nonlinear Programming*. Athena Scientific, 1999.

[3] D. Bertsekas and J. Tsitsiklis. *Parallel and Distributed Computation*. Prentice-Hall, 1989.

[4] S. Buchegger and J. Y. Le Boudec. Performance analysis of the confidant protocol (cooperation of nodes - fairness in dynamic ad-hoc networks). In *Proc. of MobiHoc*, June 2002.

[5] L. Buttyan and J. P. Hubaux. Enforcing service availability in mobile ad-hoc wans. In *Proc. of IEEE/ACM Workshop on Mobile Ad Hoc Networking and Computing (MobiHOC)*, August 2000.

[6] L. Buttyan and J. P. Hubaux. Stimulating cooperation in self-organizing mobile ad hoc networks. *ACM/Kluwer Mobile Networks and Applications*, 8(5), October 2003.

[7] X. R. Cao, H. X. Shen, R. Milito, and P. Wirth. Internet pricing with a game theoretical approach: concepts and examples. *IEEE/ACM Trans. on Networking*, 10(2):208–216, 2002.

[8] K. Chen and K. Nahrstedt. ipass: an incentive compatible auction scheme to enable packet forwarding service in manet. In *Proc. of IEEE ICDCS*, 2004.

[9] Wei-Peng Chen and Lui Sha. An energy-aware data-centric generic utility based approach in wireless sensor networks. In *IPSN'04: Proceedings of the third international symposium on Information processing in sensor networks*, pages 215–224, New York, NY, USA, 2004. ACM Press.

[10] R. Cocchi, S. Shenker, D. Estrin, and L. Zhang. Pricing in computer networks: Motivation, formulation, and example. *IEEE/ACM Trans. on Networking*, 1(6):614–627, 1993.

[11] J. Crowcroft, R. Gibbens, F. Kelly, and S. Ostring. Modelling incentives for collaboration in mobile ad hoc networks. In *Proc. of Workshop Modeling and Optimization in Mobile, Ad Hoc and Wireless Networks (WiOpt)*, 2003.

[12] M. de Berg, M. van Kreveld, M. Overmars, and O. Schwarzkopf. *Computational Geometry: Algorithms and Applications*. Springer, 2000.

[13] P. Gupta and P.R. Kumar. The capacity of wireless networks. *IEEE Trans. on Information Theory*, pages 388–404, 2000.

[14] Tina M. Heikkinen. On congestion pricing in a wireless network. *Wireless Networks*, 8(4):347–354, 2002.

[15] K. Jain, J. Padhye, V. Padmanabhan, and L. Qiu. Impact on interference on multi-hop wireless network performance. In *Proc. of Mobicom*, September 2003.

[16] D. Julian, M. Chiang, D. O'Neill, and S. Boyd. Qos and fairness constrained convex optimization of resource allocation for wireless cellular and ad hoc networks. In *Proc. of IEEE INFOCOM*, pages 477–486, June 2002.

[17] K. Kar, S. Sarkar, and L. Tassiulas. A low-overhead rate control algorithms for maximizing aggregate receiver utility for multirate multicast sessions. In *Proc. of SPIE ITCOM*, 2001.

[18] K. Kar, S. Sarkar, and L. Tassiulas. A simple rate control algorithm for maximizing total user utility. In *Proc. of INFOCOM*, 2001.

[19] F. P. Kelly. Charging and rate control for elastic traffic. *European Trans. on Telecommunications*, 8:33–37, 1997.

[20] F. P. Kelly, A. K. Maulloo, and D. K. H. Tan. Rate control in communication networks: Shadow prices, proportional fairness and stability. *Journal of the Operational Research Society*, 49:237–252, 1998.

[21] S. Kunniyur and R. Srikant. End-to-end congestion control: Utility functions, random losses and ecn marks. In *Proc. of INFOCOM*, 2000.

[22] S. Kunniyur and R. Srikant. A time-scale decomposition approach to adaptive ecn marking. *IEEE Tran. on Automatic Control*, June 2002.

[23] R. J. La and V. Anantharam. Utility-based rate control in the internet for elastic traffic. *IEEE/ACM Trans. on Networking*, 10(2):272–286, 2002.

[24] X Lin and NB Shroff. The impact of imperfect scheduling on cross-layer rate control in multihop wireless networks.

[25] X Lin and NB Shroff. Joint rate control and scheduling in multihop wireless networks. In *Proc. of the IEEE Conference on Decision and Control*, 2004.

[26] S. H. Low and D. E. Lapsley. Optimization flow control, i: Basic algorithm and convergence. *IEEE/ACM Trans. on Networking*, 7(6):861–874, 1999.

[27] H. Luo, S. Lu, and V. Bharghavan. A new model for packet scheduling in multihop wireless networks. In *Proc. of ACM Mobicom*, pages 76–86, 2000.

[28] G. Berger-Sabbatel M. Heusse, F. Rousseau and A. Duda. Performance anomaly of 802.11b. In *Proc. INFOCOM*, 2003.

[29] T. Nandagopal, T.-E. Kim, X. Gao, and V. Bharghavan. Achieving mac layer fairness in wireless packet networks. In *Proc. of ACM Mobicom*, pages 87–98, 2000.

[30] G. Owen. *Game Theory*. Academic Press, 1995.

[31] C. Perkins and E. Royer. Ad-hoc on-demand distance vector routing. In *Proc. of IEEE Workshop on Mobile Computing Systems and Applications (WMCSA '99)*, 1999.

[32] Y. Qiu and P. Marbach. Bandwidth allocation in ad-hoc networks: A price-based approach. In *Proc. of INFOCOM*, 2003.

[33] R. Wouhaybi R. Liao and A. Campbell. Incentive engineering in wireless lan based access networks. In *Proc. of 10th IEEE International Conference on Network Protocols (ICNP)*, Nov 2002.

[34] T. Salonidis and L. Tassiulas. Distributed dynamic scheduling for end-to-end rate guarantees in wireless ad hoc networks. In *Proc. of ACM MOBICOM*, 2005.

[35] Kai Chen Samarth H. Shah and Klara Nahrstedt. Available bandwidth estimation in ieee 802.11-based wireless networks. In *Proc. of 1st ISMA/CAIDA Workshop on Bandwidth Estimation (BEst 2003)*, 2003.

[36] C. U. Saraydar, N. B. Mandayam, and D. J. Goodman. Pricing and power control in a multicell wireless data network. *IEEE Journal on Selected Areas in Communications*, 19(10):1883–1892, Oct 2001.

[37] C. U. Saraydar, N. B. Mandayam, and D. J. Goodman. Efficient power control via pricing in wireless data networks. *IEEE Trans. Commun.*, 50(2):291–303, Feb 2002.

[38] S. H. Shah, K. Chen, and K. Nahrstedt. Dynamic bandwidth management for single-hop ad hoc wireless networks. In *Proc. of IEEE International Conference on Pervasive Computing and Communications (PerCom)*, March 2003.

[39] V. Srinivasan, P. Nuggehalli, C. F. Chiasserini, and R. R. Rao. Cooperation in wireless ad hoc networks. In *Proc. of IEEE INFOCOM*, 2003.

[40] L. Tassiulas and S. Sarkar. Maxmin fair scheduling in wireless networks. In *Proc. of INFOCOM*, pages 763–772, 2002.

[41] A. Urpi, M. Bonuccelli, and S. Giordano. Modelling cooperation in mobile ad hoc networks: a formal description of selfishness. In *Proc. of Workshop Modeling and Optimization in Mobile, Ad Hoc and Wireless Networks (WiOpt)*, 2003.

[42] H. Yaiche, R. R. Mazumdar, and C. Rosenberg. A game theoretic framework for bandwidth allocation and pricing in broadband networks. *IEEE/ACM Trans. on Networking*, 8(5):667–678, October 2000.

[43] S. Zhong, Y. Yang, and J. Chen. Sprite: A simple, cheat-proof, credit-based system for mobile ad hoc networks. In *Proc. of IEEE INFOCOM*, 2003.

Vita

Yuan Xue was born in Harbin, China in 1976. She received her Bachelor of Science degree in Computer Science from Harbin Institute of Technology, Harbin, China in 1998. In January 2000, she was admitted to the Department of Computer Science in the University of Illinois at Urbana-Champaign. She received her Master of Science degree in Computer Science in 2002. In summer 2000, she worked as a research assistant at the National Center for Supercomputing Applications (NCSA) at Urbana, Illinois. Since 2001, she has worked in the MONET (Multimedia Operating Systems and Networking) research group headed by Professor Klara Nahrstedt. Her research interests include networking and distributed systems with a focus on wireless network, mobile system, QoS support and network security. She is a recipient of Vodafone Fellowship in the College of Engineering at UIUC in 2003 and 2004. After graduation, she will join the Department of Electrical Engineering and Computer Science at Vanderbilt University as an assistant professor.